FURTHER SHOCK TUNNEL STUDIES OF SCRAMJET PHENOMENA

NASA CONTRACT NO. NAGW - 674

by: R.G. Morgan, A. Paull,
N.A. Morris, R.J. Stalker

RESEARCH REPORT NO. 10/86

FURTHER SHOCK TUNNEL STUDIES OF SCRAMJET PHENOMENA.

NASA CONTRACT NO. NAGW - 674.

R.G Morgan

A.Paull

N.A.Morris

R.J.Stalker

CONTENTS

	PAGE
NOTATION	I
ABSTRACT	III
LIST OF FIGURES	VI
INTRODUCTION	1
SECTIONS:	
A. Silane Combustion limits	7
B. Pitot Rake Measurements	17
C. Source Flow Nozzles	21
D. Boundary Layer Heat Transfer	24
E. Film Cooling	26
F. Multi-Staged expansions	34
G. Shock Induced Ignition	44
TABLE OF TEST CONDITIONS	51
REFERENCES	52
ACKNOWLEDGEMENTS	54
APPENDIX	55
FIGURES	58

NOTATION

C_p	Specific heat at constant pressure	J kg^{-1} K^{-1}
H_s	Stagnation enthalpy	MJ/kg
I	Injector location	
I_{sp}	Net specific impulse	sec
J_v	Bessel function of order v	
K	Thermal conductivity	W m^{-1} k^{-1}
L	Length scale parameter	m
M_I	Intake Mach number	
M_J	Hydrogen jet Mach number	
$\dot{m}_o$	Mass flow rate of injected gas	kg s^{-1} m^{-1}
P	Local static pressure	kPa
P_I	Intake static pressure	kPa
P_s	Stagnation pressure	MPa
$\dot{q}$	Surface heat transfer rate	W cm^{-2}
$\dot{q}_o$	Flux of heat across fuel/air interface	W m^{-2}
R_e	Freestream unit Reynolds number	m^{-1}
ST	Start of diverging section	
T_I	Intake static temperature	K
T_W	Wall surface temperature	K
U_I	Air velocity at intake	ms^{-1}
U_o	Velocity of injected layer	m s^{-1}
X	Wetted length measured from intake	mm
Y_o	Thickness of injected layer	m
Y	Cross stream co-ordinate	
Z_n	**Nth zero of Jv-1**	
θ_D	**Thrust surface divergence angle**	**degrees**

ϕ	Equivalence ratio	
λ	Insulating layer mass flux power law coefficient	
v	$\frac{1}{\lambda + 2}$	
ρ	Density	kg m^{-3}
ρ_o	Density of injected layer	kg m^{-3}
α	Proportion of fuel in insulating layer	
Γ	The gamma function	
ΔT	Temperature difference between injected layer and room temperature	K

ABSTRACT

This report is part of a continuing study of scramjet related phenomena being undertaken by the University of Queensland, using the shock tunnel T3 at the Australian National University. Simple two dimensional models were used with a combination of wall and central injectors.

Silane as an additive to hydrogen fuel was studied over a range of temperatures and pressures to evaluate its' effect as an ignition aid. At all these conditions the effect of silane concentration was investigated. Silane at concentrations sometimes as low as 2.5% was found to be effective in inducing ignition at conditions where hydrogen alone was unable to burn . Towards the low temperature ignition limits an unsteady combustion effect was observed. This is not understood at present, but it is suggested that it might be connected with the selective burning of the silane fuel component at temperatures where the heat release is not sufficient to ignite the hydrogen.

The film cooling effect of surface injected hydrogen was measured over a wider range of equivalence ratio than before. In order to test a simple model for the transfer of heat through the fuel layer to the wall, the injection of hydrogen into nitrogen and air, helium into air and nitrogen into air were all tried. The simple model, which does not include combustion effects, was found to be effective for qualitative comparisons between different injection conditions. Good quantitative correlations to specific experimental data may be obtained by adjustment of a parameter which governs the effective diffusivity of

heat across the fuel layer. but it cannot at present be considered a true predictive technique. Values of the order 10 times that of the molecular thermal conductivitv are required.

Heat transfer measurements without injection were repeated to confirm previous indications of heating rates lower than simple flat plate predictions for laminar boundarv lavers in equilibrium flow. The previous results were reproduced and the discrepancies are discussed in terms of the model geometrv and departures of the flow from equilibrium.

In the thrust producing mode, attempts were made to increase specific impulse with wall injection. This was bv means of a staged expansion, and, in a slight departure from two dimensional flow, transverse injection from wall mounted circular jets. Some improvements were evident at the lower enthalpies. The performance of wall injected scramjets in shock tubes still appears to be limited bv the existence of a layer of cold fuel attached to the wall.

In order to confirm that the pressure disturbances seen on the wall were also present in the duct, a pitot rake was mounted from the top of the model and spanned the mixing and combustion region of the fuel jet. Clear evidence of transverse pressure disturbances was seen.

Some preliminarv tests were also performed on shock induced ignition, to investigate the possibilitv in flight of injecting fuel upstream of the combustion chamber, where it could mix but not burn. Ignition of the premixed fuel and air mixture would subsequentlv occur due to shock heating at the combustion chamber intake.

Hydrogen was injected at a condition where it could not sustain combustion, and it was then heated by the passage of an oblique shock wave. In the central injection mode, ignition followed rapidly after shock reflection.

In the wall injection mode it was not possible to induce ignition under conditions where hydrogen would not burn without compression. Moreover, under conditions where combustion was possible, the passage of the shock did nothing to enhance combustion. The failure of shock stabilized combustion with wall injection is attributed to the quenching effect of the cold model walls. It is still thought that the technique might be successful with heated walls or with heated fuel.

LIST OF FIGURES

1. Schematic of experimental apparatus.

2. Mach 4.5 configuration.

3. Pressure profiles, ignition limit 20% SiH4/H2, M=3.4. Constant area duct. 0.3, T= 400 - 445K. P=24 kPa.

4. Pressure vs time, constant area duct, 20% SiH4/H2, T=415K, P=24kPa, H=1.07 MJ/kg.

5. Pressure profiles, ignition limit 20% SiH4/H2, M=3.3, constant area duct, T=705K, P=15 kPa, H=1.94 MJ/kg.

6. Pressure profiles, 20% SiH4/H2, M=3.3, constant area duct, T=970K, P=10 kPa, constant area duct.

7. Pressure profiles, effect of concentration of silane at mach 4.5, H=3.43 MJ/kg, T=625K, P=30 kPa, constant area duct.

8. Pressure vs time, constant pressure burning of 10% SiH4/H2 at mach 4.5, H=2.65 MJ/kg, T=480K, P=30 kPa, constant area duct.

9. Pressure profiles for constant area duct, effect of concentration of silane at mach 4.5, H=2.65 MJ/kg, P=30kPa, T=480K.

10. Pressure profiles for constant area duct, effect of concentration of silane at mach 4.5, H=1.90 MJ/kg, P=30kPa, T=400K.

11. Pressure profiles for constant area duct, effect of concentration of silane at mach 5, H=8.7 MJ/kg, P=20 kPa, T=1500K.

12. Pressure profiles for constant area duct, effect of concentration of silane at mach 5, H=6.2 MJ/kg, P=20 kPa, T=1000K.

13. Pressure profiles for constant area duct, effect of concentration of silane at mach 5, H=4.2 MJ/kg, P=20 kPa, T=650K.

14. Pressure profiles for constant area duct, effect of concentration of silane at mach 5, H=3.43 MJ/kg, P=20 kPa, T=540K.

15. Pressure profiles for constant area duct, effect of concentration of silane at mach 5, H=2.65 MJ/kg, P=20 kPa, T=410K.

16. Pressure profile for constant area duct at mach 5, 20% SiH4/H2 injection, H=1.9 MJ/kg, P=20 kPa, T=350K.

17. Pressure profile for constant area duct at mach 5, 17.4% Ar/H2 injection, H=4.2 MJ/kg, P=20 kPa, T=650K.

18. Pressure profiles for constant area duct at mach 5, 17.4% Ar/H2 injection, H=8.7 MJ/kg, P=20 kPa, T=1500K.

19. Diagram of 15 degree divergence thrust surface without cowl.

20. Diagram of 15 degree divergence thrust surface with cowl.

21. Diagram of 15 degree divergence symmetrical thrust surface .

22. Thrust contribution due to an expansion wave passing through a mach number gradient.

23. Thrust contribution due to a burning fuel jet.

24. Pitot profiles across an open duct. 15 degree divergence. M=3.5. P=160 kPa. T=1700 K. =1.0 .

25. Pitot profiles across an open duct. 15 degree divergence. M=3.5. P=160 kPa. T=2500K. =1.27.

26. Pitot profiles across a closed duct. 15 degree divergence. M=3.5. P=160 kPa. T=2500K. =1.0.1.85.

27. Pitot profiles across a symmetrical duct. 15 degree divergence. M=3.5. P=3.5. T=2500K. =1.09.

28. Central injectors. source flow and standard.

29. Wall injectors. Source flow and standard.

30a. Pressure profiles for central injection from a source flow and a cylindrical nozzle into a constant area duct. H=4.2 MJ.kg. =1.38. M=3.5.

30b. Heat transfer rates for central injection from a source flow and cylindrical nozzle into a constant area duct. H=4.2 MJ/kg. =1.38. M=3.5.

31a. Pressure profiles for central injection from a source flow with a cylindrical nozzle into a constant area duct. H=8.7 MJ/kg. =1.72. M=3.5.

31b. Heat transfer rates for central injection from a source flow and a cylindrical nozzle into a constant area duct. H=8.7 MJ/kg. =1.72 . M=3.5

32a. Pressure profiles for wall injection from a source flow and a cylindrical nozzle into a constant area duct. H=4.2 MJ/kg. =1.48. M=3.5.

32b. Heat transfer rates for wall injection from a source flow and a cylindrical nozzle into a constant area duct. H=4.2 MJ/kg. =1.48. M=3.5

33a. Pressure profiles for wall injection from a source flow and a cylindrical nozzle into a constant area duct.H=8.7 Mj/kg. =2.0. M=3.5.

33b. Heat transfer profiles for wall injection from a source flow and cylindrical nozzle into a constant area duct. H=8.7 MJ/kg. =2.0. M=3.5.

34a. Predicted and measured values of the heat transfer rate for a constant area duct with injector. H=8.7 MJ/kg. M=3.5.

34b. Predicted and measured values of the heat transfer rate for a 15 degree diverging duct with injector. H=8.7 MJ/kg. M=3.5

34c. Predicted and measured values of the heat transfer rate for a 15 degree diverging duct with injector. H=4.2 MJ/kg. M=3.5

35. Heat transfer rates for the injection of hydrogen into a nitrogen test gas in a constant area duct. H=4.2 MJ/kg. M=3.5. 1.6 mm throat.

36. Heat transfer rates for the injection of hydrogen into a nitrogen test gas in a constant area duct. H=8.7 MJ/kg. M=3.5. 0.3 mm throat.

37. Heat transfer rates for the injection of hydrogen into a nitrogen test gas in a constant area duct. H=8.7 MJ/kg. M=3.5. 1.6 mm throat.

38. Heat transfer rates in a constant area duct when hydrogen is injected into a nitrogen test gas with different injectors. H=8.7 MJ/kg. M=3.5.

39. Heat transfer rates in a constant area duct when hydrogen is injected into a nitrogen test gas with different injectors. H=4.2 MJ/kg. M=3.5.

40. Schematic of simple heat transfer model.

41. Variation of m v with m .M=3.5.

42. Variation of T/v with m . M=3.5.

43a. Pressure profiles for the injection of hydrogen into a constant area duct. nitrogen. air test gases. H=8.7 MJ/kg. =1.35. M=3.5.

43b. Heat transfer rates for the injection hydrogen into a constant area duct. nitrogen. air test gases. H=8.7 MJ/kg. =1.35. M=3.5.

44a. Pressure profiles for the injection of hydrogen into a constant area duct. nitrogen. air test gases. H=8.7 MJ/kg. =2.60. M=3.5.

44b. Heat transfer rates for the injection of hydrogen into a constant area duct. nitrogen. air test gases. H=8.7 MJ/kg. =2.6. M=3.5

45. Heat transfer rates for the injection of nitrogen into air and hydrogen into nitrogen at similar values of m v . H=8.7 MJ/kg. M=3.5.

46. Proposed central injector expanded from centre line.

47. Schematic of 2 stage expansion nozzle.

48. Schematic of expansion wall jet interaction.

49. Isp/ . Comparison of dual and single stage expansions.

50. P/X. Dual stage expansion. short duct. parallel wall injection. M=3.5. Hs =4.2 and 8.7 Mj/kg.

51. Isp/phi Dual stage expansion. long duct. parallel wall injection. M=3.5. Hs=4.2 and 4.2 Mj/kg.

52. P/X. Dual stage expansion. long duct. parallel wall injection. 0.9 mm throat, Hs=8.7 Mj/kg and 4.2 Mj/kg.

53. Schematic of transverse and parallel injection.

54. Isp/phi Transverse injection. Dual stage expansion. long duct. M=3.5. Hs=8.7.6.1 and 4.2 Mj/kg.

55. Isp/phi. Various configurations of wall injection. Hs=8.7 and 4.2 Mj/kg, M=3.5.

56. Isp/phi. Long duct. dual and single stage expansions. 27% transverse injection. Hs=8.7.6.1.and 4.2 Mj/kg. M=3.5.

57. Comparison of transverse and parallel injection. long duct. single expansion. P/x and T/x. M=3.5

58. Central injection shock stabilized combustion rig.

59. P/x. Shock stabilized combustion central injection. 5 degree shock. M=5.

60. Wall injection shock stabilized combustion rig.

61. P/X. Shock stabilized combustion wall injection. 10 degree shock.Hs=8.7 Mj/kg.

62. P/X. Shock stabilized combustion wall injection. 10 degree shock. Hydrogen and helium injection comparisons. Hs=8.7 Mj/kg, M=5.

63. P/X. Shock stabilized combustion wall injection. 10 degree shock. M=3.5. Hs=8.7 Mj/kg.

64. P/X. Shock stabilized combustion wall injection. 10 degree shock. M=3.5. Hs=6.1 Mj/kg.

65. P/X. Shock stabilized combustion wall injection. 10 degree shock. M=3.5, Hs=4.2 Mj/kg.

66. P/X. Silane injection from the wall. M=3.5. Hs=4.2 Mj/kg. 0.5.

67. Effect of freestream oxygen radical concentration on ignition delay times in 20% SiH4/H2 mixtures. results of computer simulations.

INTRODUCTION AND CONCLUSIONS

This constitutes the second progress report on Shock Tunnel Studies of Scramjet Phenomena under NASA contract No. NAGW-674.
The purpose of the study was to look more closely at some of the features identified in the first progress report. Ref 1.
The report is divided into sections as outlined below.

Section A. Silane combustion.

Preliminary tests in 1985 showed the effectiveness of silane as an ignition aid when mixed with hydrogen at 20% by volume. Further experiments were performed using silane at different concentrations and over a wider range of pressure and enthalpies. The silane was found to be effective at concentrations as low as 5%.

In order to confirm that the combustion enhancement was due to the chemical kinetics of the silane, rather than a gas dynamic effect, control experiments were performed using a mixture of argon and hydrogen. The concentration was adjusted to produce a mixture with the same molecular weight as the 20% silane mix. It was found that this mixture was unable to burn at conditions where the silane mixture burned vigorously. This was taken as confirmation of the chemical nature of the silane ignition mechanism.

In studies of wall injection the existence of a quenched layer attached to the wall was postulated to explain the low values of specific impulse, and also the lack of combustion at low equivalence ratios. Silane provides a convenient means of checking this theory, as

it is capable of spontaneous combustion at the wall temperature. A 20% silane mixture was injected from the wall into a constant area duct at an equivalence ratio which would not support combustion with hydrogen alone. Large pressure rises were recorded down the duct, which is consistent with the existence of a layer of mixed air and fuel which is attached to the wall, but unable to burn due to its' low temperature. This suggests that shock tunnel experiments with cold wall might be better able to simulate flight conditions with hot walls by the use of small concentrations of silane. At present attempts to investigate modifications, such as transverse wall injection and staged expansions, are restricted because the presence of the wall quenched zone is the predominant factor in determining the amount of heat release and thrust.

Section B. Pitot rake measurements.

Static pressure measurements have shown the existence of disturbances along the wall and the thrust surface which are consistent with the simple theory developed for the operation of a two dimensional scramjet. These disturbances would be expected to reflect off the walls and propagate across the duct, creating significant transverse pressure gradients. A pitot rake was constructed to measure the transverse pitot pressure profiles behind a normal bow shock, and this was used in several thrust producing configurations. As expected, transverse pressure disturbances were observed.

Section A. Source flow nozzles.

The fuel injection nozzles used in the experiments are of simple construction with sudden changes of geometry. and in some cases a lack of symmetry. Equivalence ratio control is by means of adjusting hydrogen reservoir pressure, and differences in mach number and jet thickness occur between shots. The nozzles are not correctly expanded for all conditions. and freestream pressure is established through a series of shocks and expansions. This is necessary in order to maintain a reasonable run rate in the limited tunnel time available. It is difficult to model the flow through the nozzles accurately, and the effects of the variations between conditions are not known. Control experiments were therefore performed with source flow nozzles for both wall and central injection. The nozzles were designed with the same throat area as the standard nozzles. but with uniform diverging sections in the supersonic regions. While these nozzles were still not operated at perfectly expanded conditions, they did provide comparisons for the effects of internal nozzle geometry on otherwise identical runs.

No difference could be observed between the nozzles from either pressure or heat transfer measurements.

Section D. Fuel off boundary layer heat transfer measurements.

Fuel off heat transfer measurements with a wall injector fitted taken during the test program in 1985 showed surprisingly low values of heat transfer when compared to flat plate predictions. The difference

between this and previous heat transfer work was that the presence of the wall injector provided a step which caused the boundary layer to temporarily separate.

This work was repeated with new instrumentation to confirm the result, and comparisons were also made with experiments by previous workers on different models. The same results were again obtained, and the discrepancies are attributed to non equilibrium flow effects, and also to the fact that the model was not a flat plate and flat plate predictions would not be expected to apply precisely.

Section E. Film cooling studies.

The effectiveness of wall injected hydrogen as a coolant was demonstrated in 1985. The data obtained was mainly at high equivalence ratios, and no theoretical treatment was offered to explain the results. More work is reported here giving more data at low equivalence ratios, and a simple predictive technique is presented.

The model gives a good qualitative explanation of the results, and identifies that the critical parameter for assessing the cooling effect of a non reacting insulating layer is the product of mass flow rate with the thickness of the jet.

Section F. Two stage divergence and transverse injection.

The first experiments with wall injection were performed in 1985. and for theoretical reasons it was expected that an improvement in performance could be produced by means of a multistaged expansion and transverse circular jets of fuel injected upstream of the parallel wall component.

Both techniques were to a certain extent successful. but interpretation of the results is complicated by the presence of the wall quenching layer.

The two stage expansion was successful in encouraging combustion in an expanding section which is simultaneously developing thrust. but the thrust obtained on further expansion of the flow was disappointing.

Transverse injection of the fuel was seen to give ignition at slightly lower equivalence ratios than parallel injection. but this improvement in performance was not maintained when the equivalence ratio was increased.

Section G. Shock Induced Ignition.

Weight minimization of scramjets is just as important as thermodynamic performance if a flight engine is to be produced. One means of reducing weight is to inject the fuel upstream of the intake. where it can mix but it is not hot enough to burn. Ignition can later be initiated by compressions at the combustion chamber intake.

This effect was examined for both wall and central injection by means of an oblique shock wave passing through the duct. For the central injector rapid combustion of the premixed fuel occurred after the shock at freestream conditions that would not normally support combustion.

With wall injection no such effect was observed, and at conditions where combustion was possible no improvement was produced by the shock heating. This is again attributed to the presence of a quenched layer attached to the wall, and emphasises the need for heated walls or heated fuel for comprehensive studies of any combustion effects with wall injection.

SECTION A

COMBUSTION LIMITS OF SILANE

Silane was mixed with hydrogen at different molar ratios and was centrally injected into a constant area duct. Silane concentration was varied by adding additional hydrogen to a pre-prepared 20% silane/hydrogen mixture . Convection currents caused by a heating coil secured to the bottom of the mixing cylinder were used to mix the gases. Work was carried out at three mach numbers and intake pressures. Temperatures were reduced for each case by reducing the enthalpy of the air flow, thus yielding a range of ignition conditions. Mach 3.4 and 5 contoured nozzles were used. Mach 4.5 flows were produced by using a model intake attachment in conjunction with the mach 5 nozzle. This attachment was in the form of two plates inclined at 2.57 degrees as shown in figure 2.

COMBUSTION LIMIT OF 20% SILANE/H2 MIXTURES AT MACH 3.4

Work at this mach number for determining the combustion limits of silane /hydrogen mixtures was performed at the University of Queensland using shock tunnel TQ .

A 20% mole fraction mixture of silane in hydrogen was centrally injected into a constant area duct with flows of a nominal mach number of 3.4. Figure 2 ,with the compression wedges removed, represents the

above configuration. Figure 3 shows that with a static intake pressure of 24 kPa that the temperature must be reduced to around 400K before the silane mixture is extinguished.

It should be noted that the temperatures listed in the figure are nominal, but they do indicate the relative magnitudes of the temperature changes involved.

At 415K the combustion becomes unstable and the pressure rise shown in figure 3 is due in fact to a pressure rise propagating upstream with time. It is suggested that this might be due to a thermal choking effect associated with an increased ignition delay time which would prevent combustion until the air/fuel mixture has travelled the length of the duct. Once combustion starts at the end of the duct, the heat release is such that steady flow cannot be maintained, and a shock is created which travels upstream. Figure 4 illustrates this effect with pressure against time traces at stations along the length of the duct. An unsteady effect was observed near the combustion limits for silane/H2 mixtures at all mach numbers and concentrations of silane .

Experiments at mach 3.3 show that 20% silane mixtures are extinguished at 705K when the pressure is reduced to 15 kPa (see figure 5).However, vigorous burning is observed at an even lower pressure of 10 kPa and a temperature of 970K (figure 6). Experiments at intermediate conditions to establish a smaller range of temperatures where silane is shown not to burn are planned, but the present results give a clear indication of the sensitivity of the combustion temperature limit with pressure at these low pressures.

COMBUSTION LIMITS OF 20%, 10%, AND 5% SILANE / HYDROGEN MIXTURES AT FLOWS OF MACH 4.5

Work at this mach number was performed at the A.N.U. in Canberra using shock tunnel T3.

Again the mixture was injected into a constant area duct configuration using central injection. Experiments were performed at three enthalpies namely 3.43, 2.65, and 1.9 MJ/kg which correspond to an intake pressure of 30 kPa and temperatures of 625K, 480K, and 400K respectively.

At 30 kPa and 625K (3.43 MJ/kg), the 20 % and 10% mixtures burned with about the same amount of heat release, but the 5% mixture was apparently extinguished (at least over the length of the duct which was considered). This is shown in figure 7 in plots of duct static pressure normalized with stagnation pressure plotted against distance along the duct. The 20% mixture appears to burn with a marginally shorter ignition delay time than the 10% mixture.

At 30kPa and 480K (2.65 MJ/kg) all of the mixtures show an unusual pattern of behaviour. The pressures along the length of the duct rise up to a particular level, and then stay roughly constant despite the falling stagnation pressures. This is illustrated in figure 8 where the pressures at stations 3,4,5 and 6 are plotted against test time for the 10% mixture. When normalized against stagnation pressure, duct static pressure vs distance traces appear unsteady, so for this

condition plots of normalized pressures are taken at comparable stagnation pressure (figure 9). These show the 10% mixture burning with the greatest pressure rise followed by the 5% mixture then the 20% mixture. This effect is not understood but appears to occur only at these lower temperatures. The fact that there appears to be unsteady burning of the 5% mixture at this temperature despite no combustion at the higher temperature cannot be explained at this stage.

At 30 kPa and 400K (1.9 MJ/kg), the same unsteady effect was observed with plots of normalized static pressures vs distance along the duct (figure 10) showing the 5% mixture giving the greatest pressure rise followed by the 10% then 20% mixtures. The decrease in heat release with silane concentration suggests that the pressure rises are not due to the selective burning of the silane component of the mixture and that the hydrogen is somehow being burnt as well at these low temperatures.

The mach 4.5 condition was obtained by use of a scoop intake (figure 2) and in this series of tests, it proved difficult to achieve perfectly steady normalized pressure traces. This may be the cause of the apparently anomalous result produced at mach 4.5.

COMBUSTION LIMITS OF 20%, 10%, 5% AND 2.5% SILANE/HYDROGEN MIXTURES AT MACH 5

A silane /hydrogen mixture was injected into a mach 5 air flow at equivalence ratios from 0.7 to 1.3. The effects of varying the silane concentration was investigated over a range of enthalpies.

In the enthalpy range 8.7 to 3.43 Mj/kg. which corresponds to intake temperatures in the range 1500 to 540 K. steady combustion was observed. Hydrogen fuel alone had previously been found not to burn at these conditions. At an enthalpy of 2.65 Mj/kg a combustion effect was observed, but it was not steady.

This is an effect which has been observed with silane over a range of conditions as the temperature approaches the lower limits for combustion. A possible explanation for this effect would be that the silane is burning. but the temperature rise is insufficient to ignite the hydrogen. The scramjet would therefore see a low equivalence ratio silane fuel jet which would probably be completely burned and produce constant heat release as the intake pressure drops. This effect would tend to hold the internal duct pressures high as the intake pressure dropped. leading to unsteady duct pressures when normalized to the intake or stagnation pressures. In this unsteady region the duct pressure rises would be expected to increase with silane concentration. and this was observed in some cases.

This is in contradiction with the data obtained at mach 4.5, and suggests that there may be two mechanisms for unsteady combustion at low enthalpies. The first, consisting of a thermal choking effect, and the second being selective combustion of the silane alone.

At 8.7 Mj/kg silane was injected at concentrations of 5% and 20%, and no significant difference between the two was observed. This is shown in Figure 11 and suggests that at the higher temperatures that raising the level of silane concentration has only marginal benefit.

At 6.1 Mj/kg silane was injected at 2.5% and 20% and the same steady pressures were achieved down the duct, but with a slightly longer delay in the 2.5% case. This is illustrated in figure 12.

At 4.2 Mj/kg silane was injected at 2.5, 5, 10 and 20% concentrations, and the effect on delay times was seen to change strongly between 2.5 and 5% but not much between 5% and 20% (Figure 13). The steady pressure levels downstream in the duct were again seen to be fairly independent of silane concentration.

At 3.43 Mj/kg all concentrations showed a significantly increased ignition delay (Figure 14), with not much variation between the concentrations. However in the down stream regions of the duct, higher pressures were achieved with the lower silane concentrations.

At 2.65 Mj/kg the combustion effects were not steady, as mentioned above and the higher concentrations of silane were seen to produce higher pressures. This is shown in Figure 15.

At 1.9 Mj/kg silane injected at a concentration of 20% did not produce any ignition (Figure 16) and no further work was done at this condition.

The mach 5 tests produced very steady time resolved traces, and thr results are considered to be more reliable than those presented for mach 4.5.

In conclusion to this section, it is noted at the higher enthalpies 5% silane is adequate for ignition, and no improvement is produced for higher concentrations. At lower enthalpies, combustion proceeds faster but with less heat release, as the silane concentration is increased.

The unsteady effects at the lower temperature ignition limit, while an interesting phenomena, cannot be explained completely at this stage. This is not considered to be critical because in practice, flight conditions which promote unsteady burning will be avoided. However, it will be important to define the limits where these effects are observed.

HYDROGEN / ARGON MIXTURES

A Hydrogen/Argon mixture equivalent in molecular weight to a 20% silane in hydrogen mixture was centrally injected into a constant area duct. Fuel was injected such that the mass flow rate of the argon/hydrogen mixture was equal to the mass flow rate of a 20% silane/hydrogen mixture injected at an equivalence ratio of about one based on the hydrogen content of the fuel. Flow conditions which did not support hydrogen combustion but did support combustion of a 20% silane/hydrogen mixture were used. This was done to test whether the increased molecular weight over pure hydrogen fuel was a contributing factor in the mechanism of burning when silane was added to hydrogen.

Figure 17 shows pressure profiles for fuel on and fuel off cases with a hydrogen/argon mixture at a flow condition of mach 5 and a freestream enthalpy of 4.2 MJ/kg. It is clearly evident that there is no burning.

The freestream temperature was increased by increasing the flow enthalpy to 8.7 MJ/kg and still no combustion was observed. This is shown in figure 18. It was concluded therefore that increased molecular weight of a silane/ hydrogen mixture over pure hydrogen had no significant effect on the reactivity of the fuel. Rather, burning is due to the chemical kinetic mechanisms related to the breakdown of silane.

Recent numerical analysis has shown that the ignition of silane is very sensitive to the presence of oxygen atoms created in the shock tube and frozen in the freestream flow. This effect is discussed in the appendix and represents an important difference between shock tunnel simulations and real flight conditions.

WALL INJECTION OF SILANE.

The presence of the cold model walls represents a sink of heat to the flow. because in the short duration of the tests the wall temperature does not rise significantly above ambient. The cooling effect of the wall penetrates a significant distance into the flow. With central injection this does not have a critical effect on the development of combustion.

However. when the fuel is injected from the wall, there is always a region whose temperature will be held below the ignition temperature, regardless of how much combustion may take place further away from the wall. The hydrogen contained in this low temperature region appears to correspond to an equivalence ratio of approximately 1.5, because no ignition at all is possible at lower equivalence ratios. This represents a serious defect in the ability of shock tunnel tests to accurately model a real flight situation with aerodynamically heated walls.

The fuel in the quenched region may be mixed with oxygen, with only the low temperature inhibiting combustion. To confirm that this is indeed the case, and that the lack of combustion is not the result of some other cause, a test was done with the injection of a 20% silane hydrogen mixture.

The fuel was injected at an equivalence ratio of 0.5 into a flow of enthalpy 4.2 Mj/kg. With hydrogen injection alone no combustion would be expected at this condition. The results of this test are shown in Fig 66, and it can be seen by the pressure rise above the fuel off levels that it burnt well.

This result is significant in that it demonstrates that oxygen is diffusing to the fuel layer close to the wall, and that it is thermal effects which are preventing it from burning. This gives encouragement to efforts which are currently being made to design a model which can use heated fuel, and possibly even heated walls. It also suggests that in the absence of the above, silane might be used to investigate other aspects of combustion which are difficult to study properly in the presence of an extensive layer of quenched fuel. This includes the use of staged expansions and transverse injection discussed in section F.

SECTION B

PRESSURE PROFILES ACROSS A DIVERGING DUCT

For these experiments, a "pitot rake" was secured to the model to take a pressure profile normal to the flow direction. Three cases at mach 3.5 with central fuel injection were tried, 15 degree divergence thrust surface without cowl (fig. 19), 15 degree divergence thrust surface with cowl (fig. 20), and twin 15 degree divergence thrust surfaces (fig. 21). Measurements were those of stagnation pressure behind bow shocks created by the presence of the blunt pitot probes.

Pressure disturbances measured on the walls of the thrust surface indicate the presence of compression and expansion waves in the flow that are consistent with a simple model that has been developed for the combustion and thrust production mechanisms in a two dimensional scramjet (ref. 2). These waves will reflect off the walls and should produce corresponding transverse pressure gradients across the duct. This series of experiments has been developed to confirm the presence of such transverse disturbances and add further credibility to the theoretical model. A full treatment to predict the quantitative transverse pressure profiles for these test cases has not yet been performed, but the results are still significant in confirming the presence of such effects.

EXPLANATION OF THE MODEL

Heat release from the fuel jet results in a subsequent drop in mach number in the jet because of increased temperature. Because of the existence of a negative gradient of mach number from the edge of the burning jet to the middle, the expansion waves produced by the divergence, create reflected compression waves and then expansion waves as they progress through the burning jet. This is illustrated in figure 22, which shows the passage of a single expansion wave through a mach number gradient. Integration of the effects of all the expansion waves in the expansion fan passing through the fuel jet produces a net pressure rise on the thrust surface. Compression and expansion waves reflect off solid surfaces and continue on to the rear of the duct where they are sensed by the pitot rake.

Coupled with this effect is the production of compression waves due to the mixing and burning of the injected fuel, and their subsequent reflection from the thrust surface as shown in Figure 23. The compression are later followed by expansion waves from the combustion region, but the net result in a confined duct is a pressure and thrust increase.

Wave propagation paths will be different for each of the different configurations and each is discussed separately, together with experimental results.

To carry out a full analysis , mach number profiles for the burning hydrogen jet would be obtained from a two dimensional mixing and combustion program (8). Integral expressions for the strength of reflected expansion and compression waves from the mach number gradient could then be evaluated to give pressure profiles (ref 2).

OPEN DUCT - 15 DEGREES DIVERGENCE

When the scramjet is configured as a closed duct, expansion waves propagating from the end of the shock tunnel nozzle clear the intake of the scramjet and have no effect on the thrust surface pressure measurements. However, for this configuration with only one surface, to ensure that expansion waves from the nozzle exit did not impinge on the instrumented part of the thrust surface, the nozzle was extended by a sector which fitted between the side plates of the scramjet. As seen in figure 19, the first expansion wave encountered by the thrust surface from the edge of the nozzle extension is well downstream of the surface pressure transducers. Note that expansions propagating from the edge of the nozzle are bent 15 degrees in towards the thrust surface by the presence of the expansion fan at the corner of the diverging section. The pitot rake experiences these expansions due to the lack of a top cowl.

Plots of pitot pressure versus y (distance from datum A) are shown in figures 24 and 25 for fuel off and fuel on cases at two freestream enthalpies, 6.1 and 8.7 MJ/Kg. It appears from these plots that changing the enthalpy of the air flow has marginal effect on the stagnation pressures across the duct.

CLOSED DUCT - 15 DEGREES DIVERGENCE

With a closed duct, expansions created by the start of divergence reflect off the top cowl and continue on down the duct. Coupled with this effect is that of the compressions and expansions reflected from the mach number gradient caused by the presence of the burning fuel jet. Overall pitot pressures are lower than those for the case when the duct has no cowl. This is probably due to multiple reflections of the expansion caused by the start of divergence. For this case, the pitot rake was traversed up and down the width of the duct for the fuel on case with equivalence ratio of one. Hydrogen at a higher equivalence ratio was injected and had little effect on the pressure profile. Plots of fuel on and fuel off pressure profiles at a freestream enthalpy of 8.7 MJ/kg are shown in figure 26.

SYMMETRICAL DUCT - 15 DEGREES DIVERGENCE

When the scramjet was configured as a symmetrical duct, there was a more marked difference between fuel on and fuel off results compared with the closed duct case. Plots of fuel off and fuel on pressure profiles at a freestream enthalpy of 8.7 MJ/Kg are shown in figure 27.

COMMENT

Although the results of the pitot survey cannot be fully interpreted until the computations mentioned above had been performed, they do indicate the presence of substantial transverse pressure gradients. This is consistent with the thrust production mechanisms postulated in reference (2).

SECTION C

SOURCE FLOW NOZZLE

Fuel nozzles used in the experiments to date have been designed to give a wide range of equivalence ratios with the simplest possible design and a minimum of structural adjustments between operating conditions. This was done to make optimum use of the limited tunnel test time which is available to the project.

The nozzle consists of a removable two dimensional throat, and the mass flow rate and Mach Number are controlled by the setting of the fuel reservoir pressure. Figures 28a and 29a show the standard nozzle configurations for wall and central injection. Ref (1) Figure 3 shows the range of injection conditions which may be achieved with the wall injectors. For a given injection condition the nozzle exit pressure will not in general be matched to the free stream pressure, and a series of compressions and expansions will be created as the pressures equalize. It is not known what effect an under or over expanded jet will have on the mixing and combustion rates of the scramjet, and this process is difficult to model numerically with the abrupt changes in geometry of the standard injector.

However previous experience with wall injection suggests that it is the equivalence ratio alone which controls the amount of mixing and combustion. Ref (1) presents data in Figures 8 and 9 comparing runs with similar equivalence ratios, but obtained with different throats which produce different exit pressures. No significant difference is apparent between the two injectors for either of the enthalpies considered.

In order to further investigate this effect nozzles with the same throat sizes,

but with different geometries were constructed. The geometry of the new nozzles was chosen so that it would be more ameanable to numerical analysis, as well as giving a direct comparison with the standard injectors.

A comparison was made between two different injectors for both central and wall injection. The two injectors used were a cylindrical nozzle and a source-flow nozzle. Figures 28b and 29b show the different structures of the two injectors for central and well injection. Both injectors are two dimensional and expand the fuel from a 0.9 mm throat (wall injection) and a 1.6 mm throat (central injection) to 5 mm at the nozzle exit. The source-flow nozzle expands the fuel so that the flow through the nozzle is similar to that from a two-dimensional line mass source.

For both central and wall injection pressure and heat transfer measurements were taken simultaneously. The freestream test gas was air and the stagnation enthalpies of the test gas were either 4.2 mJ/kg or 8.7 mJ/kg. Hydrogen fuel was injected from the wall injector at equivalence ratios of 1.45 and 2.0 into a test gas of stagnation enthalpy 4.2 mJ/kg respectively and from the central injector at equivalence ratios of 1.4 and 1.7 respectively.

The results of the central injection experiments are given in Figures 30a, 30b, 31a and 31b and the wall injection results are given in Figures 32a, 32b, 33a and 33b. From the normalized pressure results it is seen that for both the wall and central injectors and at either test condition, little difference is produced by the different injectors. The heat transfer measurements also reflect this result, however they are not as conclusive due to the considerable scatter observed.

In conclusion, no difference between the results for a source-flow nozzle and

a cylindrical nozzle could be detected within the experimental accuracy. Coupled with previous data for the effect of throat size at a given equivalence ratio, it still seems that the equivalence ratio is the factor of most significance in determining the mixing and combustion rates.

SECTION D

BOUNDARY LAYER HEAT TRANSFER

Previously reported work, Ref (1), measured heat transfer rates to the scramjet walls at lower levels than would be predicted by flat plate predictions. A series of tests was performed with different heat transfer gauges to confirm the reproducability of these results.

Heat transfer measurements to the wall of a constant area duct and a 15^{o} diverging duct, both with 5 mm steps, were taken simultaneously with pressure measurements. Experiments were done at an intake Mach number of 3.5 and enthalpies of 4.2 and 8.7 MJ/kg. From the pressure measurements and the intake conditions emperical predictions of the heat transfer rate are made using the correlations of Ref 3 for a flat plate laminar boundary layer and following the treatment of Ref 4 for a turbulent boundary layer. The intake conditions are determined from the stagnation conditions using a computer model for the non-equilibrium expansion of a reacting gas down the nozzle, Ref 5.

Similar measurements have been taken previously and are recorded in Ref 1. For those experiments the measured heat transfer rate was of order 1/10 of the predicted value for a turbulent boundary layer and was less than or equal to the predicted value for a laminar flow. Moreover, there was a greater deviation between the measured and predicted laminar values when more expansions were experienced by the flow, and this deviation was more pronounced at higher enthalpies.

The results of the latest experiments and predictions for a laminar boundary layer are given in Figures 34a, 34b and 34c. The turbulent boundary layer

predictions were again of order ten times those measured and from these figures it is concluded that the boundary layer is laminar. It can be seen that the same trends were observed again. It is also seen that the predicted values approach the measured values at the downstream end of the duct. A possible explanation for the low measured values lies in the non equilibrium chemistry of the flow at the higher enthalpies.

The test gas in a reflected shock tunnel is produced by expanding the gas from a high pressure and temperature reservoir which is in equilibrium, and, due to the high temperatures, significant amounts of dissociation occur, particularly of oxygen molecules. During the expansion the dissociated products recombine at a finite rate, and if the nozzle is sufficiently short equilibrium composition will not be maintained. This leads to a reduction of temperature, and hence heat transfer rate, as the chemical energy which would be released on recombination is stored. This effect increases with stagnation enthalpy, and can be shown to be significant at the conditions relevant to this study, Ref. 6.

As the result of expansion from the trailing edge of the injector and from the start of the divergent section further departures from equilibrium will occur, and further lowering of the heating rates might be expected. Further downstream the condition is nearer to equilibrium and therefore the measured and predicted values approach each other. This effect has been observed before in the same facility, Ref 6, and is more significant at higher stagnation enthalpies.

Another possible cause of the lower than expected heating rates in the diverging duct might be in the interaction of the corner expansion with the boundary layer on the side walls. The effect of the expansion in the low mach

number boundary layer would be to create a cross flow along the wall, which might spill coded boundary layer gases on to the thrust surface and reduce the heat transfer rate.

SECTION E

FILM COOLING STUDIES

An initial series of experiments was reported in Ref 1 to investigate the use of wall injected hydrogen as a combustion chamber coolant. The study demonstrated the effectiveness of the fuel layer in shielding the model walls from the heat of the flow. New results are presented in this report to give a more comprehensive set of data for the testing of theoretical models.

Results are given for the following three conditions:

(1) Injection of hydrogen into a nitrogen test gas,

(2) Injection of hydrogen into an air test gas,

(3) Injection of nitrogen into an air test gas.

All experiments used a constant area duct with the hydrogen or nitrogen being injected from behind a 5 mm step. Different equivalence ratios were obtained by varying the reservoir pressure of hydrogen and using different injectors.

1. Hydrogen injected into a nitrogen test gas.

Those experiments were done to model the cooling effect of injecting hydrogen into a test gas in which combustion does not occur. Nitrogen was chosen as the test gas as its molecular weight is close to that of air. Partial mixing of the two gases occurs and heating of the wall results from heat being transported from the test gas by the mixing process in addition to thermal diffusion through the mixed and unmixed layers of hydrogen. Axial convection also transports heat downstream.

In this section, due to the analogy which is drawn between nitrogen and air, the term "equivalence ratio" is used as an alternative measure of the mass flow rate of hydrogen. The injection of hydrogen at an equivalence ratio of one is to be interpreted as injecting hydrogen with the mass flow rate which is required for a stoichiometric mixture with air.

The heat transfer results for the test gas at enthalpies of 4.2 MJ/kg and 8.7 MJ/kg are given in Figures 35, 36 and 37. It is seen that for a given injector the increase in equivalence ratio produces an increased cooling effect. This results because the increase in mass flow rate (equivalence ratio) increases both the thickness of the hydrogen layer and the velocity of the hydrogen in this layer. Thus heat takes longer to diffuse through the thicker hydrogen layer and in addition is convected more rapidly downstream. These effects reinforce each other so that the heat reaches the wall further downstream.

When the fuel is not injected and the stagnation enthalpy was 8.7 MJ/kg the heat transfer rate at the downstream end of the duct was approximately 80 W/cm. It is also seen from Figure 36 that far downstream the heat transfer rate when fuel is injected approaches the fuel off heat levels.

In Figure 38 the heat transfer rates are displayed for the injection of hydrogen from a 0.3 mm and 0.9 mm nozzle at equivalence ratios of 1.39 and 1.13 respectively. It was seen from Figures 35, 36 and 37 that the heat transfer rate is dependent on equivalence ratio. However, from Figure 38 it can be seen that the Mach number is also affecting the heat transfer rate as the same value of $\dot{m}_o y_o$ for different injectors is equivalent to a different mach number.

A simple model for the heating of the thrust surface is to assume that a portion of the hydrogen is trapped in a layer of constant thickness along this surface; see Figure 40. If it is assumed that heat diffuses across this boundary layer and is converted downstream and if gas dynamic effects are ignored so that the heat equation

$$k \frac{\partial^2 T}{\partial y^2} - \rho C_o u_o \left[\frac{y}{y_o} \right]^{\lambda} \frac{\partial T}{\partial x} = 0 \tag{1}$$

can be used, then using Laplace transforms it can be shown that the flux of heat into the thrust surface is

$$\dot{q} = \dot{q}_o - \left[\dot{q}_o + \frac{\Delta T}{y_o} k\alpha^{\frac{-1}{\lambda+1}} \right] \frac{\alpha^{\alpha-\nu}}{\Gamma(\nu)} \sum_{n=1}^{\infty} \frac{Z_n^{\nu-2}}{J_\nu(Z_n)} \exp\left[- \frac{Z_n^2}{4\nu^2} \frac{x}{L} \right] \tag{2}$$

where the length is scaled with respect to

$$L = \frac{C_p}{k} \alpha^{\frac{\lambda+2}{\lambda+1}} \dot{m}_o y_o ; \quad \dot{m}_o = \rho_o u_o y_o \tag{3}$$

The velocity profile of the boundary layer is given by $\rho u = \rho_o u_o \left[\frac{y}{y_o} \right]^{\lambda}$ where y_o is the thickness of the injected layer when expanded to the local free stream pressure. It is assumed that the fuel expands isentropically from its reservoir pressure to the intake pressure with a mass flow rate which is determined experimentally as a function of reservoir pressure for each nozzle. The quantity ΔT is the difference between room temperature and the temperature of the isentropically expanded fuel. This term is present because of the boundary condition at $x = o$. This boundary condition is inconsistent with the velocity profile (except if $\lambda = 2$) and only serves to approximate the boundary condition so that an analytical solution can be obtained.

Equation 1 assumes that transverse heat transfer is solely by means of thermal conduction. It is in fact augmented by turbulent transport and by the diffusion of species which may or may not be reacting. However, if it is assumed that an equation of the form of equation 1 may still be used, but with a revised value of conductivity to account for the extra heat transfer mechanisms, then a solution of the form of equation 2 will still apply. In Ref 7 the value of the effective conductivity was adjusted and good agreement was obtained with the experimental results. However a value of the order ten times that of the standard thermal conductivity was needed. As we have at present no independent scientific method for predicting the rate of heat transfer across the mixing layer, the analysis will be used in this report only to provide quantitative comparisons between different conditions.

There are two distinct variables $\dot{m}_o y_o$ and $\frac{\Delta T}{y_o}$, which can be varied using different reservoir pressures and nozzles. In Figures 41 and 42 $\dot{m}_o y_o$ and $\frac{\Delta T}{y_o}$ are respectively drawn a functions of $\dot{m}_o$ for the three injectors used and for a test gas at enthalpies of 4.2 MJ/kg and 8.7 MJ/kg. From Figure 42 it is seen that for a given injector $\frac{\Delta T}{y_o}$ is effectively constant for sufficiently large values of $\dot{m}_o$. Hence as an increase in $\dot{m}_o$ for a given injector increases $\dot{m}_o y_o$ (Figure 41) then from equation 2 an increase in $\dot{m}_o$ results in increased cooling the length scale is approximately a linear function of the mass flow (i.e. the thickness of the layer is approximately constant).

In Figure 38 the heat transfer rates are given for values of $\dot{m}_o y_o$ of 4.28×10^{-4} kg/sec (ϕ = 1.39) through at 0.3mm throat and 4.75×10^{-4} kg/sec ($\phi = 8 \times 1.13$) through a 0.9 mm throat. It is seen that the heating rates are similar. An explanation for this can be derived from equation (2). The value

of $\dot{q}_o$ is assumed to be the fuel off heat flux to the wall, which for a test gas of enthalpy of 8.7 Mj/kg is approximately 80 W/c_m^2. The value of the conductivity constant k for hydrogen at 300 K and 1 atm is 0.18 W/mK, but due to the turbulent transport and the variations of k with temperature, a precise value of k is unknown. However, even if k were to increase by a factor of five and α was not too small it is seen from Figure 42 that would still only be a second order correction to $\dot{q}_o$. Thus if two injectors of different throat size were to inject hydrogen so that $\dot{m}_o y_o$ is the same for both then the heat flux into the wall should be similar.

A result contrary to Figure 38 is given in Figure 39 which displays the heat transfer rates for injection through the 0.9 mm and 1.6 mm throat with values of $\dot{m}_o y_o$ of 1.3 x 10^{-3} kg/sec (ϕ = 1.93), and 2.5 10^{-3} kg/sec (ϕ = 2.49) respectively. The enthalpy of the test gas was 4.2 MJ/kg. Therefore under the above assumptions the heat transfer rates should not be the same. The assumption that $\frac{\Delta T}{y_o} K \alpha^{\frac{-1}{\lambda+1}}$ is of second order to $\dot{q}_o$ will be less accurate for the lower enthalpy test gas. Furthermore if $\dot{m}$, or equivalence ratio, is the same for the two injectors then it is seen from Figure 42 that by using larger throat the value of $\frac{\Delta T}{y_o}$ decreases and thus by equation 2 the heat transfer rate is increased. Hence if this effect were no longer second order, then for the above mass fluxes the cooling effect created by the larger value of $\dot{m}_o y_o$ using the 1.6 mm throat may be offset by the heating effect created by using the larger throat.

2. Hydrogen injected into an air test gas.

In Figures 43a, 43b, 44a and 44b the pressure and heat transfer rates recorded for the injection of hydrogen into an air test gas are compared with injection into a nitrogen test gas. Both gases had an enthalpy of 8.7 MJ/kg. The hydrogen was injected through the 0.3 mm and 0.9 mm throat at equivalence ratios of 1.34 and 2.7 respectively. It was reported in Ref 1.that burning started at an equivalence ratio of 1.3. At lower equivalence ratios it is believed that the close proximity of the wall quenches the burning. This is confirmed in Figure 43a where it is seen that only a slight increase in pressure is observed for an equivalence ratio of 1.35. Furthermore this pressure rise is significant only towards the end of the duct. Additional confirmation is obtained from the heat transfer results in Figure 43b where it is seen that the heat transfer rate from the nitrogen test gas is the same as from the air.

From Figure 44a it is seen that pressure rises occur everywhere downstream of the injector when hydrogen is injected at an equivalence ratio of 2.6. Thus some of the fuel has been burnt. It is seen in Figure 44b that in the downstream position of the duct the heat transfer rate for an air test gas appears to be higher than a nitrogen test gas, which is assumed to be the result of burning. It is observed that a significant pressure rise does not occur until halfway down the duct, and yet the heat transfer rate increases only in the last quarter of the duct. This delay in the heating rate also supports the theory that burning will not occur at the wall, for if it did there would be no delay time. The delay time is caused by the convection process transporting heat downstream while it diffuses across the unburnt layer of hydrogen.

3. Nitrogen injected into an air test gas.

The heat transfer rates when nitrogen is injected into an air test gas at 8.7 MJ/kg and when hydrogen is injected into a nitrogen test gas at the same enthalpy are given in Figure 45. These measurements have been taken to gauge the cooling effect that the injection of oxygen would have. Oxygen was not injected as the injection valve uses an oil lubricant which would burn on contact with the oxygen. The conductivity constants of nitrogen and oxygen at 1 atm and $300^{o}K$ are 0.0260 W/mK and .0262 W/mK and the specific heats are 2080 J/kgK and 1820 J/kgK respectively. Hence little difference is expected between the two gases. The conductivity constant and specific heat for hydrogen are .181 W/mK and 14460 J/kgK respectively, so that the value of k/cp for both nitrogen and hydrogen is 1.25×10^{-5} kg/sec m. The values of $\dot{m}_o y_o$ for the nitrogen and hydrogen injection are 2.8×10^{-3} kg/sec and 3.2×10^{-3} kg/sec, so that if $\frac{\Delta T}{y_o} \; K \; \alpha^{\frac{-1}{\lambda+1}}$ is of second order to $\dot{q}$ then the heat transfer rates would be expected to coincide. From Figure 45 it is seen that heating first occurs at the same distance downstream of the injector, however towards the end of the duct the hydrogen injection would appear to give a greater cooling rate than the nitrogen injection. This is not understood.

Conclusions.

At the higher enthalpies an increase in $\dot{m}_o y_o$ gives greater insulation to the thrust surface. At lower enthalpies effects which are second order at the higher enthalpies are now equally as important. The simple model proposed for the heating of the thrust surface is qualitatively useful. However, due to the lack of an accurate value of the effective diffusivity constant it is limited in its ability to predict quantitative results.

SECTION F

2 STAGE DIVERGENCE.

Previous experiments with wall injection showed low values of thrust and specific impulse. This was attributed to two effects,Ref 1. Firstly, combustion was prevented from spreading to the wall by cooling effects. This leads to a loss of performance which is equivalent to hydrogen representing an equivalence ratio of ~ 1.5 being wasted.

This is a feature of the cold walls in the shock tunnel tests which would not be expected to apply in a flight situation. Several means are under investigation at the moment to make the shock tunnel tests more representative of real conditions, but they do not apply to the present report. They include preheated fuel, heated walls and a geometrical configuration using a central injector configured to look like a wall injector in so far as the expansion is concerned. The latter proposal simulates wall injection, but with no heat transfer or shear of the fuel jet on the centreline upstream of the thrust surface. This configuration is shown in Fig 46.

Secondly, as the combustion layer is attached to the wall the zone over which it generates thrust by the expansion and jet interaction mechanism, Ref 9, is limited. A means of improving this is to allow extra length in the combustion chamber before expanding the flow. This was done in previous experiments, Ref 1 Fig 17, and a limited increase in thrust was confirmed. A weight penalty would be associated with the longer combustion chamber, and it is advantageous to start expanding the flow as soon as possible after injection.

However, expansion of the jet before complete combustion is achieved can have a quenching effect on the flame, and it also slows down the spread of the jet across duct. The optimum configuration of combustion chamber and expansion nozzle is likely to be a compromise between these two effects.

It was noted in previous experiments that the thrust produced by wall injection was not very sensitive to the combustion chamber divergence angle when the expansion / jet interaction is absent. It was therefore decided to construct a combustion chamber with a 2 stage divergence. This is shown schematically in Fig 47.

The first stage includes a thrust surface inclined at 4 degrees to the intake flow. This geometry was shown in Ref 1 Fig 15 to produce significant thrust due solely to compressions from the burning fuel jet. Because only a small pressure drop is associated with a 4 degree expansion , it was hoped that the jet would continue to mix and react and spread across the duct in the first thrust producing stage. When subsequently expanded by the second stage the thickness of the jet should be such that substantial thrust could be produced by the expansion interaction method.

The advantage over a single expansion of 15 degrees is twofold.

Firstly , if the full 15 degrees expansion is introduced too early, no further combustion will take place. By limiting the initial expansion to 4 degrees, thrust may be developed in a region that is still supporting combustion.

Secondly, the final expansion takes place at a point where the jet has had time to spread away from the wall. Combustion creates a region of reduced Mach number attached to the wall, and after the passage of the corner expansion this region will be at a higher static pressure than the free stream flow. This high pressure region is subsequently

eliminated by a system of expansions and compressions, but it creates a region of increased wall static pressure downstream of the corner which produces a thrust increment. It can be seen from Fig 48 that the zone of increased wall static pressure will grow as the jet continues to spread away from the wall. It is this principle that give extended combustion chambers potential for increased thrust from the interaction mechanism.

Short combustion chamber.4/15 degrees divergence.

The initial series of tests was done with the model configured as shown in Fig 47 with a 25 mm length of constant area duct after injection before the start of the 4 degree diverging section.

In Fig 49 the results of the dual stage divergence are compared to previous data for a single thrust surface with 15 degrees divergence. It is seen that at an enthalpy of 8.7 Mj/kg no improvement in performance was produced.

In Fig 50 the pressure against distance profiles are shown. It is seen that despite significant heat release in the 4 degree section, as shown by the pressure rise above fuel off levels, very little net thrust is developed on the downstream thrust surface. This compares unfavorably Fig 17 Ref 1, where an extended combustion chamber followed by a single 15 degree expansion gave a large pressure rise through the expansion interaction mechanism.

At an enthalpy of 4.2 Mj/kg no improvement in specific impulse was produced, as can be seen from Fig 49 b. However it can be seen from Fig 50 b that the effects of the reduced divergence are just beginning to be felt in the form of combustion induced pressure rises towards the downstream end of the first thrust surface. This would suggest that somewhat more distance for combustion was required before the

start of the 15 degree section. Consequently the two stage thrust surface was then used with an extended combustion chamber, although this does to a certain extent defeat the purpose of the two stage expansion, which is to obtain thrust in all sections where the fuel is burning.

Long combustion chamber, 4/15 degrees divergence.

At an enthalpy of 8.7 Mj/kg no improvement was produced by the extra mixing length, as may be seen by comparing Figs 51a and 49a for specific impulse, and Figs 52a and 50a for P/X dependence.

At 4.2 Mj/kg a noticeable improvement in performance was gained by adding the combustion chamber extension. This is shown both in the increased value of specific impulse , Fig 51b , and also in the development of net thrust on the second thrust surface, Fig 52b.

It would appear that in the higher enthalpy condition ,8.7 Mj/kg , the temperature after the initial expansion of 4 degrees is sufficiently high that combustion is fast , and the heat release is only limited by the quenched zone attached to the wall. The addition of extra combustion chamber length does not change this, and no increase in the difference between fuel on and fuel off was observed between Figs 50a and 52a.

However at the lower enthalpy condition , 4.2 Mj/kg , it is seen in Fig 50b that without the combustion chamber extension significant heat release only occurs towards the end of the 4 degree section , and not much net thrust is produced on either surface. This is thought to be due to the longer ignition delay at the lower temperature. In this case when a longer combustion chamber was used ignition occurred upstream of the first expansion , and increased thrust was developed on both surfaces, as seen in Fig 52b.

A similar effect has previously been observed with central injection. Ref 9 , where increasing combustion chamber length is only beneficial at the lower enthalpies. and this may also be true for wall injection.

Transverse and parallel injection.

In an attempt to improve the performance of the wall injected scramjet , a modified injector was constructed with transverse holes as well as the parallel injection throat. It was hoped that the transverse momentum of the jets would carry some of the fuel through the boundary layer and away from the quenching effect of the wall, and would also increase the mixing rates.

A schematic of the injector is shown in Fig 53. It consists of a series of holes drilled at 45 degrees to the flow and pointing downstream. The percentage of transversely injected hydrogen was controlled by changing the throat of the parallel injector, and setting the hydrogen reservoir pressure to give the required total equivalence ratio. Transverse hydrogen mass flow rates equal to 27% and 79% of that passing through the parallel injectors were produced for the 0.9 mm and the 0.1 mm throats respectively. No other combinations were used.

Reduction of the size of the quenched zone would be evident in the form of increased values of specific impulse. and also combustion would be possible at lower values of equivalence ratio. Combustion in a scramjet using fuel from a room temperature reservoir requires heating of the fuel to its' ignition temperature by transfer of heat from the free stream.

In the wall injection case this flow of heat is partially offset by the flow of heat to the wall, and is also limited by only having one fuel air interface, as opposed to two for central injectors. In the two dimensional configuration the area for heat transfer from the flow to the jet is equal to the area for transfer from the jet to the wall, and this limits the temperature which may be achieved in the jet. However a circular jet propagating transversely across a duct will have a much larger area exposed to the flow , and may be expected to get hotter.

Transverse injection,long combustion chamber.

Two stage divergence

In Fig 54 the results of transverse injection with an extended combustion chamber are shown. They are reproduced in Fig 55 for the 4.2 and 8.7 Mj/kg conditions to give a direct comparison with the other configurations.

Transverse injection at the 8.7 Mj/kg enthalpy condition again gives no improvement over any of the other results, except at low values of equivalence ratio. Combustion with transverse injection occurred at lower equivalence ratios than was possible with parallel injection alone. This is indicated by the two points on Fig 55a at equivalence ratios of 0.83 and 1.11. This would suggest that above a certain fuel injection pressure the transverse jets are to some extent penetrating the boundary layer, and burning at lower equivalence ratios than is possible for wall injection. However, the heat release from this

combustion is not reducing the size of the quenched zone in the parallel injected component, and so no increase in specific impulse is observed at higher equivalence ratios.

Also shown on Fig 54a is a data point obtained by injecting Helium instead of hydrogen. This was done for selected conditions, together with the injection of hydrogen into nitrogen test gas, to separate the effects of combustion from the physical presence of a jet of foreign gas in the flow. In this case a genuine combustion effect appears to be present as the hydrogen is producing significantly more specific impulse than the helium gas.

At 4.2 Mj/kg combustion at low equivalence ratios is again observed , and there also appears to be significant improvement in performance in the equivalence ratio range of 1 to 2.5 , as may be seen from Fig 55b. Also shown on this figure is are the results of 4.2 Mj/kg tests with a transverse component equal to 79% of the parallel injection, the only condition for which this was done. This shows no improvement over the 27% case. It had been hoped that a larger proportion of transversely injected fuel would lead to more combustion, and higher specific impulse. This effect would seem to indicate that the transverse jets are not penetrating very far into the flow, and are still restricted by wall quenching.

Further evidence of this is given in Fig 57, which compares the wall pressure and temperature profiles for a single 15 degree expansion at an enthalpy of 6.1 Mj/kg for parallel and 27% transverse injection. No difference is apparent between the pressure traces , and only a slight increase in heat transfer with transverse injection was observed. Both tests were taken at an equivalence ratio of about 2, where no thrust increment was observed with transverse injection. A more significant

result would be at equivalence ratios of order one where the transverse injection appears to be effective, but no heat transfer data was taken at those conditions.

It is possible that the transverse jets also require a layer of fuel as a thermal buffer to insulate them from the wall, and if this is not supplied by the parallel jet then more of the transverse component will be quenched. Another factor which may be significant is the effect of the expansion from the trailing edge of the injector. The strength of this expansion is dependent on the amount of fuel injected through the parallel throat. Less fuel from the parallel throat would lead to a stronger expansion and a region of cooler fuel downstream of the injector.

Long combustion chamber 15 degree single expansion.

A final series of experiments with transverse injection were performed with a long combustion chamber and a single 15 degree thrust surface. Transverse injection was a the rate of 27% of the parallel component. The results are presented in Fig 56, together with the corresponding data for the 2 stage expansion with a long combustion chamber.

Except for the 4.2 Mj/kg case , which only just seems to be on the verge of igniting for the single expansion, no difference was observed between the two conditions.

Conclusion.

In conclusion for this section, the 2 stage expansion can lead to more combustion with a short combustion chamber, but this does not lead to the development of more thrust, presumably indicating that the reacting layer has not spread far from the wall. This is shown for a low enthalpy condition in Fig 50b and Fig 49b.

For longer ducts the double expansion is able to produce more thrust at lower enthalpy than a short one , but the improvement over a single expansion with a long duct is marginal. For high enthalpy ,8.7 Mj/kg, no combination of divergence or combustion chamber length was able to produce an improvement with parallel injection.

The wall quenching layer appears to be the predominating effect , and the effectiveness of staged expansions cannot be properly measured or understood until this problem is alleviated. Several possible approaches to this problem are suggested at the beginning of this section.

The use of transverse injection was shown to be partially effective in lowering the minimum equivalence ratio for combustion. At higher equivalence ratios it did not improve specific impulse,except to a slight extent at 4.2 Mj/kg . This was taken to imply that although some of the transversely injected fuel may burn at equivalence ratios where combustion would not otherwise be possible, it did not reduce the amount of parallel injected fuel which was quenched by the wall.

No improvement was produced by injecting a larger proportion of transverse fuel. This suggests that the penetration of the transverse jets into the freestream is limited, and that combustion still relies on an insulating layer of fuel to act as a buffer to the cold walls. Because the combustion is again dominated by wall quenching it is not possible to asses the effectiveness of the transverse jets as a mixing aid. However heat transfer measurements did not show significant change in the heating rates , and it does not appear that it had a strong effect. This would again imply that it is difficult to get a hydrogen jet to penetrate into the freestream.

The use of transverse injection into a long combustion chamber, followed by a two stage expansion, did produce the highest values of specific impulse yet obtained in the shock tube for wall injection. This is shown in Fig 56c where a value of 550 sec was achieved at equivalence ratios of ~ 1.

SECTION G

SHOCK STABILIZED COMBUSTION.

For combustion of fuel in a scramjet three processes are necessary, namely mixing of the fuel and air, heating of the fuel above its ignition temperature and the allowance of sufficient time for reactions to take place. All these processes would normally be expected to occur concurrently. However, the compression process in a scramjet, which consists of an initial compression by an oblique bow shock followed by further compression at the combustion chamber intake, allows for the separation of the first of these processes.

A schematic diagram of a scramjet is shown in Fig 58. The pressures and temperatures after the bow shock will typically not be sufficient to support combustion. If fuel is injected after the bow shock, but before the combustion chamber intake, it will not burn, but as the intake is likely to be very long it may be expected to mix well with the freestream air. It will enter the combustion chamber as a premixed fuel air mixture, and some heating of the fuel will have taken place. Both fuel and air will be heated by the combustion chamber intake shock waves to form a combustible mixture. Combustion will then only depend on the ignition characteristics at the temperature and pressure after the shock. Ignition by means of a shock wave is known as shock stabilised combustion.

The combustion chamber can therefore in theory be made shorter and lighter because the mixing and heating stages are completed at the intake. An additional benefit might occur if the fuel were to be injected from the wall, and could act as a coolant for the underside of the craft. To prevent choking at the intake a sufficiently high

enthalpy and Mach number flow is required. A preliminary series of tests were performed on the T3 shock tunnel to see if this effect could be realised.

Central injection, Mach 5 flow.

The purpose of the experiments was to inject hydrogen into a flow of air at conditions which do not sustain combustion, and then to induce ignition by compression through an oblique shock wave. A schematic diagram of the experimental model is shown in Fig 58.

A mach 5 contoured nozzle was used , with which it has previously been found hydrogen does not burn. A wedge inclined at 5 degrees to the intake flow was used to create the shock wave ,and reflection of the shock from the wall was eliminated by a 5 degree corner starting at the point where the shock meets the wall. Down stream of the expansion fan the flow was contained in a constant area duct formed between the wedge and the sidewall. Equivalence ratios were high.of order 5.

In Fig 59 the results for a range of enthalpies are shown. At the higher enthalpies, Fig 59a + 59b, ignition is almost immediate after shock reflection, as may be seen by comparison of the fuel on and off pressure profiles. Before the reflection of the shock from the wall no pressure increase from combustion was observed.

As the enthalpy is reduced ignition occurs with a significant delay after shock reflection, as may be seen in Fig 59c for an enthalpy of 3.43 Mj/kg.

As the enthalpy is reduced further this delay increases, as may be seen in Figs 59d and 59e for enthalpies of 2.65 and 2.3 Mj/kg. At these last two conditions combustion was unsteady, as determined by the normalised plots of static pressure/stagnation pressure against

time. The unsteadvness was in the form of a pressure pulse starting down stream and propagating up the duct. These two results should therefore be treated with caution. but thev do serve to illustrate the effects of enthalpy on ignition delay times.

As the enthalpv was further reduced to 1.9 Mj/kg no combustion was observed at all, Fig 59f. As this was just a preliminarv look at the shock stabilised combustion effect, fuel off traces were not taken for all enthalpies. As the form of these does not change much with enthalpv, fuel off traces from different enthalpies were used where necessary for qualitative comparisons.

The passage of a shock wave through premixed fuel was found therefore to be very effective in heating the gas and inducing ignition. Large pressure rises were recorded in a flow that would not normallv support combustion. An unsteadv combustion effect was observed at the lower enthalpies which could be the onset of thermal choking.

Wall injection, Mach 5 flow.

The shock induced combustion concept was also tried with wall injection. There were two reasons for this. Firstly, if this technique is to be used on a flight vehicle, the fuel will probably be injected from the wall in order to provide boundary layer cooling.

Secondly, previous experiments with wall injection in the combustion chamber have all been affected by a cold layer of quenched fuel near the wall. It was hoped that by reflecting a shock off the model walls this quenched layer might be reduced in size and effect.

The experiments at Mach 5 were performed for the first reason.

The configuration of the model was similar to that used with central injection, but a shock turning angle of 10 degrees was used. Because the shock was reflecting off a thick low Mach number layer of fuel, disturbances were apparent upstream of the shock. The model configuration for wall injection with shock stabilisation is shown in Fig 60.

Combustion was not possible at this Mach number for wall injection without shock compression. The tests were performed at an enthalpy of 8.7 Mj/kg, and with equivalence ratios from 0 to 5.7. The results are presented in Fig 61, and it is seen that it did not burn. The pressure rises upstream of the shock apparent in Fig 61 are attributed to a shock wave interaction process rather than to combustion. This is confirmed in Fig 62 where the results of helium and hydrogen injection are compared at an equivalence ratio of 5.7 for the hydrogen case, with the helium being injected at the same pressure.

The shock ignition process was therefore found to fail for wall injection at a condition where it had been most effective for central injection, despite being compressed by means of a stronger shock. This

is provisionally being attributed to the quenching effects of the walls. This does not preclude the use of shock stabilised combustion with wall injection on a flight vehicle with hot walls.

Wall injection, Mach 3.5.

At this Mach number the purpose of the experiments was to try to reduce the extent of the wall quenching zone. Before the arrival of the shock combustion would already be established in a limited zone between the free stream and the cooled layer in the immediate vicinity of the wall. However it is thought that mixing of oxidant penetrates beyond the reacting layer and into the quenched zone. Therefore if the temperature of this mixed but unburned region could be raised, more combustion and heat release might be produced. The quickest and most uniform way to heat this region is by the passage of a shock wave, and this is why shock assisted combustion was tried.

Because this is a condition where combustion is already possible, the effectiveness of the technique would be shown by a reduction in the minimum equivalence ratio at which any burning takes place. It should also result in higher pressure levels in the equivalence ratio range 1 to 2.5 which is the only region where heat release was found to increase with equivalence ratio for wall injection.

In Fig 63 the pressure profiles are shown for an enthalpy of 8.7 Mj/kg at an equivalence ratio of 0.91. This is a condition which does not burn with a constant area duct because the equivalence ratio is too high. It still does not burn with the shock heating, showing that there is not significant reduction in the size of the quenching zone at this condition.

At enthalpies of 6.1 and Mj/kg more comprehensive data was obtained. These results are displayed in Fig 64 and Fig 65. Again it is seen that down stream of the shock, in the constant area duct section. there is no improvement in performance over the results quoted in Ref 1. This applies both to the pressure rises and the minimum equivalence ratio at which it will burn.

A possible explanation for the different results the shock wave has on central and wall injection mav lie in the effects the physical size reduction of the compression has on the heat transfer rates in the two configurations.

In the central jet heat is flowing into the mixing layer from both sides, and after the passage of the shock wave the driving temperature difference is increased, and the distance the heat has to be transferred over is reduced. There is therefore a significant increase in the rate of heat transfer to the mixing layer which, when coupled with the corresponding pressure increase, initiates combustion.

For wall injection the temperature of the jet is determined by a balance of the heat flow from the freestream to the mixing laver .and from the mixing layer to the wall. This was mentioned in Section F when discussing the effect of transverse injection.
Whilst the passage of the shock wave will increase the flow of heat from the freestream, it will also for the same reasons increase the heat transfer from the jet to the wall. The temperature rise in a wall injected jet will therefore be smaller than that produced in a central jet. From the experimental results it would appear then that the net result of the compression is that the temperature is not much

increased in those regions where the fuel and air have mixed to combustible proportions, but are prevented from burning by the cooling effects of the wall.

TABLE OF TEST CONDITIONS

H MJ/kg	M	T K	P kPa
8.70	3.50	2500	160
8.70	4.50	1740	32
8.70	5	1500	20
6.10	3.50	1700	160
6.10	4.50	1200	32
6.10	5	1000	20
4.20	3.50	1100	160
4.20	4.50	750	32
4.20	5	650	20
3.43	4.50	625	30
3.43	5	540	20
2.73	3.30	970	10
2.65	3.50	700	120
2.65	4.50	480	30
2.65	5	410	20
1.94	3.30	705	15
1.90	4.50	400	30
1.90	5	350	20
1.19	3.40	445	24
1.07	3.40	415	24
1.03	3.40	400	24

REFERENCES.

1. R.G.Morgan, A.Paull, N.A.Morris, R.J.Stalker.
"Scramjet sidewall burning - preliminary shock tunnel results."
University of Queensland,
Department of Mechanical Engineering Research Report No: 12/85.

2. M.P.Netterfield, R.J.Stalker, R.G.Morgan.
"The reflection of an expansion fan from a Mach mumber gradient in a scramjet exhaust."
University of Queensland,
Department of Mechanical Engineering Research Report No: 7/84.

3. W.D.Hayes, R.F.Probstein.
"Hypersonic flow theory."
Academic Press, New York and London. 1959.

4. J.L.Stollery, G.T.Coleman.
"A correlation between pressure and heat transfer distributions at supersonic and hypersonic speeds."
Aeronautical Quarterly, Vol. 26, pp 304-315, 1975.

5. J.A.Lordi, R.E.Mates, J.R.Moselle.
NASA rep. NASA CR-472. 1966.

6. R.A.East, R.J.Stalker, J.P.Baird.
"Laminar flet plate heat transfer measurements from a dissociated high enthalpy hypersonic air flow".
Department of Aeronautics and Astronautics,

Southampton Report No. 338. 1977.

7. A.Paull,N.A.Morris,R.G.Morgan,R.J.Stalker.
"High reynolds number heat transfer to the cold walls of a model scramjet".
To be presented to the 9th Australasian Fluid Mechanics Conference, Auckland, November 1986.

8. J.S.Evans, C.J.Schexnayder Jr., H.L.Beach Jr.,
"Application of a two - dimensional parabolic computer program to prediction of turbulent reacting flows."
NASA Tech. Paper 1169, March 1978.

9. R.J.Stalker,R.G.Morgan.
"Supersonic Combustion with a Short Thrust Nozzle".
Journal of Combustion and Flame,Vol. 57, No. 1,
July 1984, pp 55-70.

10. Allen G. McLain and C. S. R. Rao
"A Hybrid computer Program for Rapidly Solving Flowing or Static Chemical Kinetic Problems Involving Many Chemical Species."
NASA Technical Memorandum X-3403, July 1976.

11. Casimir J. Jachimowski and Allen G. McLain
"A Chemical Kinetic Mechanism for the Ignition of Silane/Hydrogen Mixtures"
NASA Technical Paper 2129, February 1983.

ACKNOWLEDGMENTS.

This work was performed under a grant from the NASA Langley Research Center, Hypersonics Propulsion Branch.

The experimental work was performed in the shock tunnel of the Physics department of the Australian National University, and the assistance of many members of the staff for all the back up support required for the operation of a major test facility is greatly appreciated.

APPENDIX

Additional work has been carried out on the simulation of the combustion of silane/hydrogen mixtures in a constant area duct. Using a one dimensional chemical kinetics program (Ref. 10) and the reaction scheme postulated by Jachimowski (Ref 11.), results have been compiled for four intake temperatures at an intake pressure of 20kPa and a mach number of five. A 20% silane in hydrogen fuel was considered for these examples. Of particular interest is the effect of freestream oxygen radical concentration on the combustion process. Comparisons are made with experiments involving central injection into a constant area duct.

Because the program is one dimensional and applies to premixed gases only, its use is restricted to the examination of the effect of chemical kinetics on ignition delay times rather than details of pressure profiles when comparing with experimental results.

Figure 67a shows that at 1500K or a freestream enthalpy of 8.7 MJ/kg, increasing the radical oxygen has little or no effect on the ignition delay time. Results from this simulation compare favourably with the experimental results for a 20% mixture as shown in figure 11, given that injection takes place at X=88.5mm. (ALPHA is the percentage mass of freestream oxygen that has dissociated). It is suggested therefore that at this high enthalpy, the high dissociation expected in a shock tunnel (ALPHA=10%) has no noticeable effect on the ignition delay.

At 1000K or a freestream enthalpy of 6.1 MJ/kg, the shock tunnel produces flows with an ALPHA of around 1.5%. According to the simulation (figure 67b), this would bring the rapid pressure rise to around 20 cm closer to the point of injection than when compared to a flow with no oxygen dissociation. Figure 12 shows a high pressure is measured closer to the point of injection than the 20 cm predicted for a zero dissociation flow which suggests that free radical oxygen does in fact aid combustion in this case.

Figure 67c shows that at 650K (4.2MJ/kg), only small amounts of free radical oxygen have a very significant effect on the ignition delay time predicted by the simulation. At this enthalpy, non-equilibrium calculations have shown that an ALPHA of 0.18% is expected in the shock tunnel. It can be seen by comparing the results for a 20% silane mixture shown in figure 13 with simulation for ALPHA=0.2% in figure 67c, that ignition delay times are around the same.

At a lower temperature of 540K, ignition delay times are dramatically increased for the lower radical concentrations, as predicted by the computer simulation (figure 67d). However, figure 14 shows that in experiments with an ALPHA of 0.13%, the 20% silane mixture ignites at about 1.5 cm from the point of injection. This compares with about 65 cm for premixed gases as predicted by the 1-D program. Similarly, at the lower temperature of 410K (figure 15), it is seen that ignition takes place at about 1.5 cm from the injection point, yet the oxygen dissociation is calculated to be only 0.06%.

Experiments suggest therefore that if the reaction scheme is valid, then freestream radical production at high enthalpies (1500K freestream temperature) has no appreciable effects on the ignition of 20% silane/hydrogen mixtures.

At the intermediate freestream temperature of 650K, oxygen radical concentrations play an important part in the combustion process of silane/hydrogen mixtures therefore shock tunnel simulations may not be representative of real flight conditions.

At the lower temperatures of 540K and 410K, experiments showed short ignition delay times despite the very low free radical oxygen concentrations produced by the shock tunnel. This suggests that combustion is occurring because of other effects. These may be the high temperature produced by the boundary layer on the injection strut and/or production of free radical oxygen in this boundary layer. If this is the major ignition mechanism, then freestream radical oxygen produced by shock tunnel flows will not have a significant effect on the combustion process. Rather, ignition will be determined by the presence of a central injection strut in hypersonic flows.

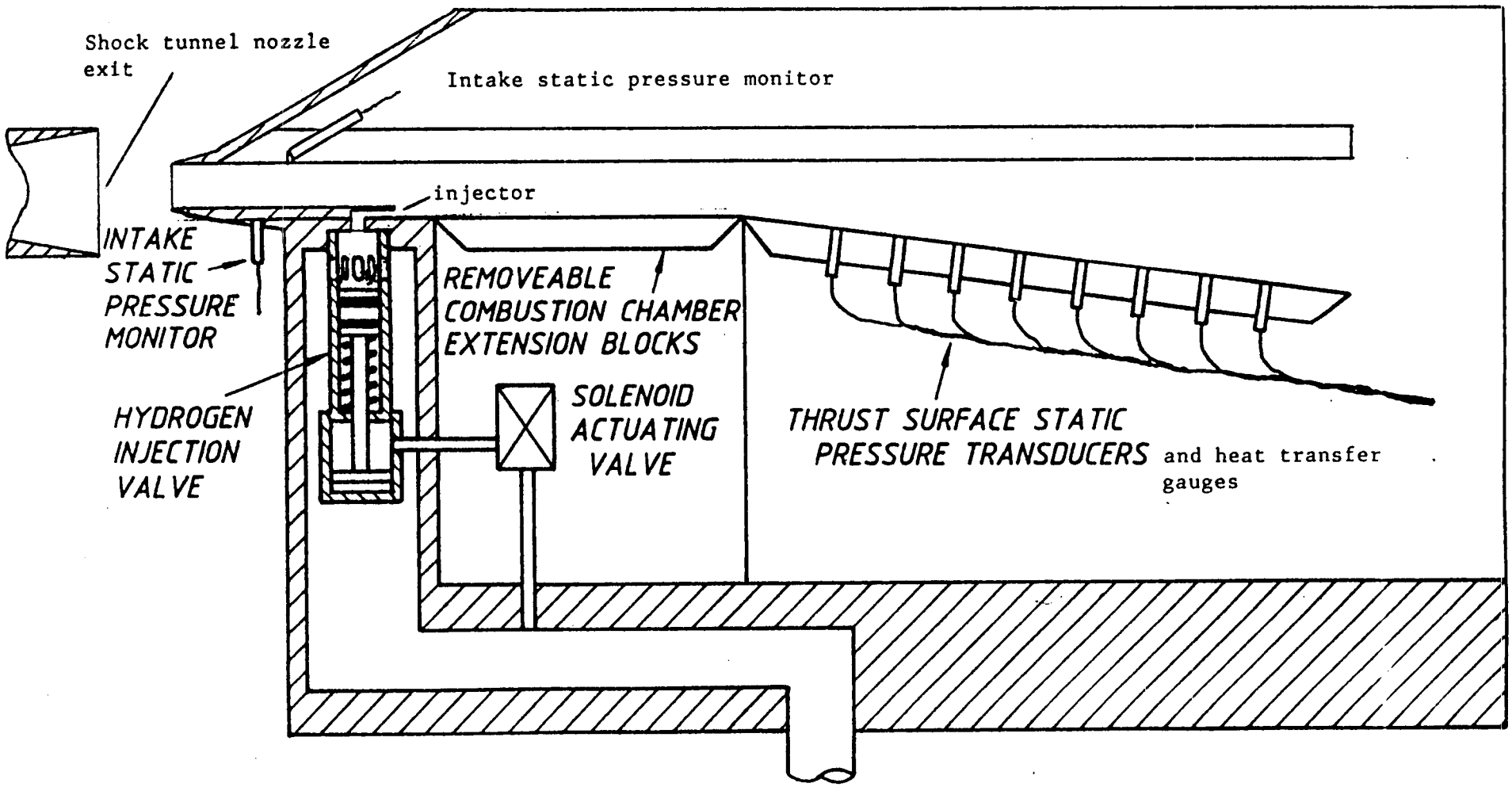

Fig 1. Schematic Diagram of Experimental Apparatus

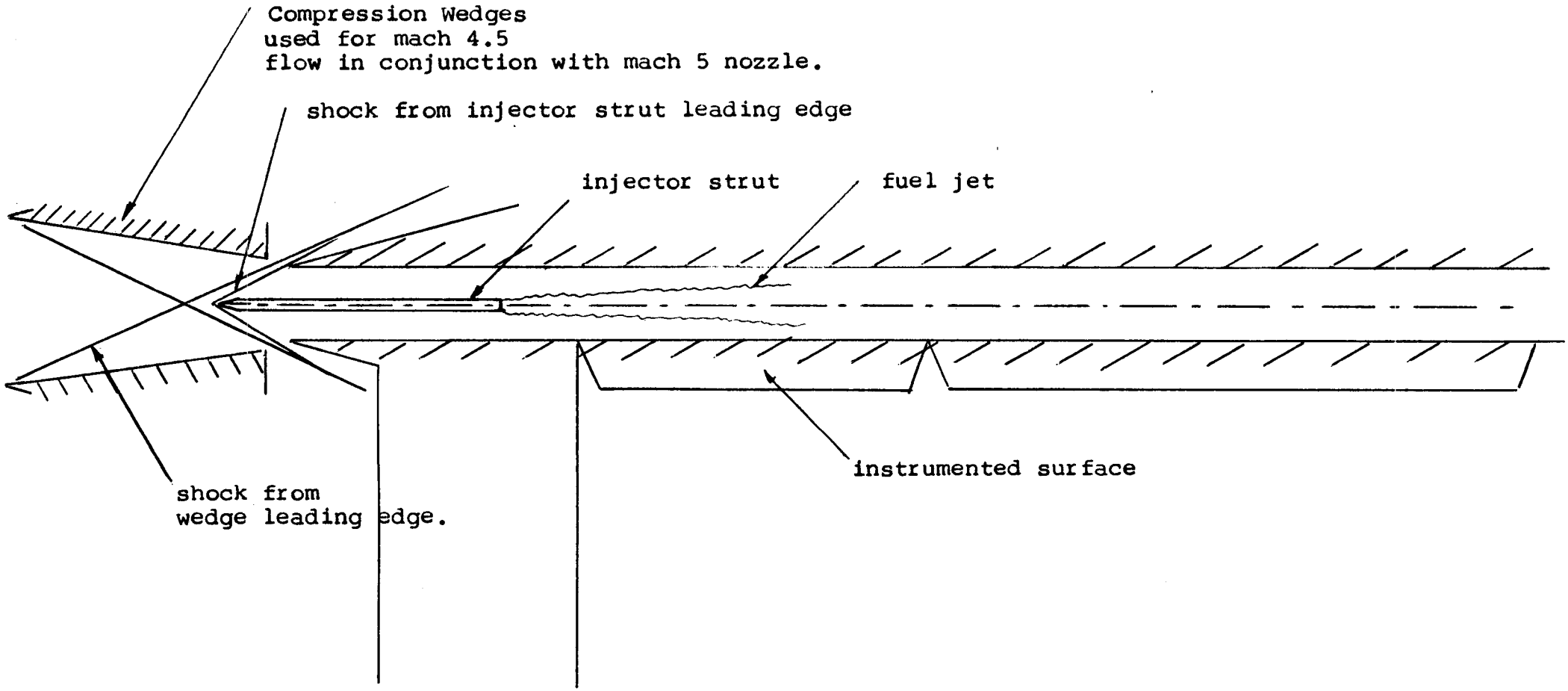

Figure 2: Constant Area Duct with central injector
and mach 4.5 intake configuration

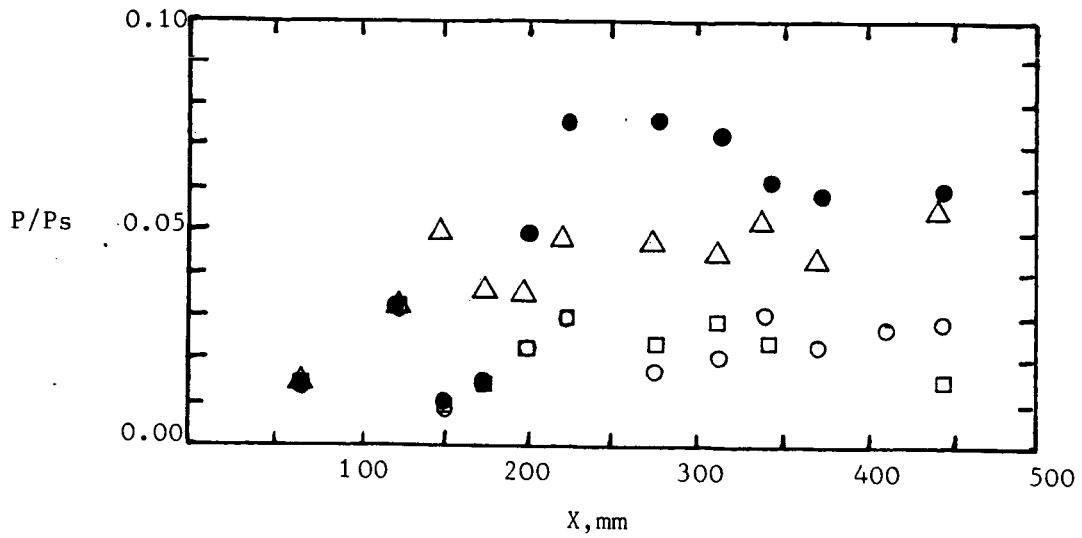

□fuel off, T= 400K

○20% SiH_4/H_2 injection, T_I = 400K

●20% SiH_4/H_2 injection, T_I = 415K

△ 20% SiH_4/H_2 injection, T_I = 445K

Fig. 3. Ignition limit of 20% SiH_4/H_2 mixtures at mach 3.4, $\phi \sim 0.3$, P_I = 24kPa

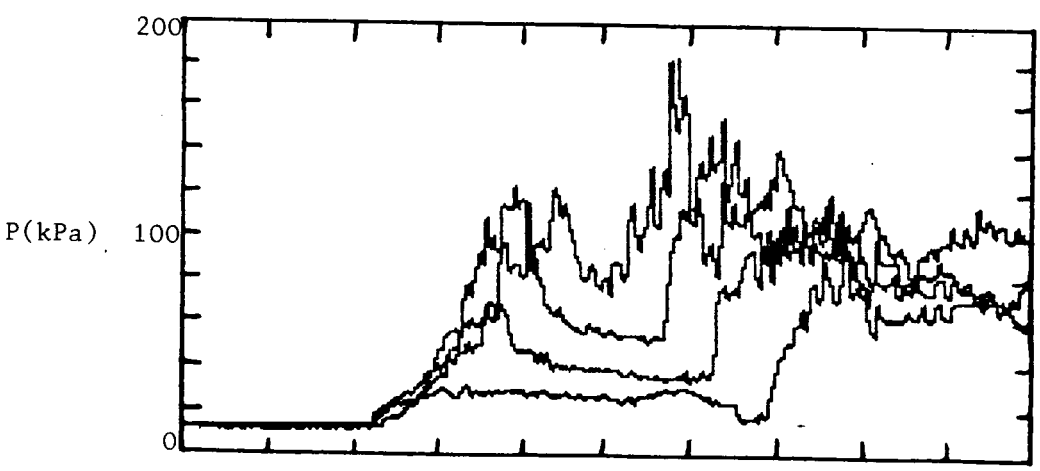

Time, 307μs per division

Station	X,mm
(3)	130.5
(4)	155.5
(5)	180.0
(6)	205.5

Fig. 4. Illustration of thermal choking at low Temperatures, 20% SiH_4/H_2, T_I = 415K, P_I = 24kPa, $\phi \sim 0.3$.

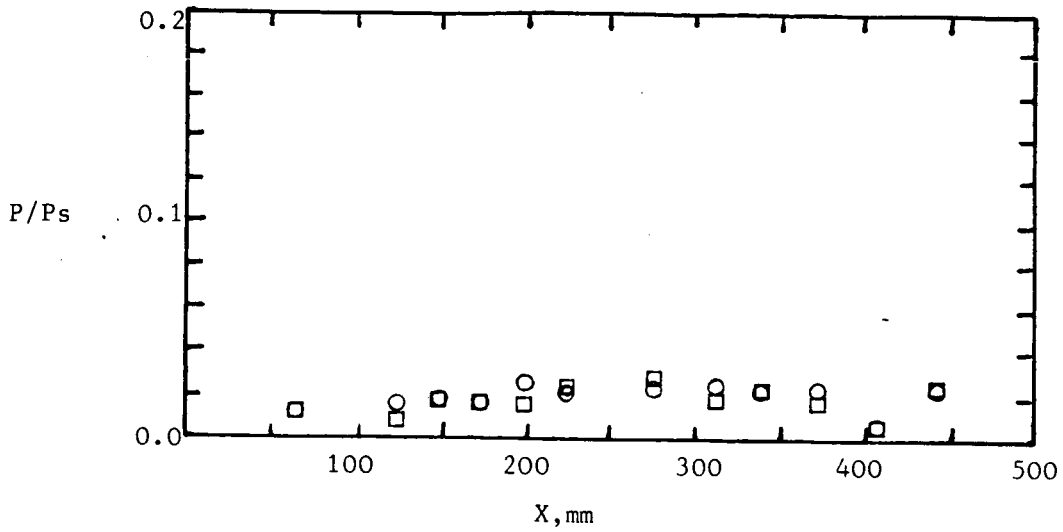

□ Fuel off, T_I = 705K

○ 20% SiH_4/H_2 injection, T_I = 705K

Fig. 5. Ignition limit of 20% SiH_4/H_2 mixture at mach 3.3, P_I = 15kPa, Φ = 0.78

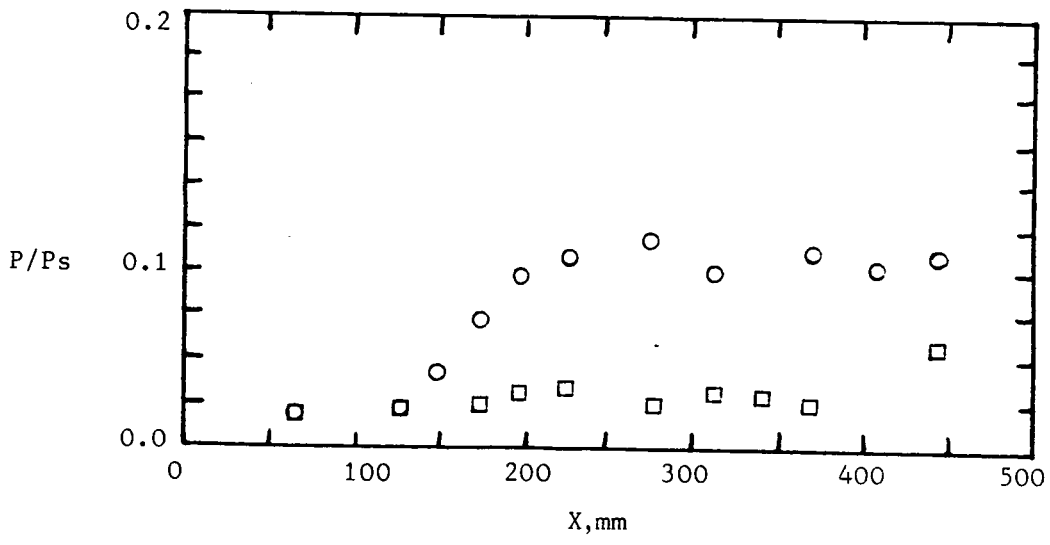

□ Fuel off, T_I = 970K

○ 20% SiH_4/H_2 injection, T_I = 970K

Fig. 6. Combustion of 20% SiH_4/H_2 mixture at mach 3.3, P_I = 10kPa, Φ = 1.58

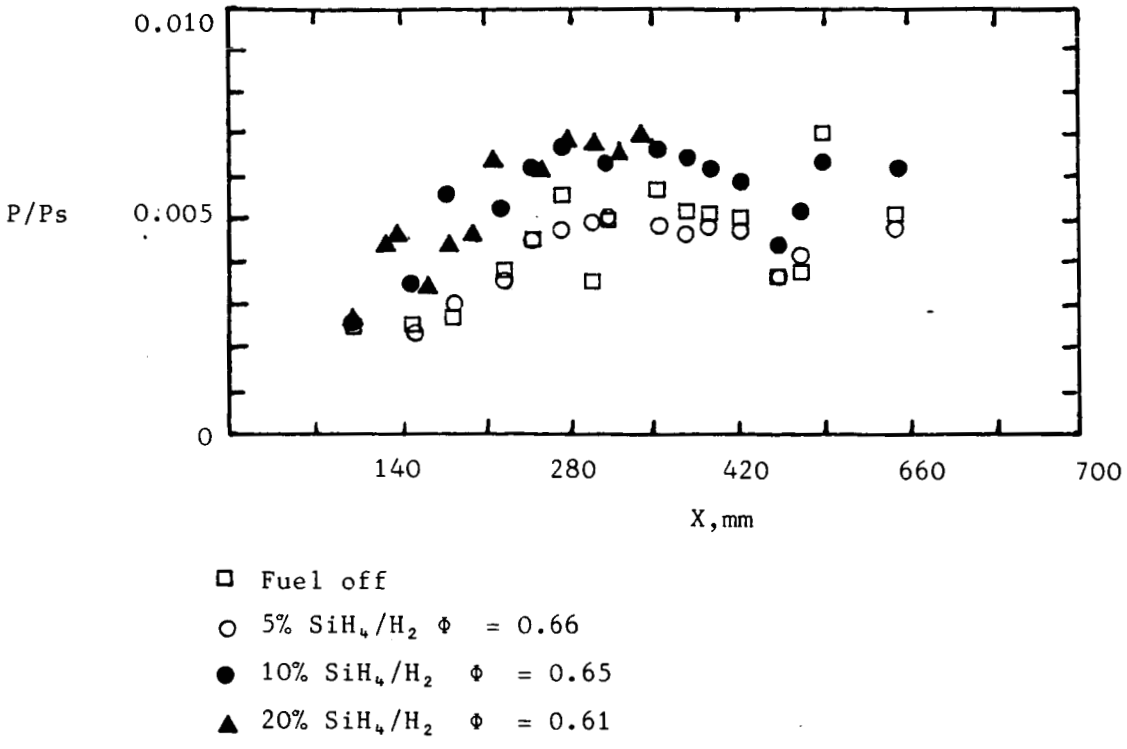

Fig. 7. Effect of concentration of silane on Combustion at mach 4.5, H_s = 3.43MJ/kg, P_I = 30kPa, T_I = 6.25K

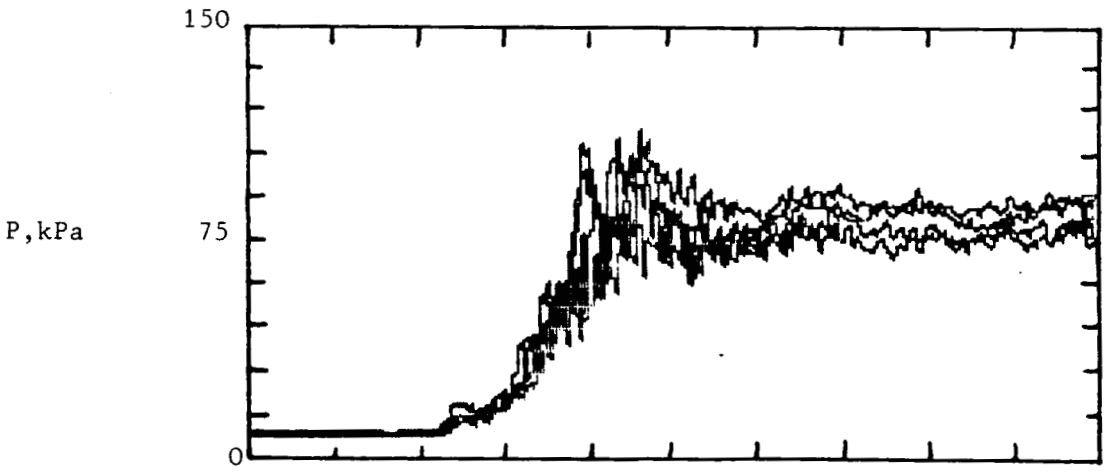

Station	X,mm
3	190.5
4	233.5
5	258.0
6	284.0

Fig. 8. Constant pressure burning of a 10% Silane Hydrogen mixture at mach 4.5, H_s = 2.65MJ/kg, P_I = 30kPa, T_I = 480K

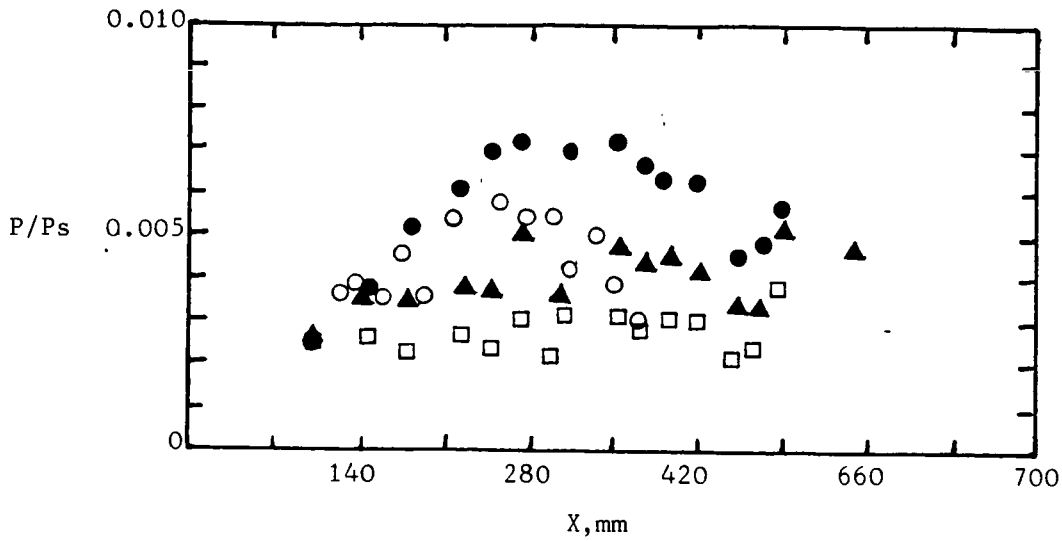

□ Fuel off

○ 5% SiH_4/H_2 injection, Φ = 0.57

● 10% SiH_4/H_2 injection, Φ = 0.65

▲ 20% SiH_4/H_2 injection, Φ = 0.58

Fig. 9. Effect of concentration of silane on combustion at mach 4.5, H_s = 2.65MJ/kg, P_I = 30kPa, T_I = 480K

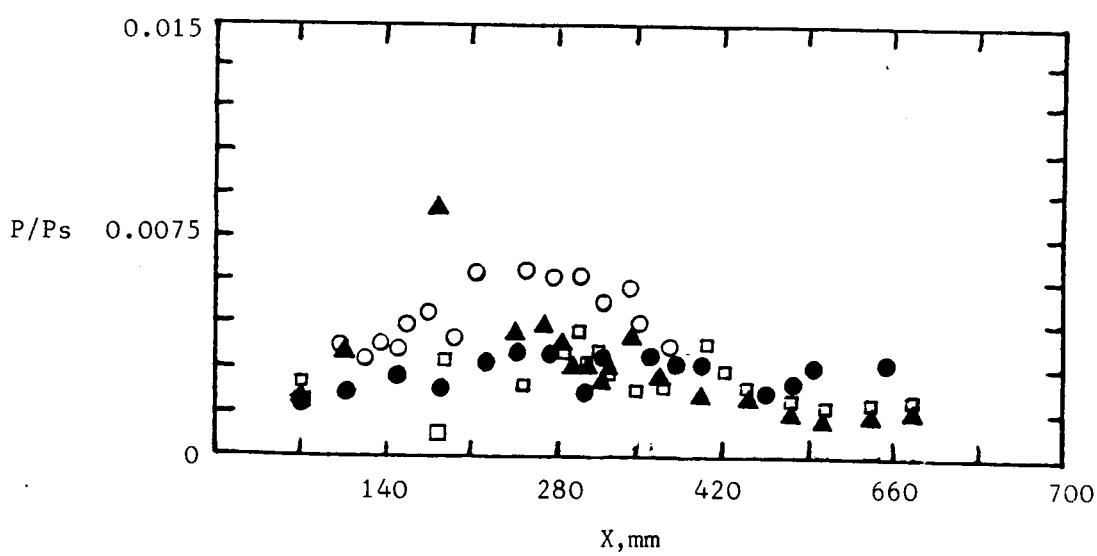

□ Fuel off

○ 5% SiH_4/H_2 injection, Φ = 0.72

● 10% SiH_4/H_2 injection, Φ = 0.63

▲ 20% SiH_4/H_2 injection, Φ = 1.07

Fig. 10. Effect of concentration of silane on combustion at mach 4.5, H_s = 1.90MJ/kg, P_I = 30kPa, T_I = 400K

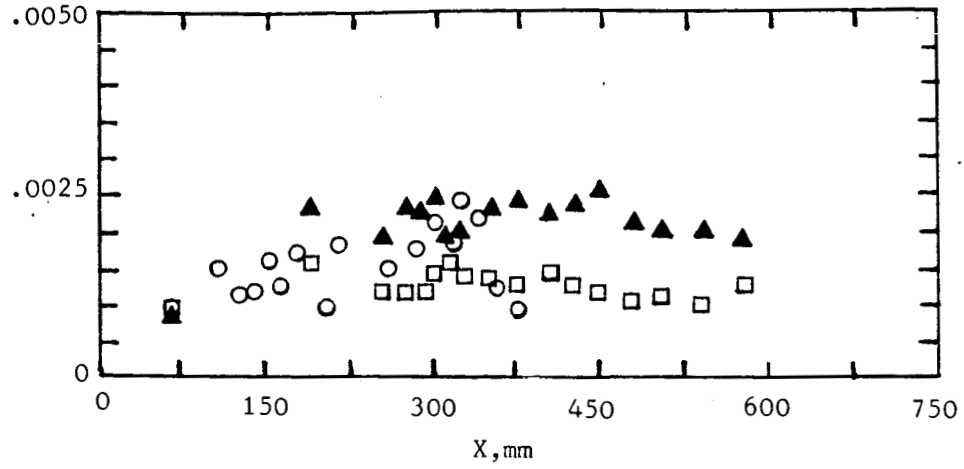

□ fuel off

○ 5% SiH_4/H_2 injection, ϕ = 1.3

▲ 20% SiH_4/H_2 injection ϕ = 1.21

Fig. 11. Effect of concentration of silane on combustion at Mach 5, H_s = 8.7 MJ/kg, P_I = 20 kPa, T_I = 1500 K

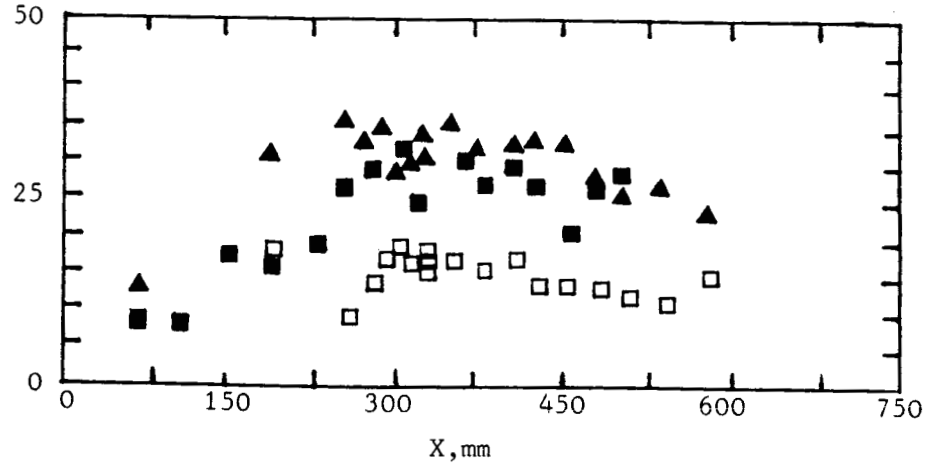

□ fuel off

■ 2.5% SiH_4/H_2 injection, ϕ = 1.08

▲ 20% SiH_4/H_2 injection, ϕ = 0.90

Fig. 12. Effect of concentration of silane on combustion at Mach 5, H_s = 6.1 MJ/kg, P_I = 20 kPa, T_I = 1000 K
(Note: Pressure is absolute due to lack of stagnation pressure information)

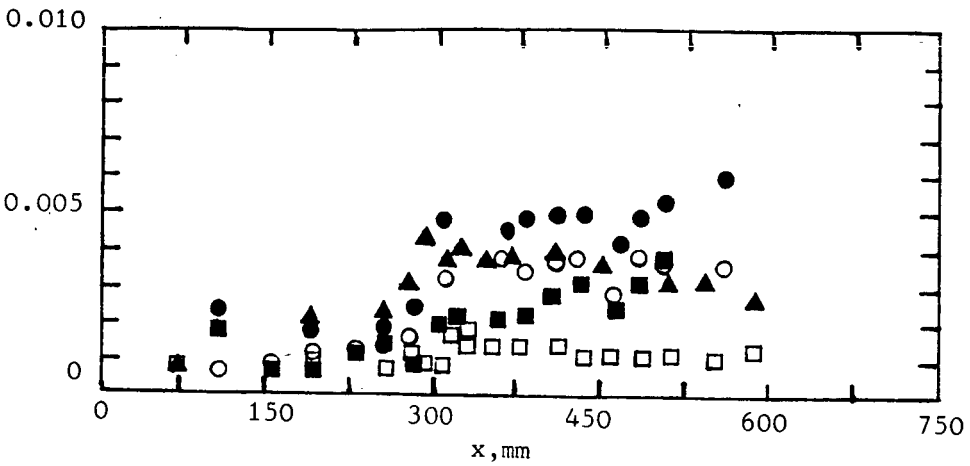

□ fuel off
■ 2.5% SiH_4/H_2 injection, ϕ = 1.03
○ 5% SiH_4 H_2 injection, ϕ = 0.92
● 10% SiH_4 H_2 injection, ϕ = 0.87
▲ 20% SiH_4 H_2 injection, ϕ = 0.99

Fig. 13. Effect of concentration of silane on combustion at Mach 5, H_s = 4.2 MJ/kg , P_I = 20 kPa, T_I = 650 K

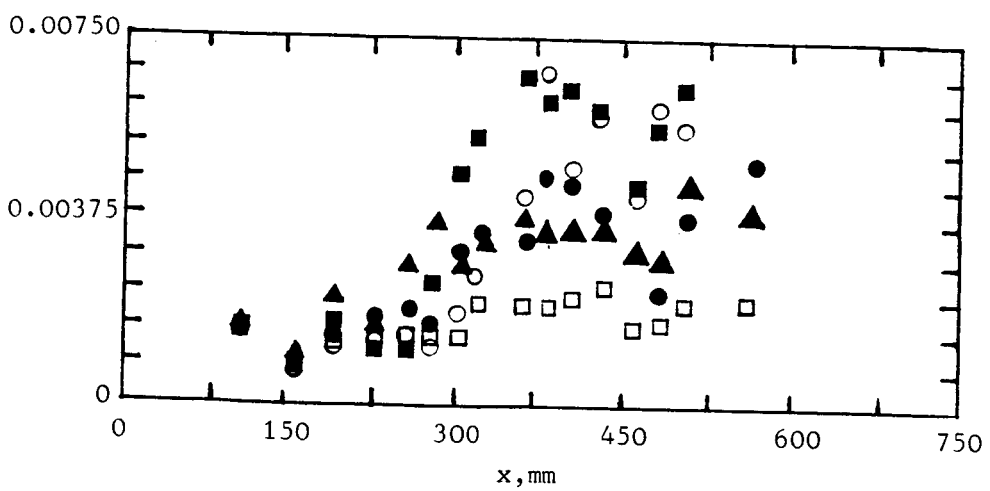

□ fuel off
■ 2.5% SiH_4/H_2 injection, ϕ = 0.95
○ 5% SiH_4/H_2 injection, ϕ = 0.92
● 10% SiH_4/H_2 injection, ϕ = 0.77
▲ 20% SiH_4 H_2 injection, ϕ = 0.87

Fig. 14. Effect of concentration of silane on combustion at Mach 5, H_s = 3.43 MJ/kg, P_I = 20 kPa, T_I = 540 K

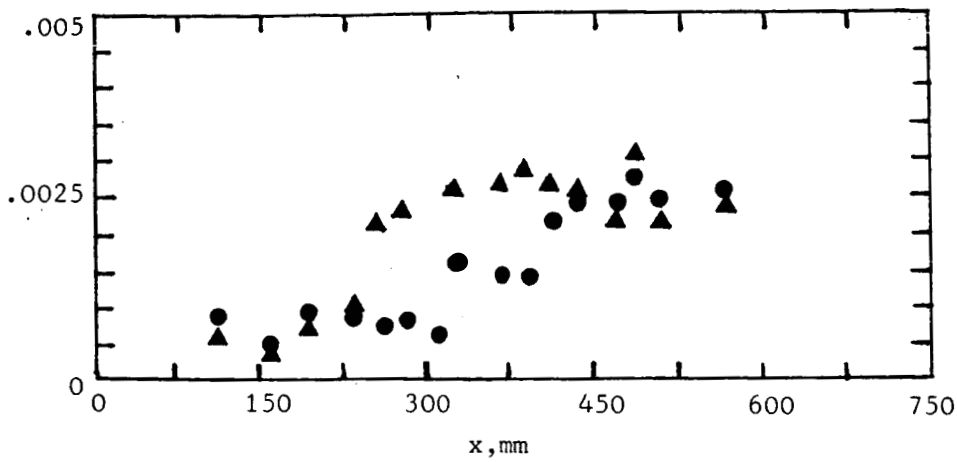

● 10% SiH_4/H_2 injection, ϕ = 0.91

▲ 20% SiH_4 H_2 injection, ϕ = 0.68

Fig. 15. Effect of concentration of silane on combustion at Mach 5, H_s = 2.65 MJ/kg, P_I = 20 kPa, T_I = 410 K

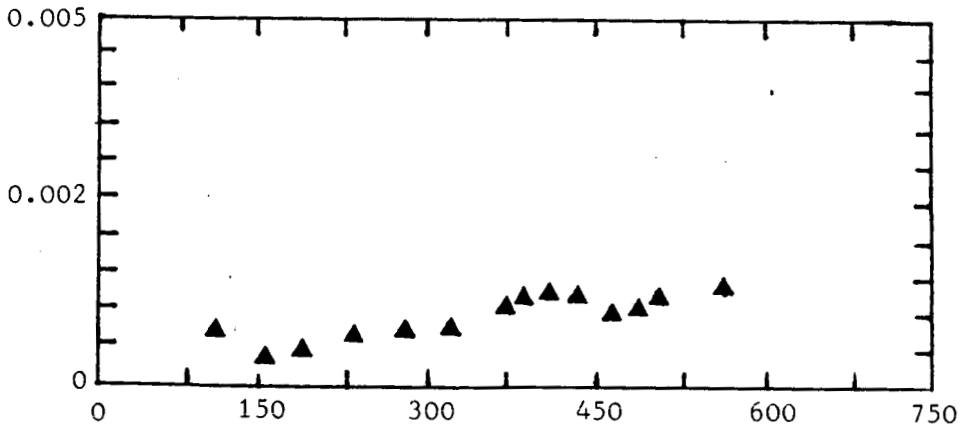

▲ 20% SiH_4/H_2 injection, ϕ = 0.83

Fig. 16. Combustion limit of 20% SiH_4/H_2 at Mach 5, H_s = 1.90 MJ/kg, T_I = 350 K

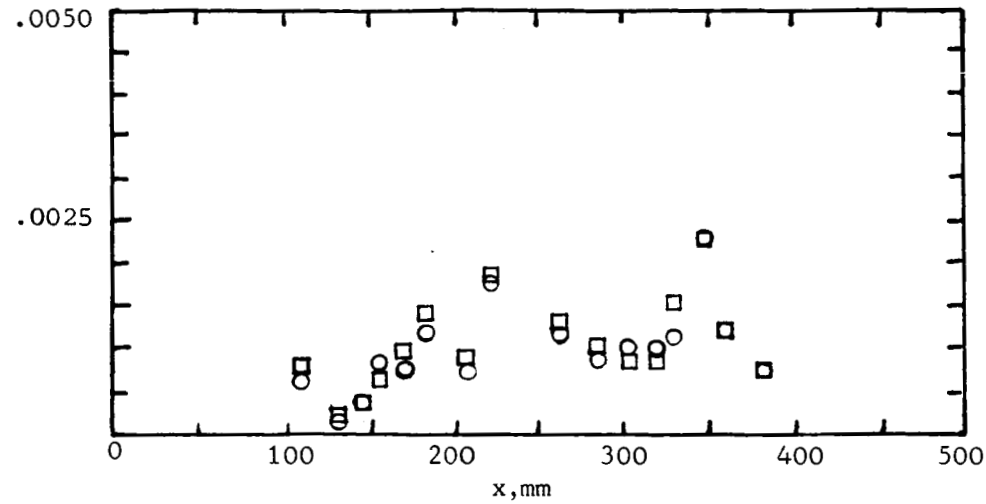

□ fuel off, H_s = 4.2 MJ/kg

○ 17.4% Ar/H_2 injection, H_s = 4.2 MJ/kg

Fig. 17. Central injection of an argon hydrogen mixture at Mach 5, T_I = 650 K, P_I 20 kPa, $\phi \approx 1$.

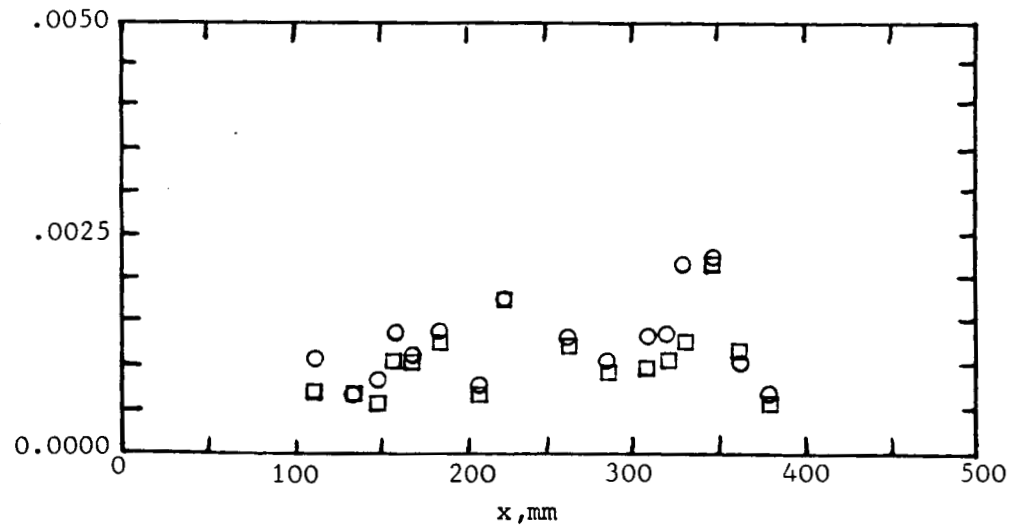

□ fuel off, H_s = 8.7 MJ/kg

○ 17.4% Ar/H_2 injection, H_s = 8.7 MJ/kg

Fig. 18. Central injection of an argon hydrogen mixture at Mach 5, T_I = 1500 K, P_I = 20 kPa, $\phi \approx 1$

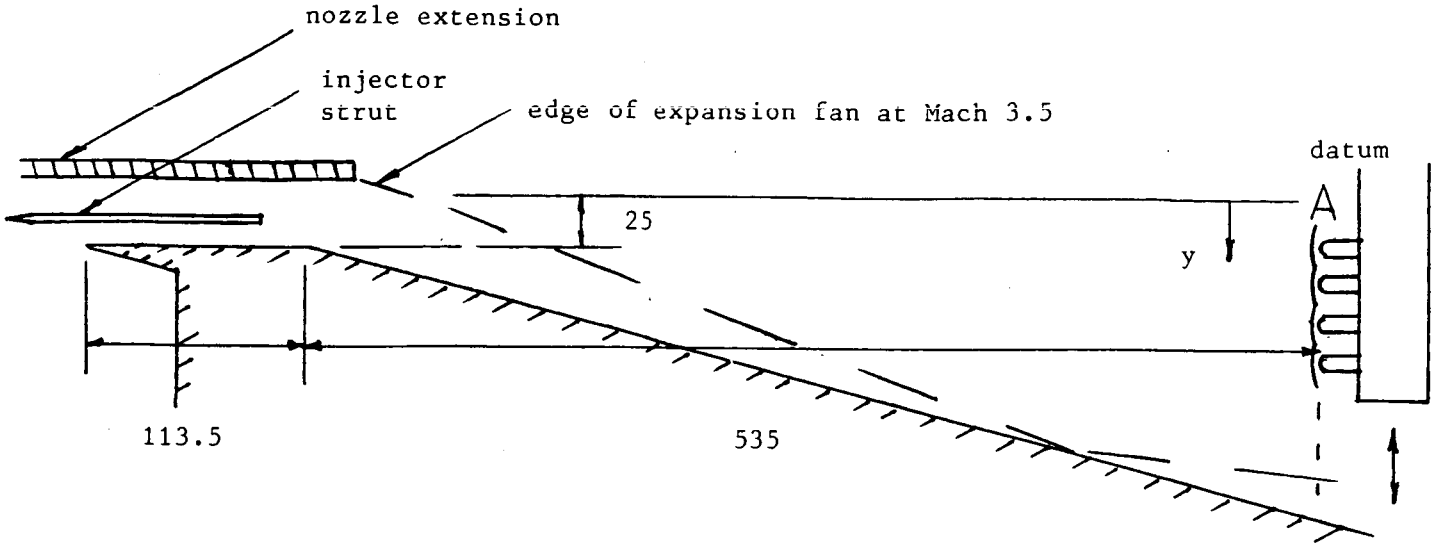

Fig. 19. 15 degree divergence thrust surface without cowl

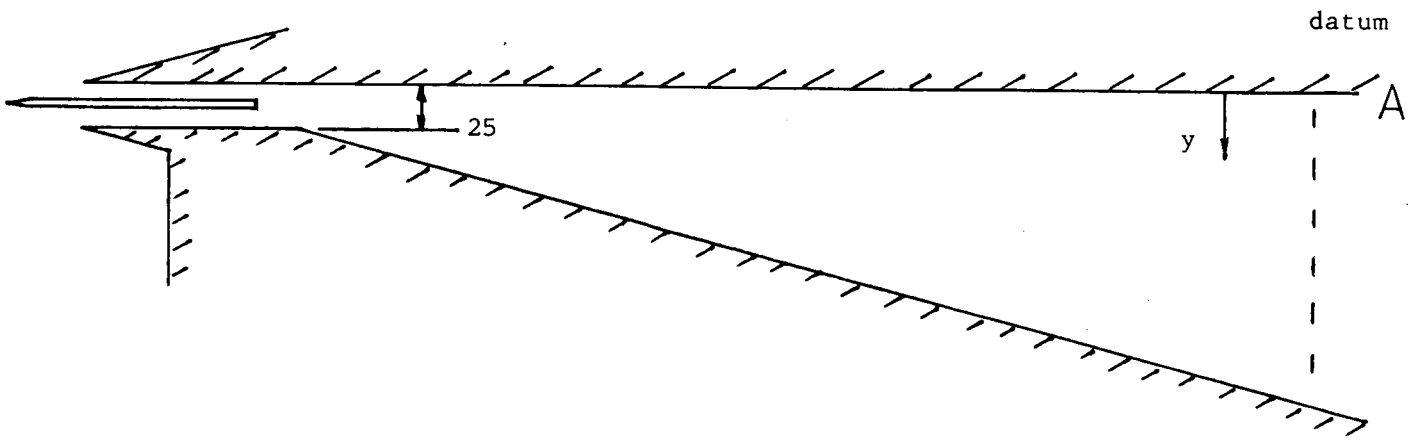

Fig. 20. 15 degree divergence thrust surface with cowl.

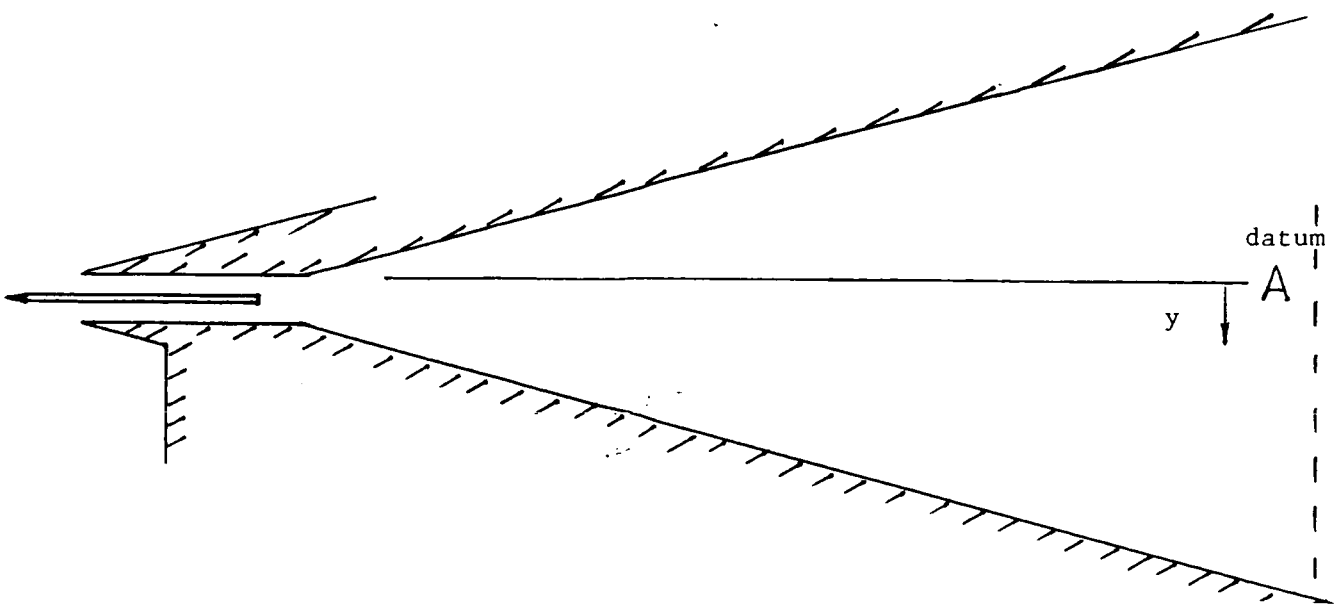

Fig. 21. 15 degree divergence symmetrical thrust surfaces

Scale 1:4

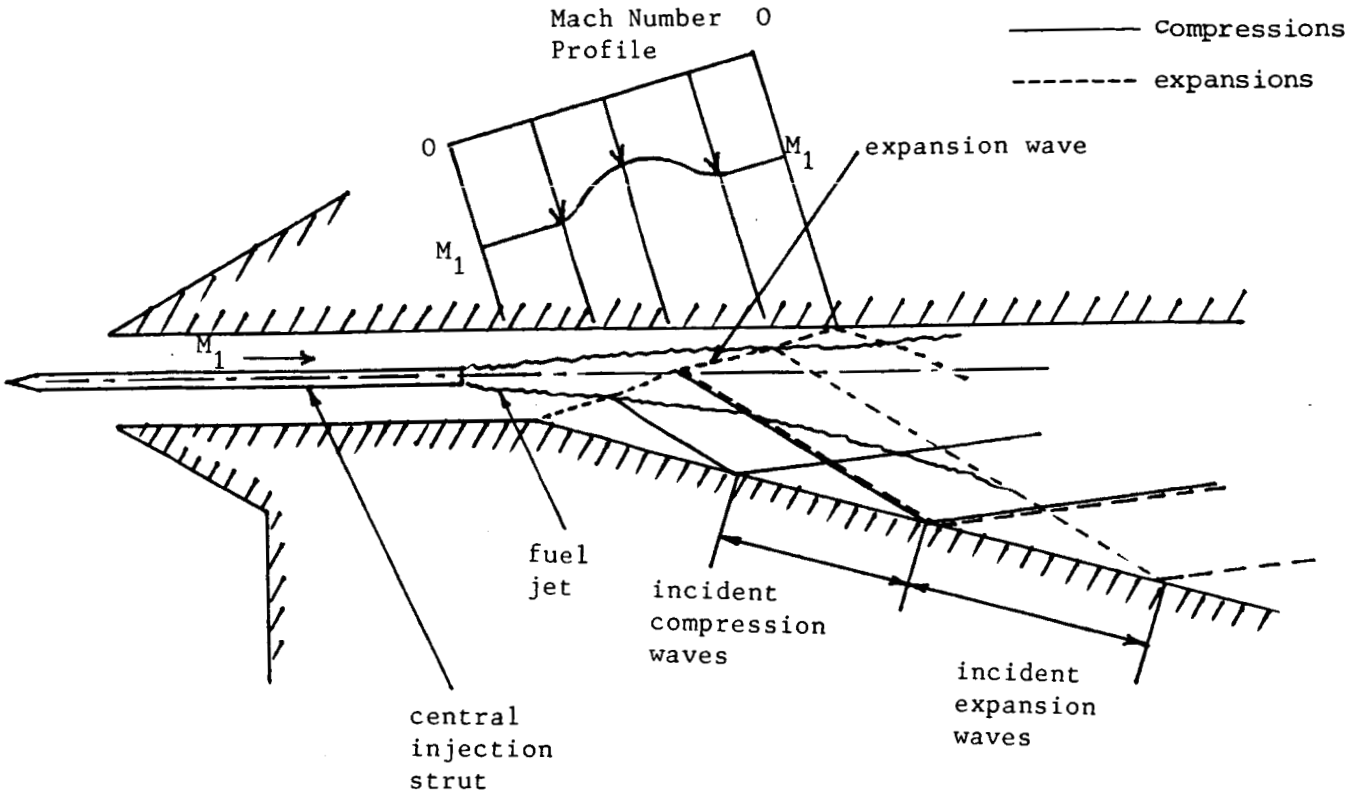

Fig. 22. Thrust contribution due to an expansion wave passing through a Mach number gradient

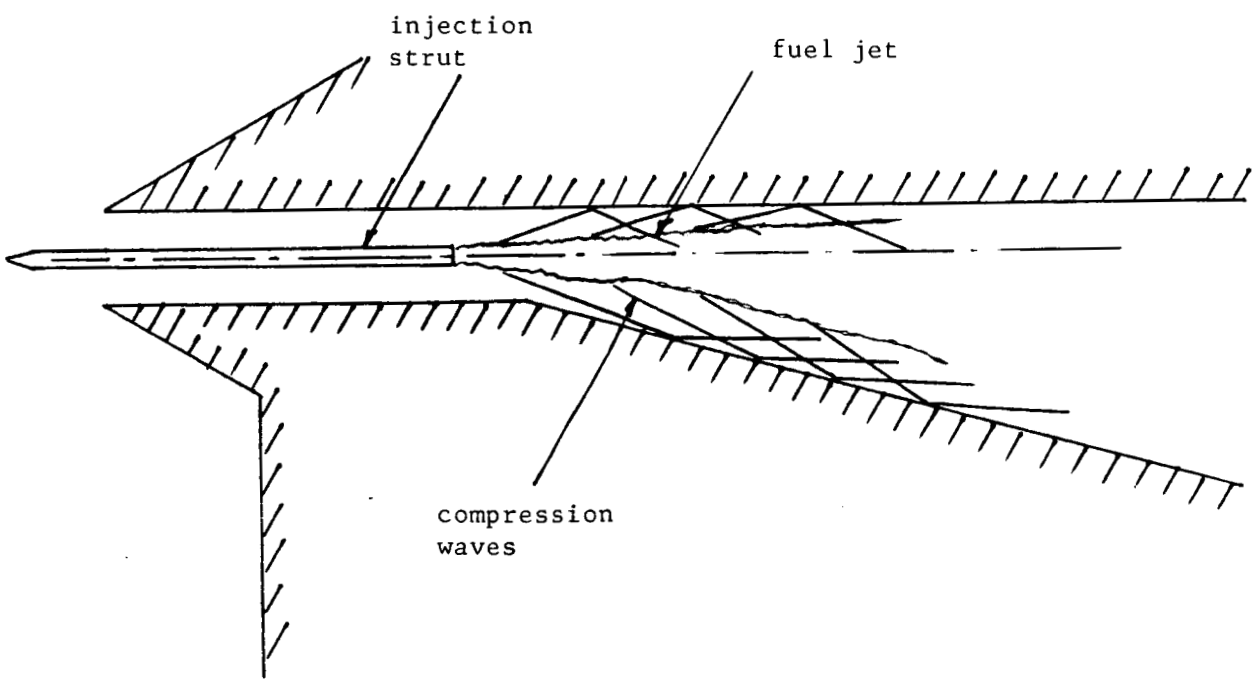

Fig. 23. Thrust contribution due to a burning fuel jet

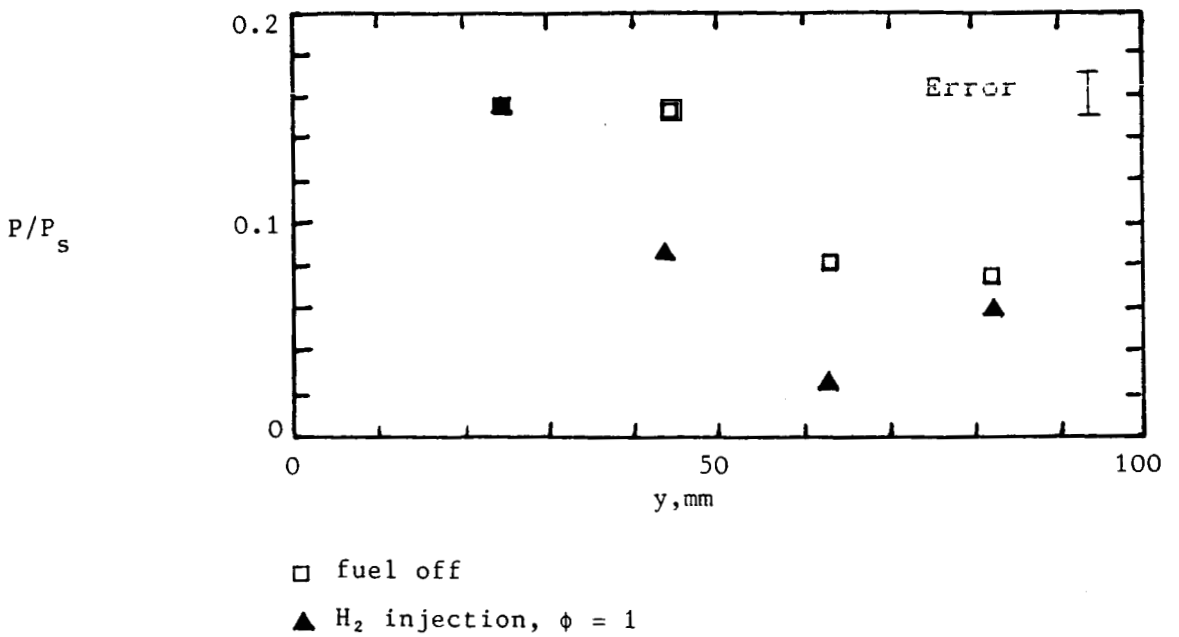

Fig. 24. Pitot profiles across an open duct with 15 degrees divergence, H_s = 6.1 MJ/kg, M_I = 3.5, T_I = 1700 K, P_I = kPa

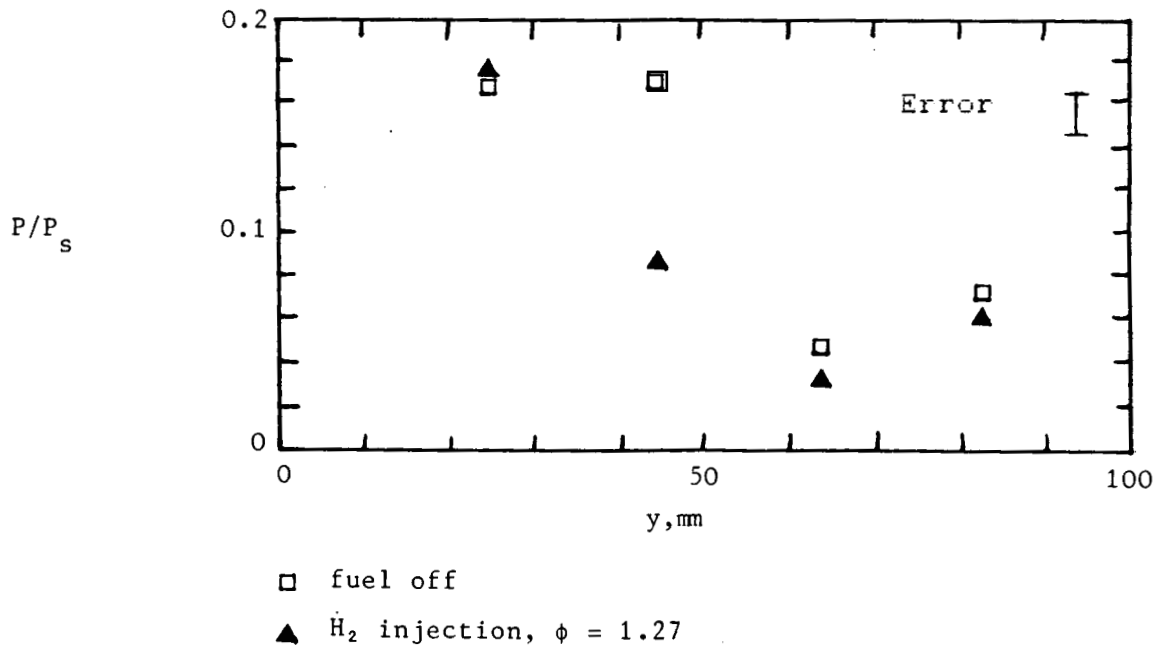

Fig. 25. Pitot profiles across an open duct with 15 degress divergence, H_s = 8.7 MJ/kg, M_I = 3.5, T_I = 2500 K, P_I = 160 kPa

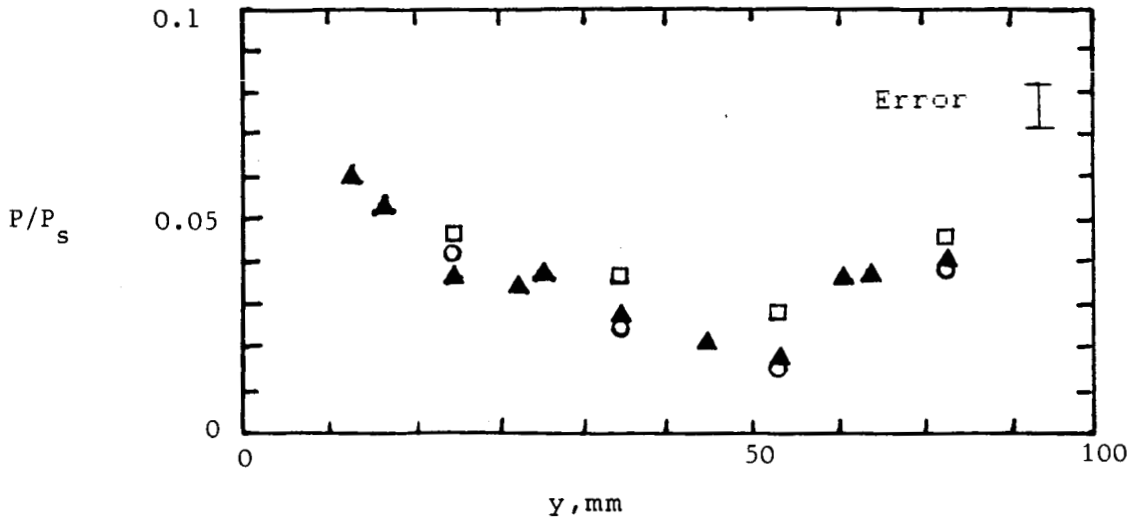

□ fuel off

▲ H_2 injection, ϕ = 1.0

○ H injection, ϕ = 1.85

Fig. 26. Pitot profiles across a closed duct with 15 degrees with divergence, H_s = 8.7 MJ/kg, M_I = 3.5, T_I = 2500 K, P_I = 160 kPa

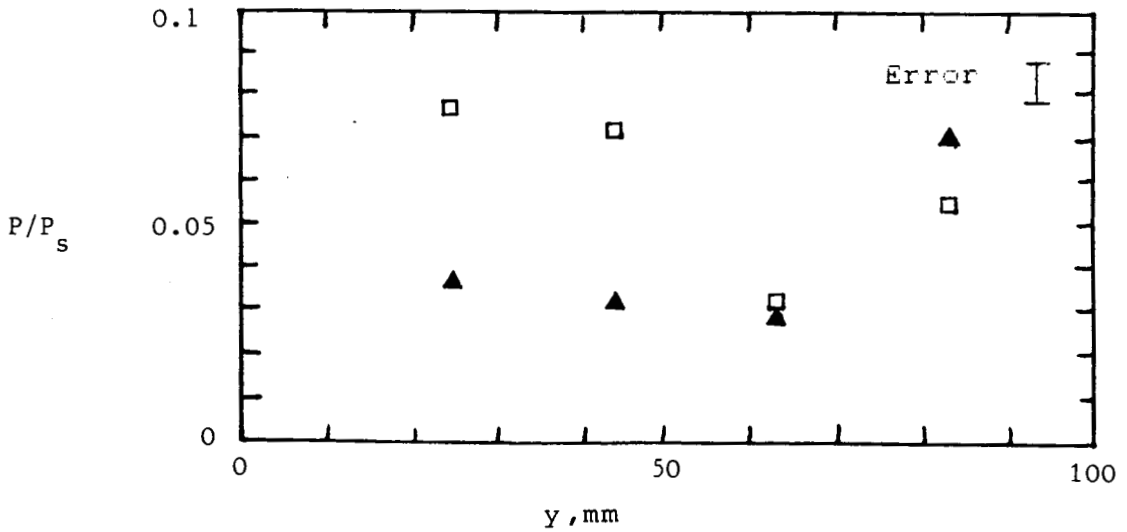

□ fuel off

▲ H_2 injection, ϕ = 1.09

Fig. 27. Pitot profiles across a symmetrical duct, 15 degress divergence, H_s = 8.7 MJ/kg, M_I = 3.5, T_I = 2500 K, P_I = 160 kPa

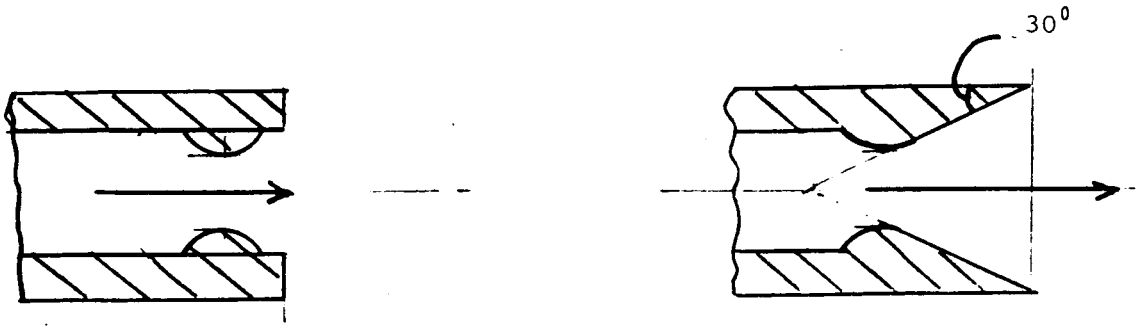

A. Standard nozzle

B. Source flow nozzle

Fig. 28. Central Injectors

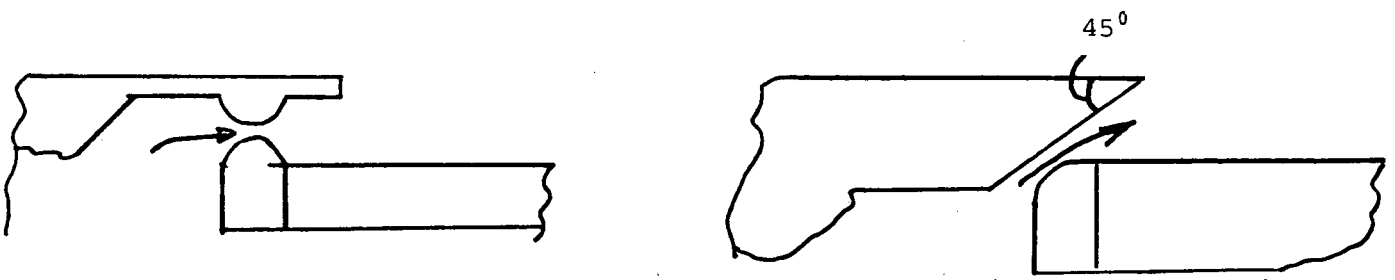

A. Standard nozzle

B. Source flow nozzle

Fig. 29. Wall injectors

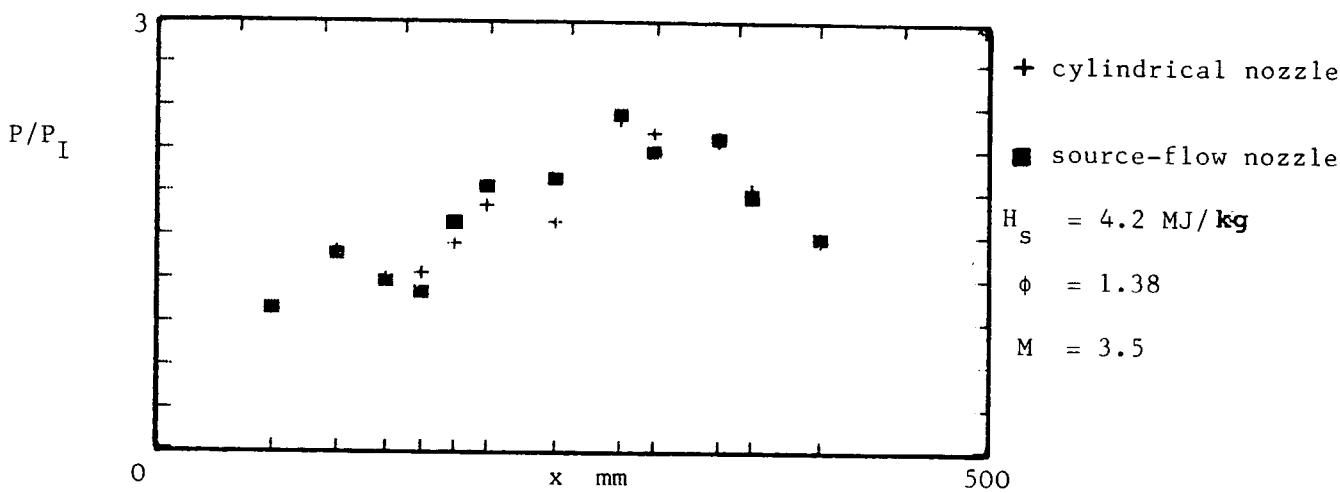

Fig. 30a. Pressure profiles for central injection from a source-flow and a cylindrical nozzle into a constant area duct.

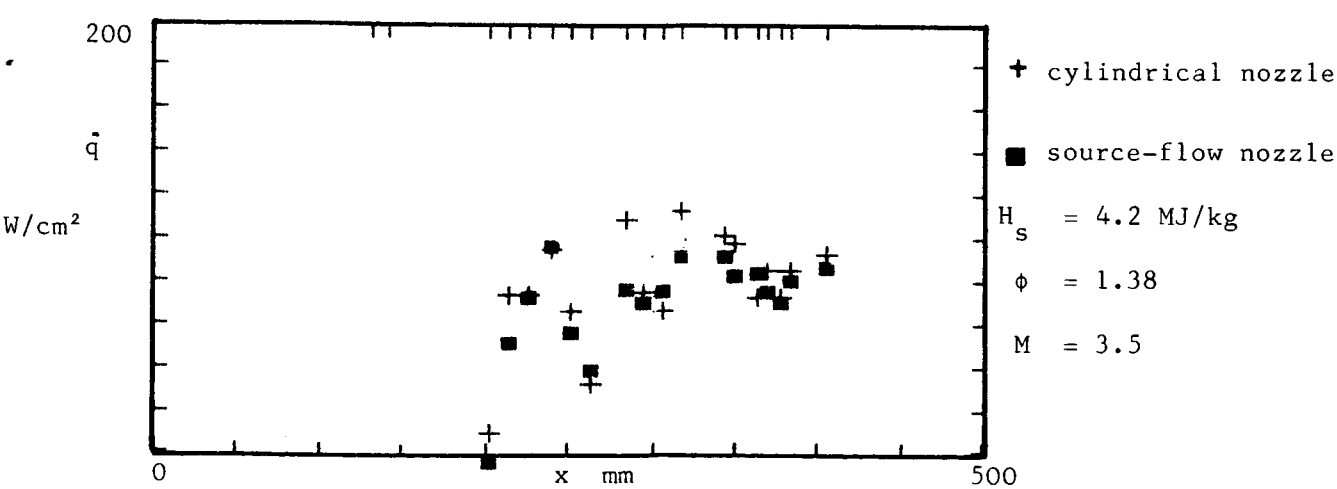

Fig. 30b. Heat transfer rates for central injection from a source-flow and a cylindrical nozzle into a constant area duct.

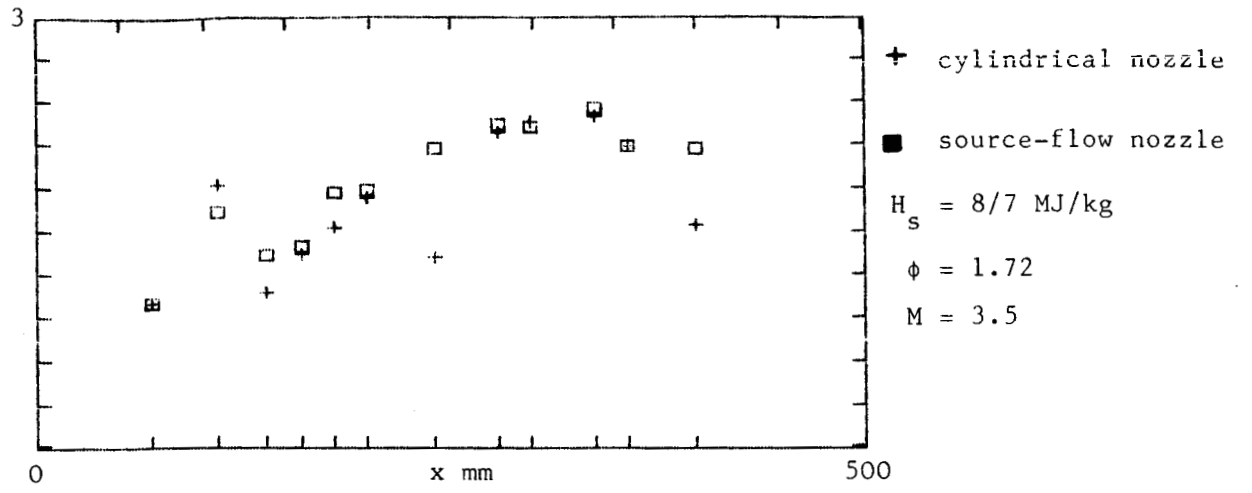

Fig. 31a. Pressure profiles for central injection from a source-flow and a cylindrical nozzle into a constant area duct.

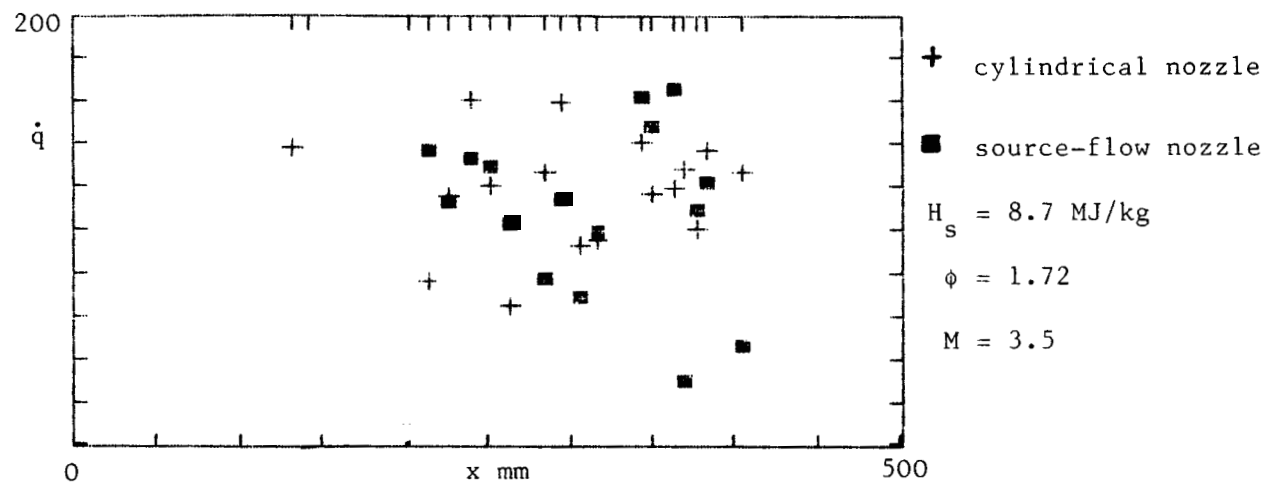

Fig. 31b. Heat transfer rates for central injection from a source-flow and a cylindrical nozzle into a constant area duct.

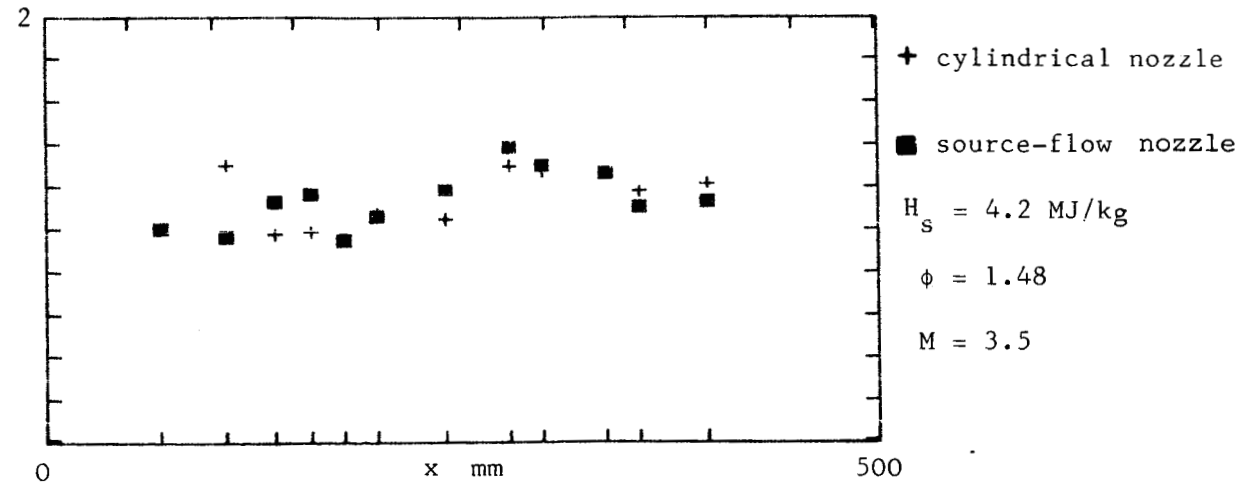

Fig. 32a. Pressure profiles for wall injection from a source-flow and a cylindrical nozzle into a constant area duct.

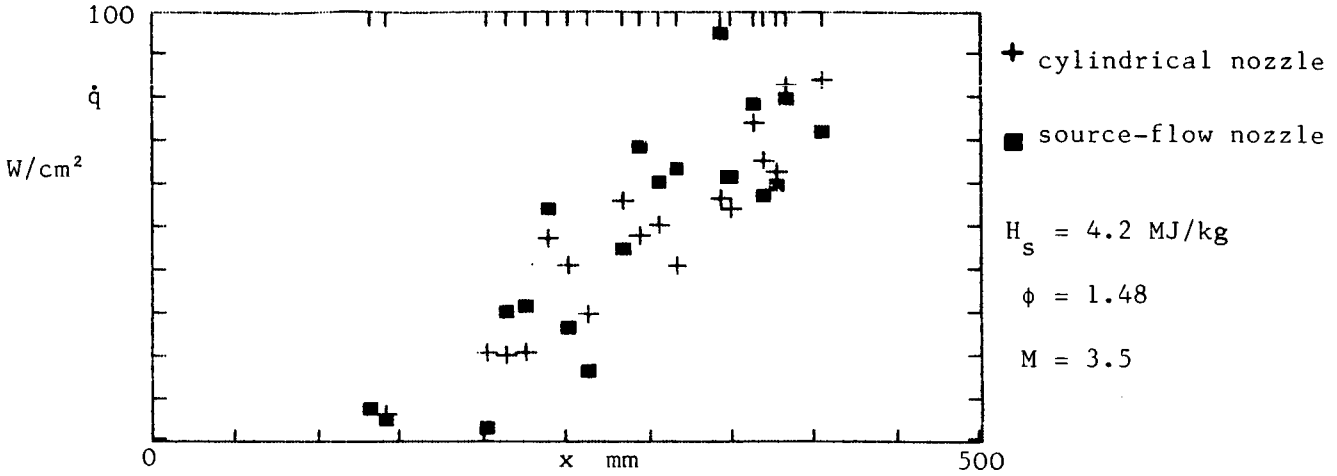

Fig. 32b. Heat transfer rates for wall injection from a source-flow and a cylindrical nozzle into a constant area duct.

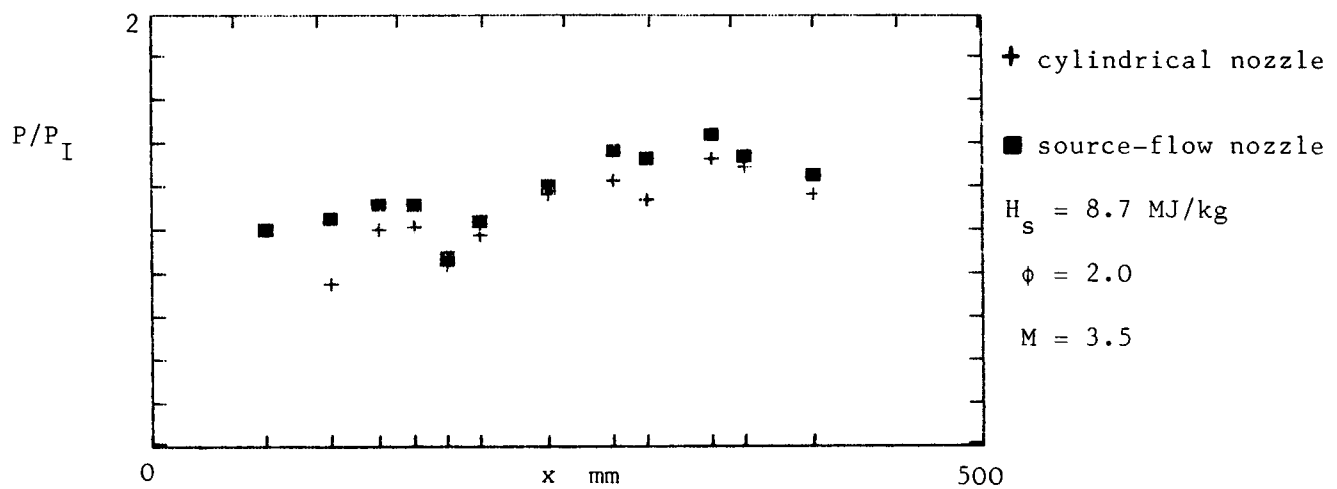

Fig. 33a. Pressure profiles for wall injection from a source-flow and a cylindrical nozzle into a constant area duct.

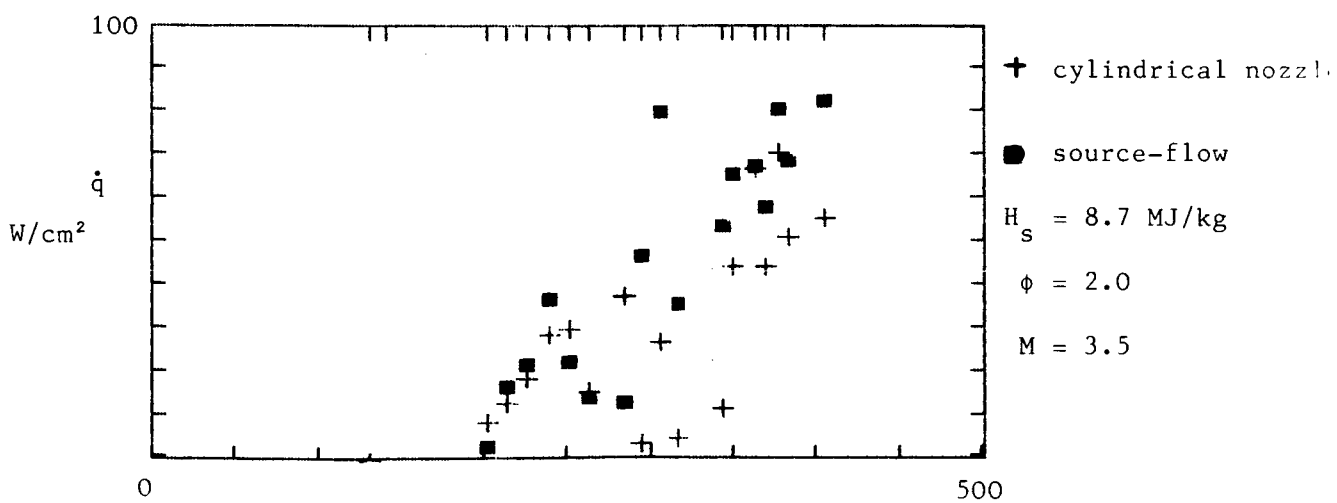

Fig. 33b. Heat transfer rates for wall injection from a source-flow and a cylindrical nozzle into a constant area duct.

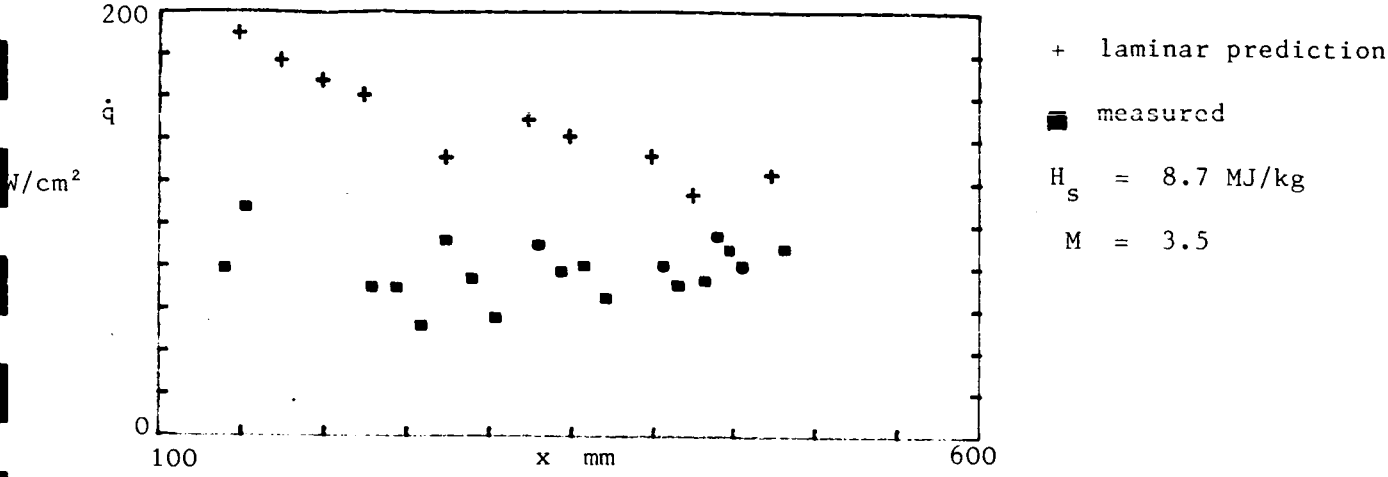

Fig. 34a. Predicted and measured values of the heat transfer rate for a constant area duct with injector.

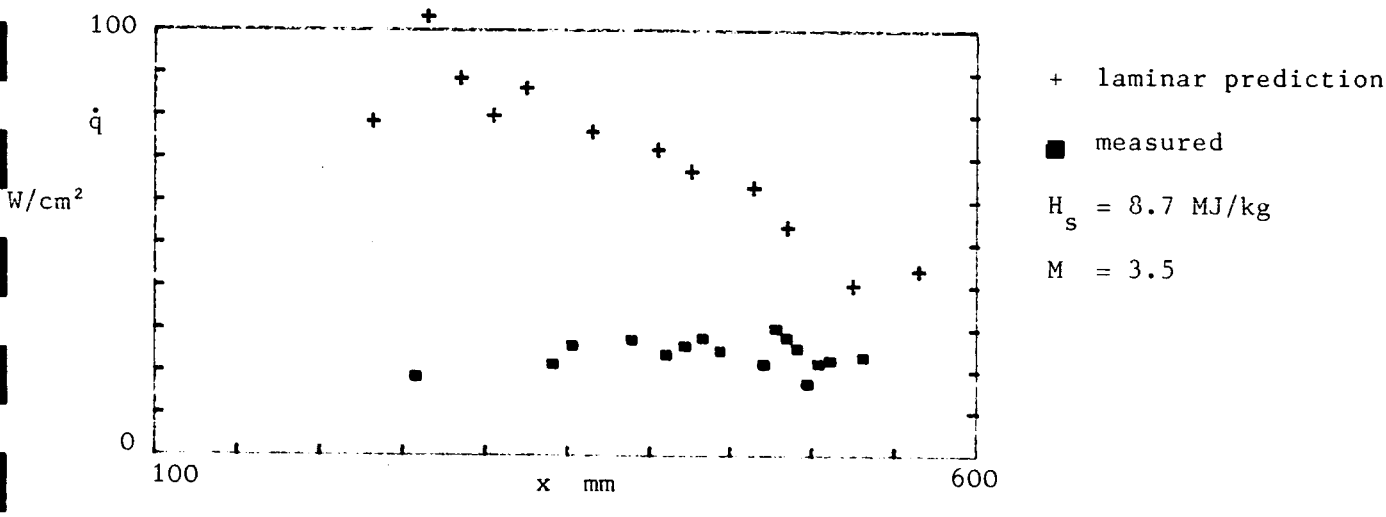

Fig. 34b. Predicted and measured values of the heat transfer rate for a 15° diverging duct with injector.

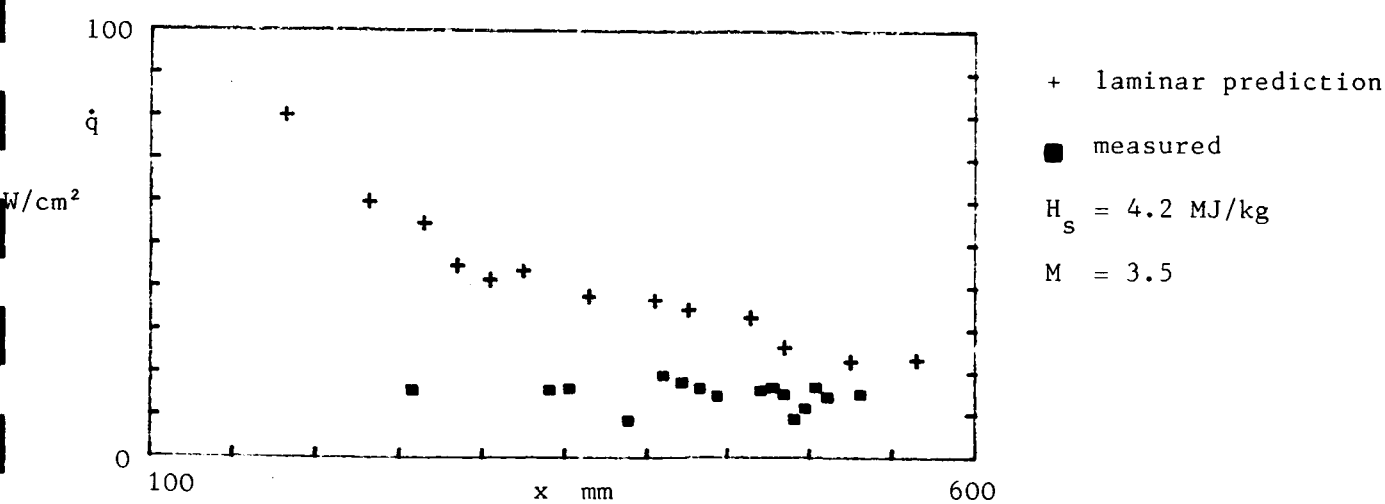

Fig. 34c. Predicted and measured values of the heat transfer rate for a 15° diverging duct with injector.

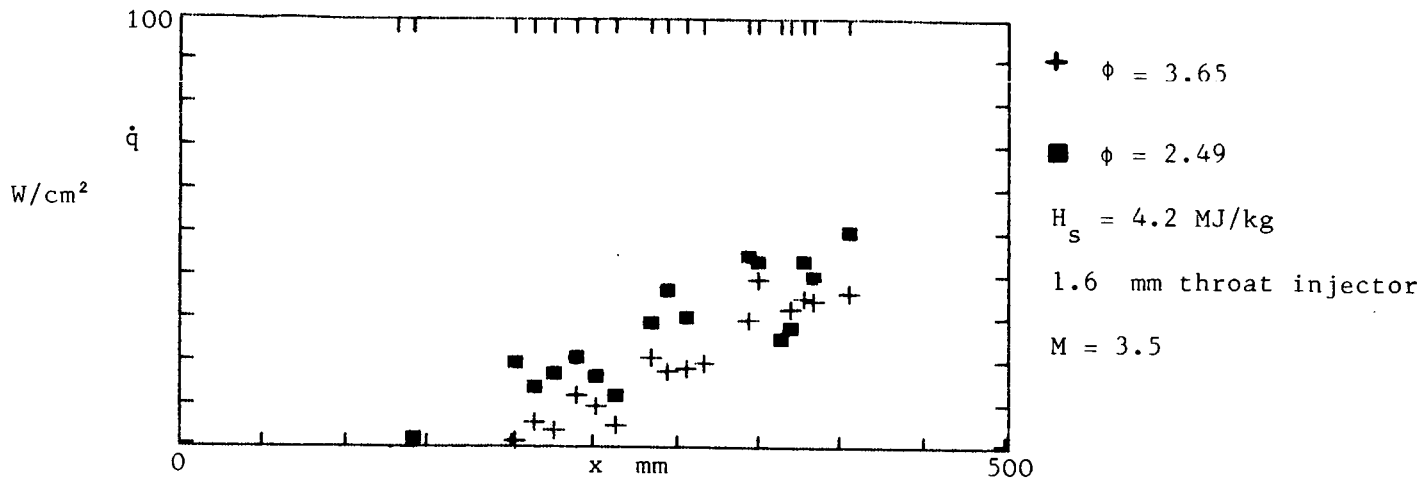

Fig. 35. Heat transfer rates for the injection of hydrogen into a nitrogen test gas in a constant area duct.

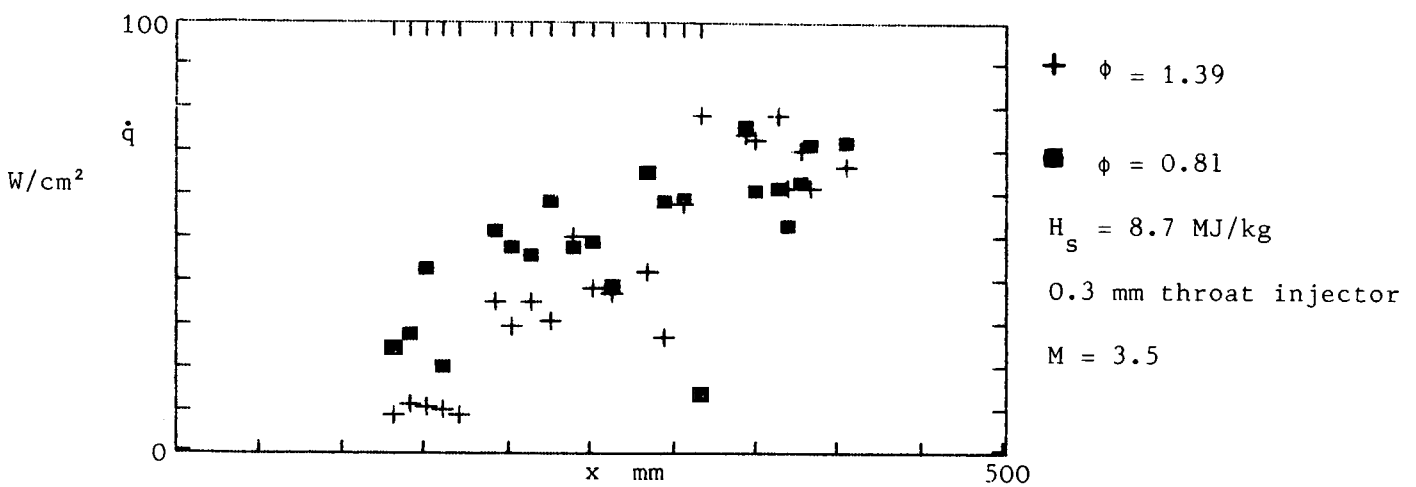

Fig. 36. Heat transfer rates for the injection of hydrogen into a nitrogen test gas in a constant area duct.

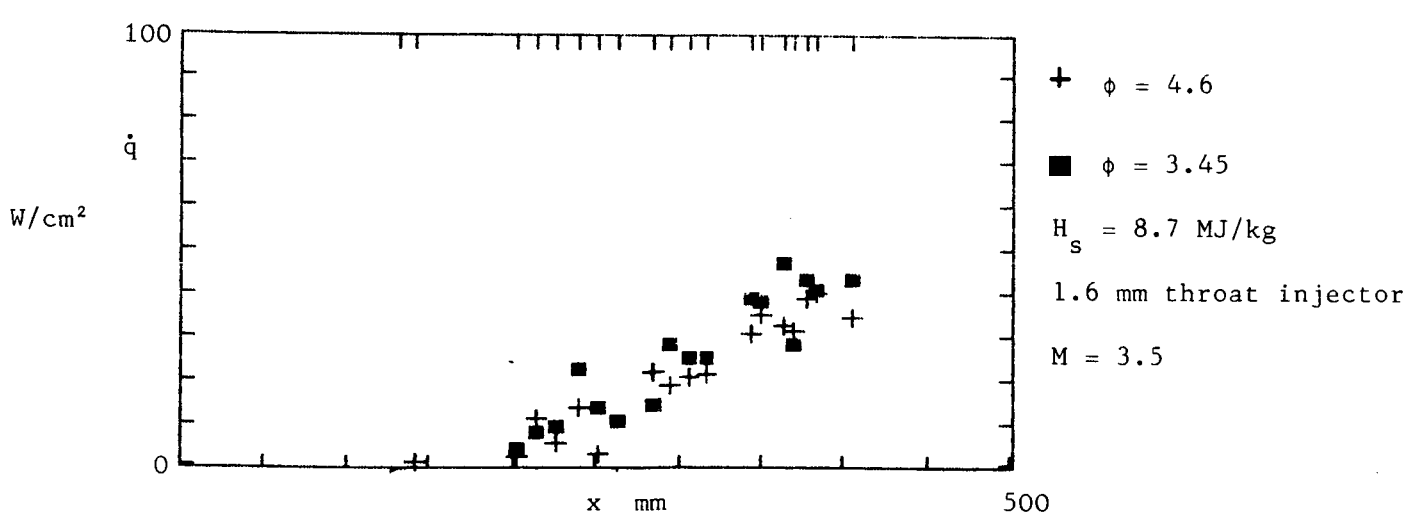

Fig. 37. Heat transfer rates for the injection of hydrogen into a nitrogen test gas in a constant area duct.

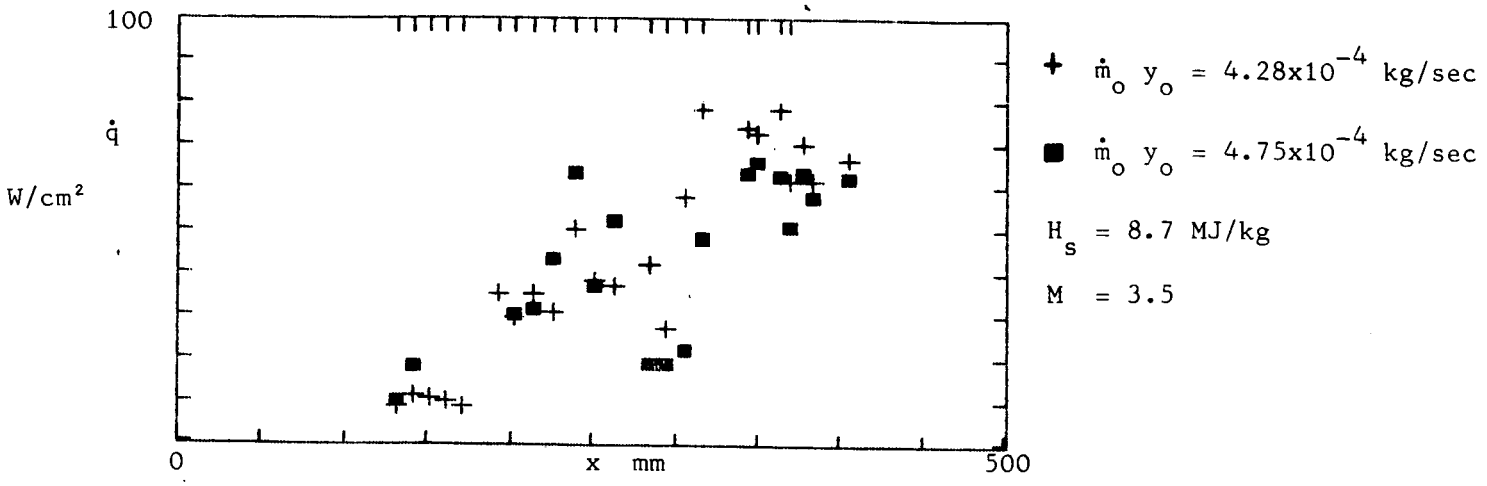

Fig. 38. Heat transfer rates in a constant areaduct when hydrogen is injected into a nitrogen test gas with different injectors.

\+ 0.3 mm throat ■ 0.9 mm throat

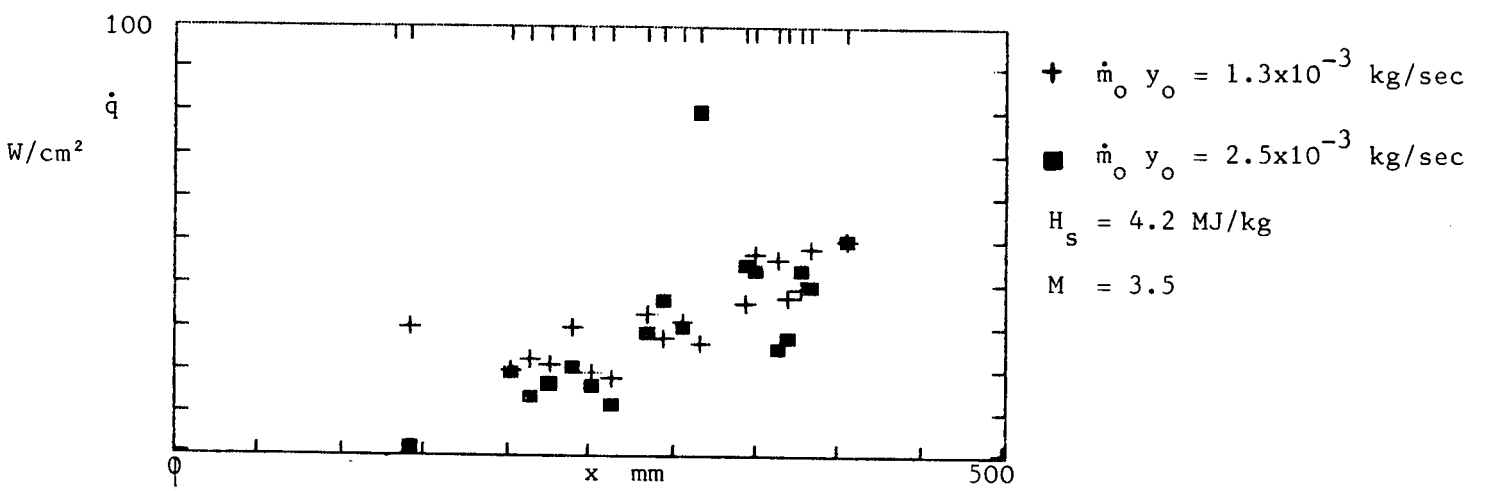

Fig. 39. Heat transfer rates in a constant area duct when dydeogen is injected into a nitrogen test gas with different injectors.

\+ 0.9 mm throat ■ 1.6 mm throat

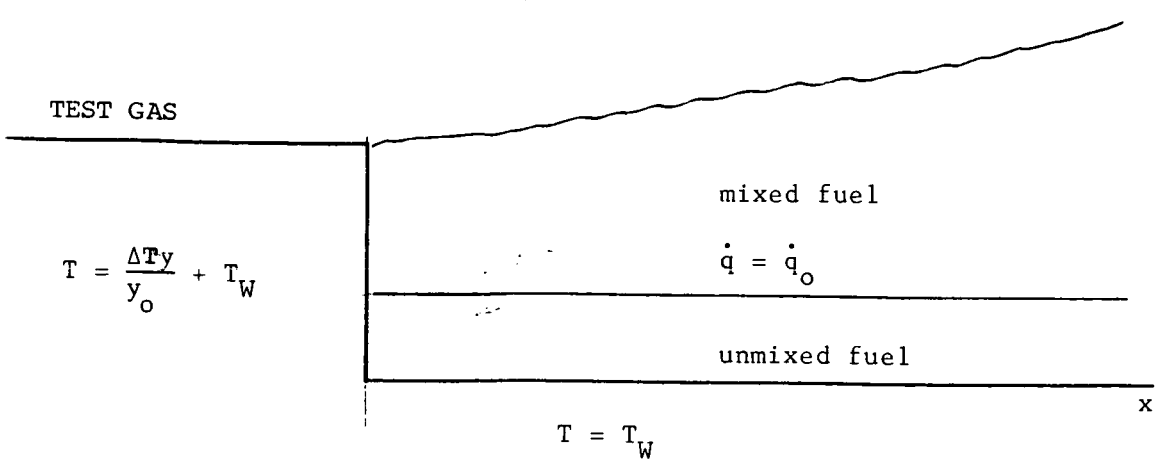

Fig. 40. Schematic of simple heat transfer model.

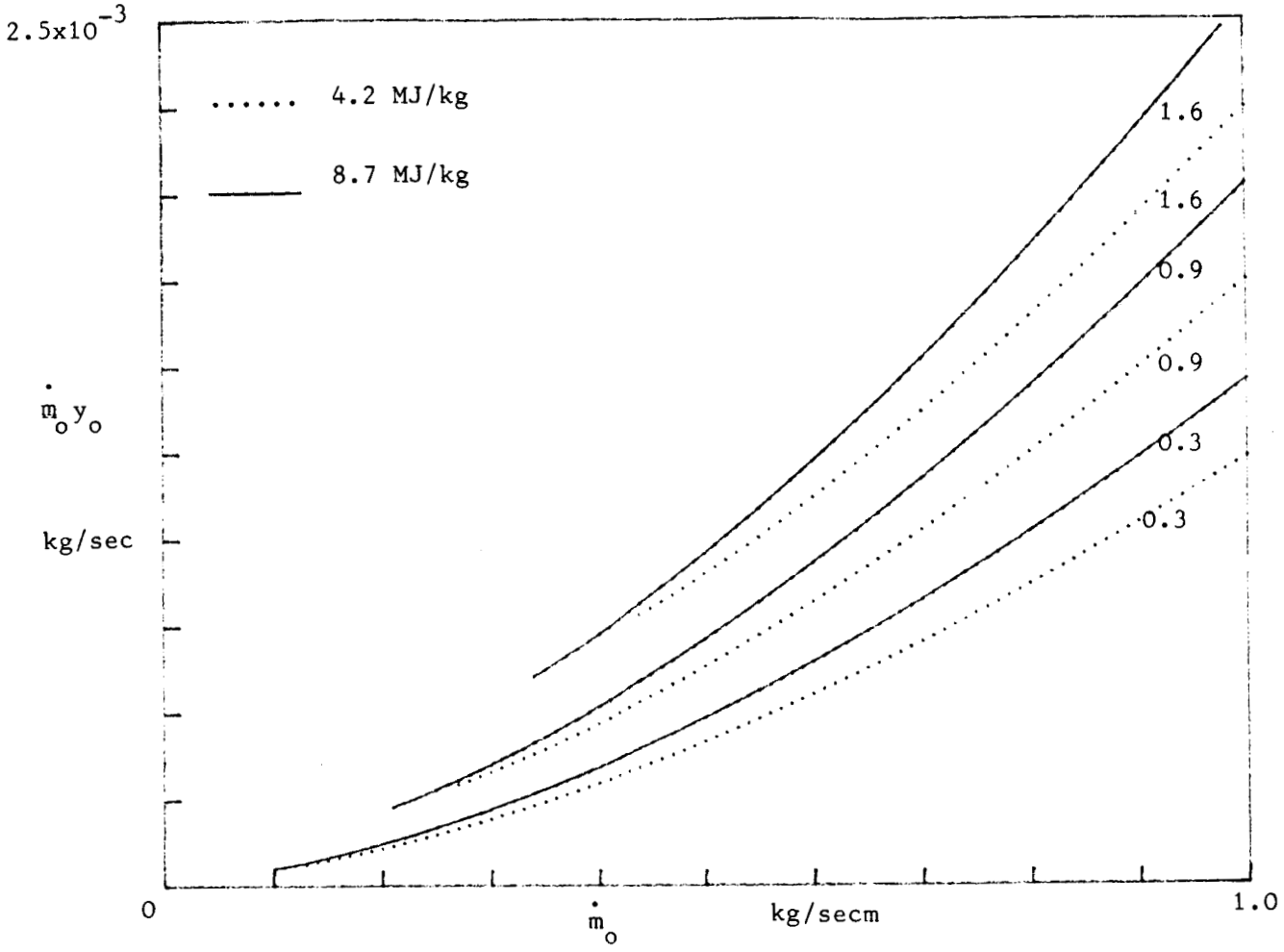

Fig. 41 The variation of $\dot{m}_o y_o$ with $\dot{m}_o$ M=3.5

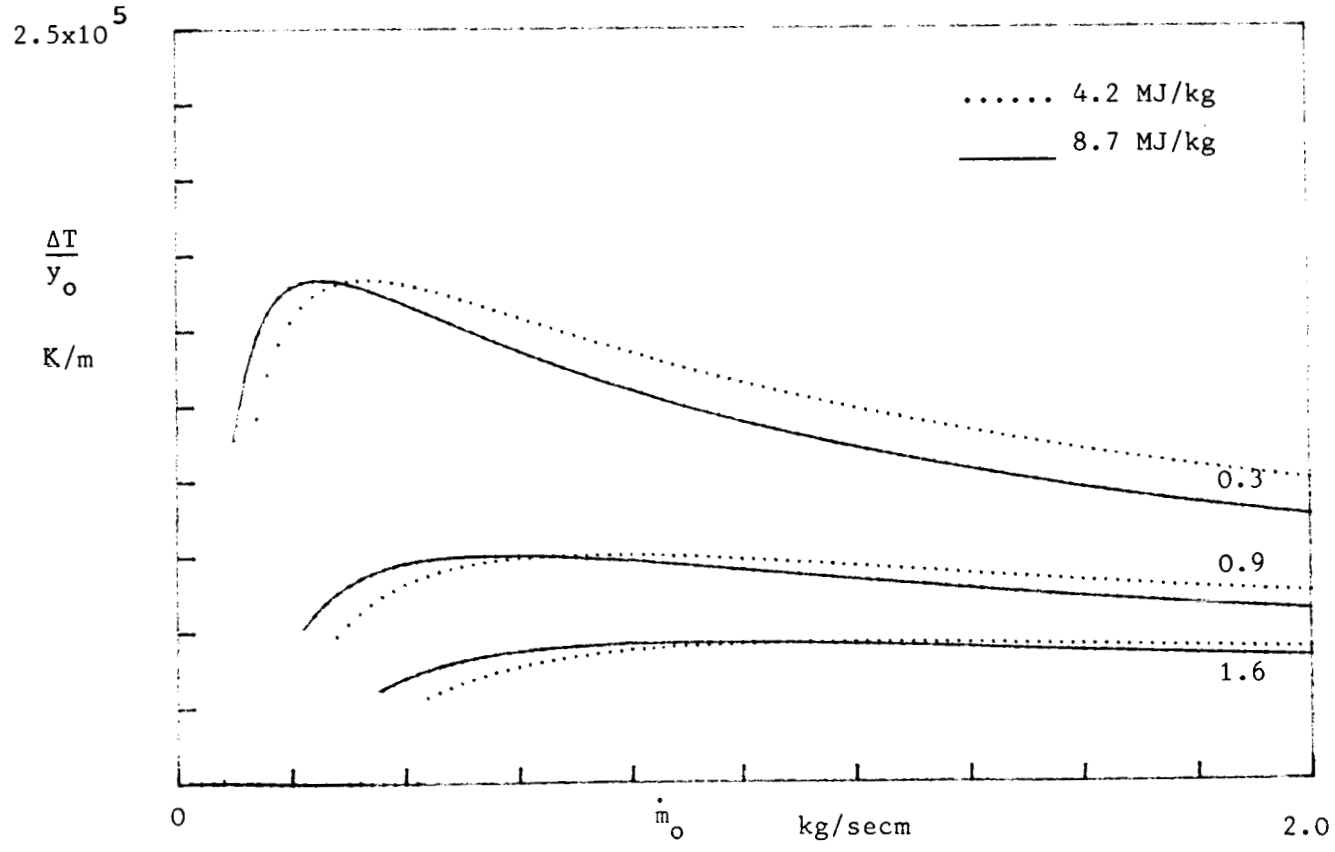

Fig. 42 The variation of $\frac{\Delta T}{y_o}$ with $\dot{m}_o$ M=3.5

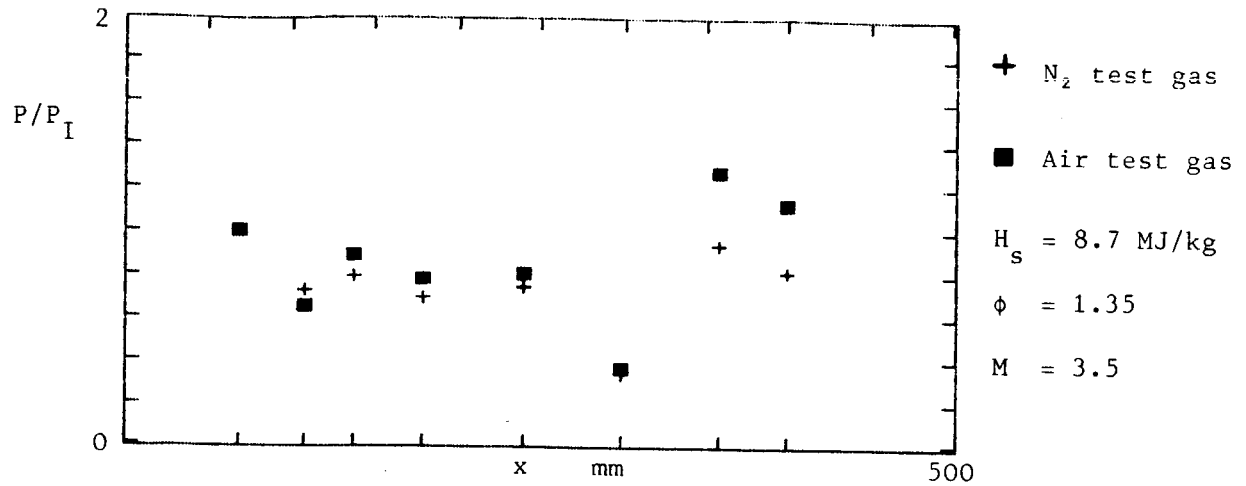

Fig. 43a. Pressure profile for the injection of hydrogen into a constant area duct and a test gas of air and nitrogen

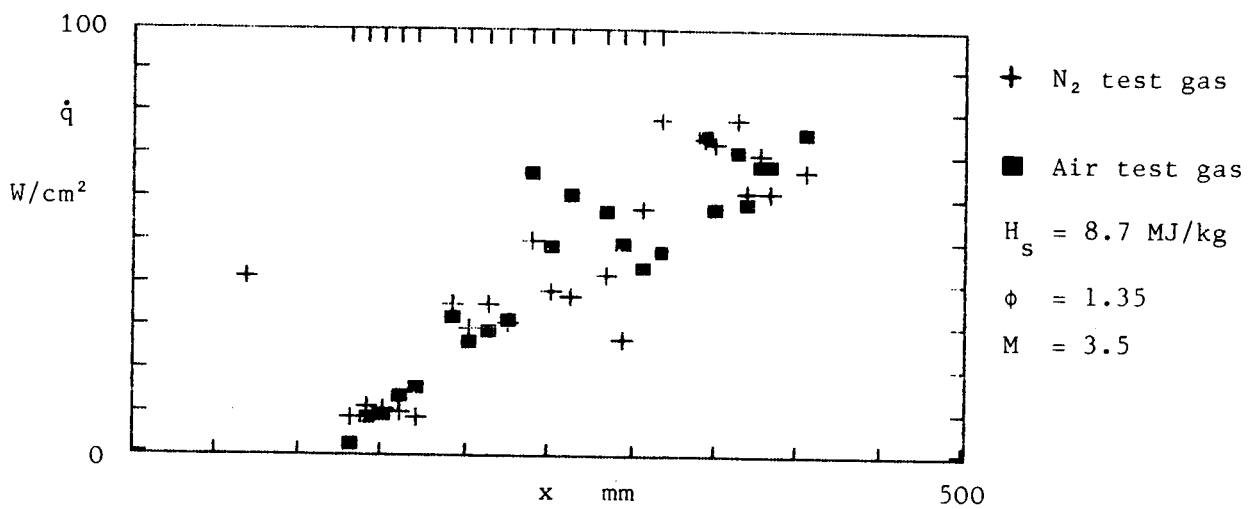

Fig. 43b. Heat transfer rates for the injection of hydrogen into a constant duct and a test gas of air and nitrogen

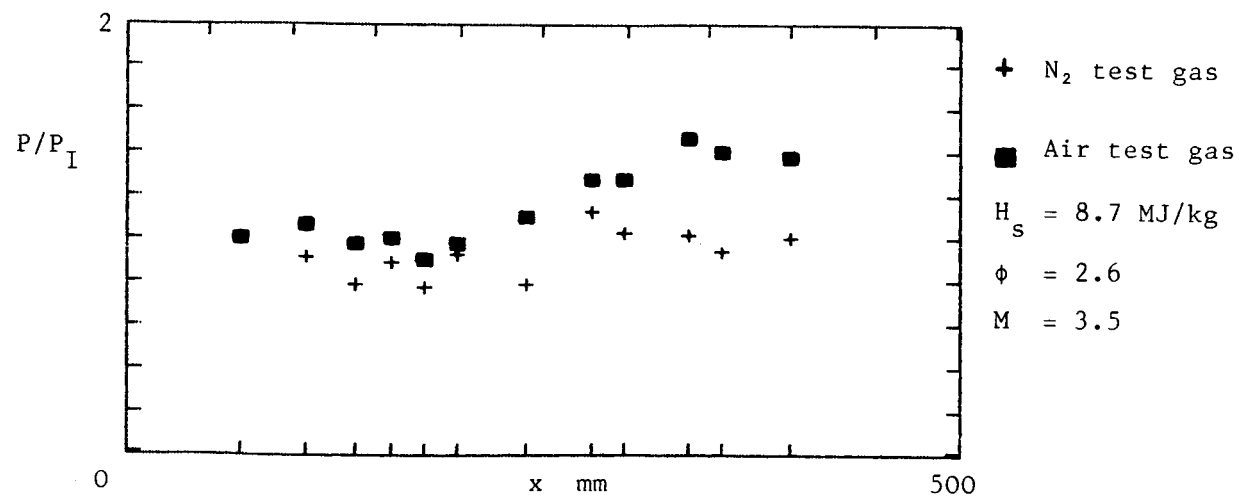

Fig. 44a. Pressure profile for the injection of hydrogen into a constant area duct and a test gas of air and nitrogen

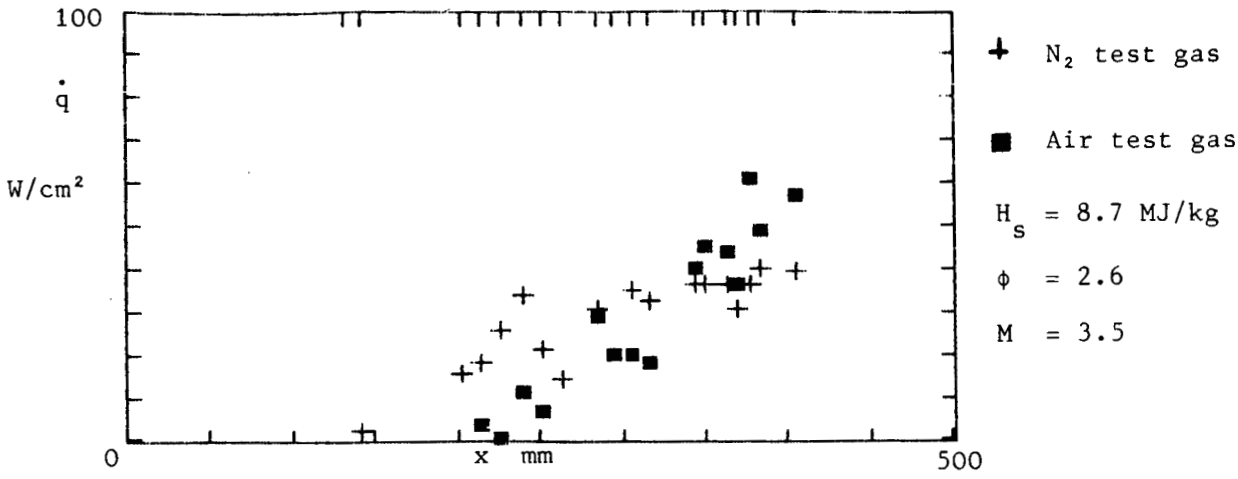

Fig. 44b. Heat transfer rates for the injection of hydrogen into a constant area duct and a test gas of air and nitrogen.

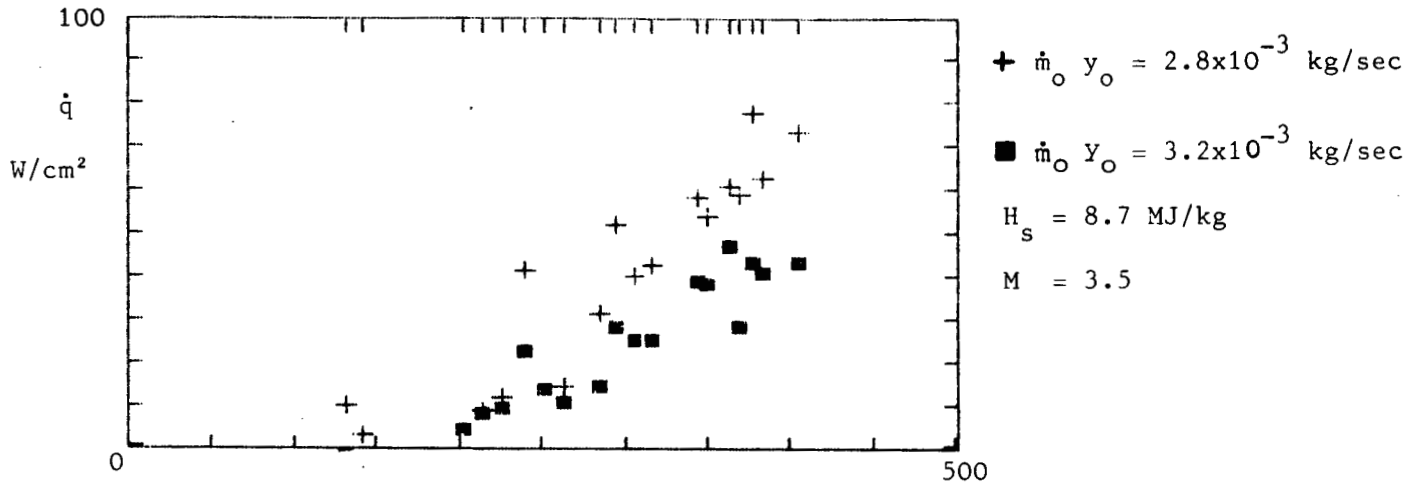

Fig. 45. Heat transfer rates for the injection of nitrogen into air and hydrogen into nitrogen at similar values of $\dot{m}_o$ y_o .

+ nitrogen - air ■ hydogen - nitrogen

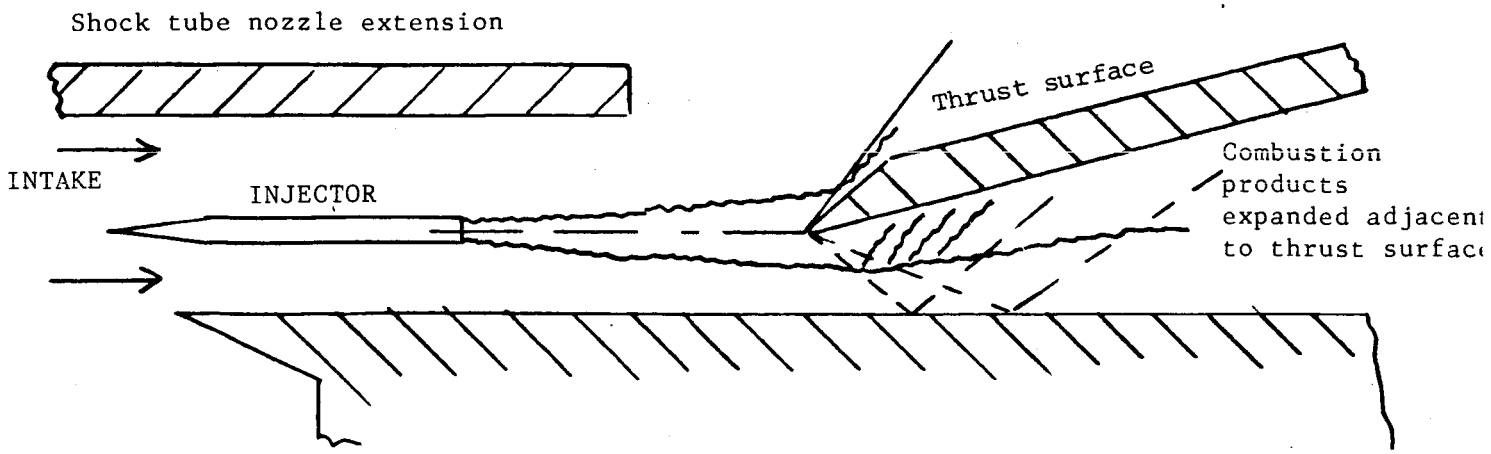

Fig. 46. Proposal for central injector expanded from the centreline in order to simulate wall injection without quenching

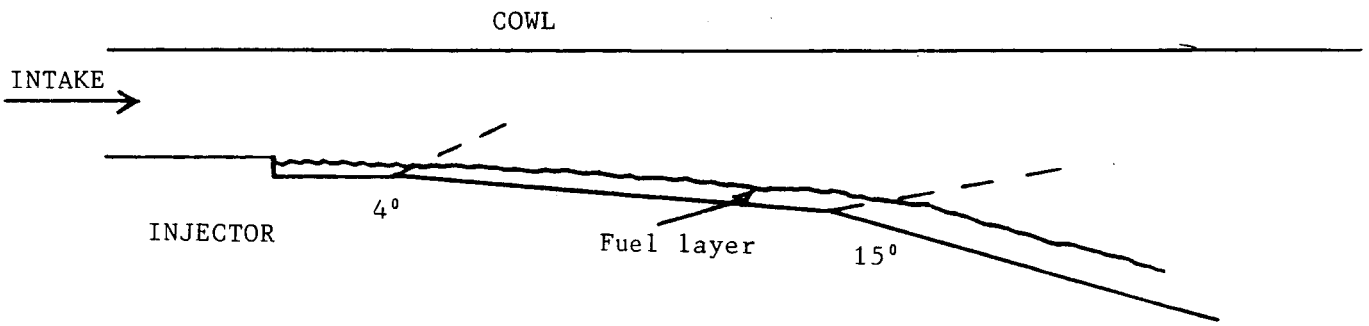

Fig. 47. Dual stage expansion

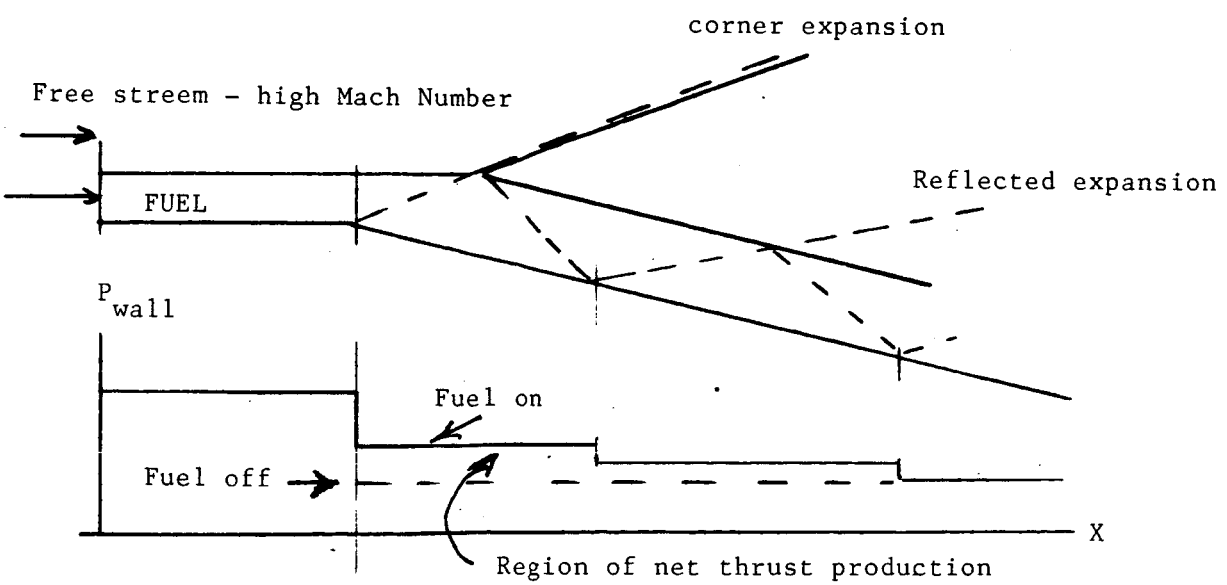

Fig. 48. Corner expansion/wall jet interaction

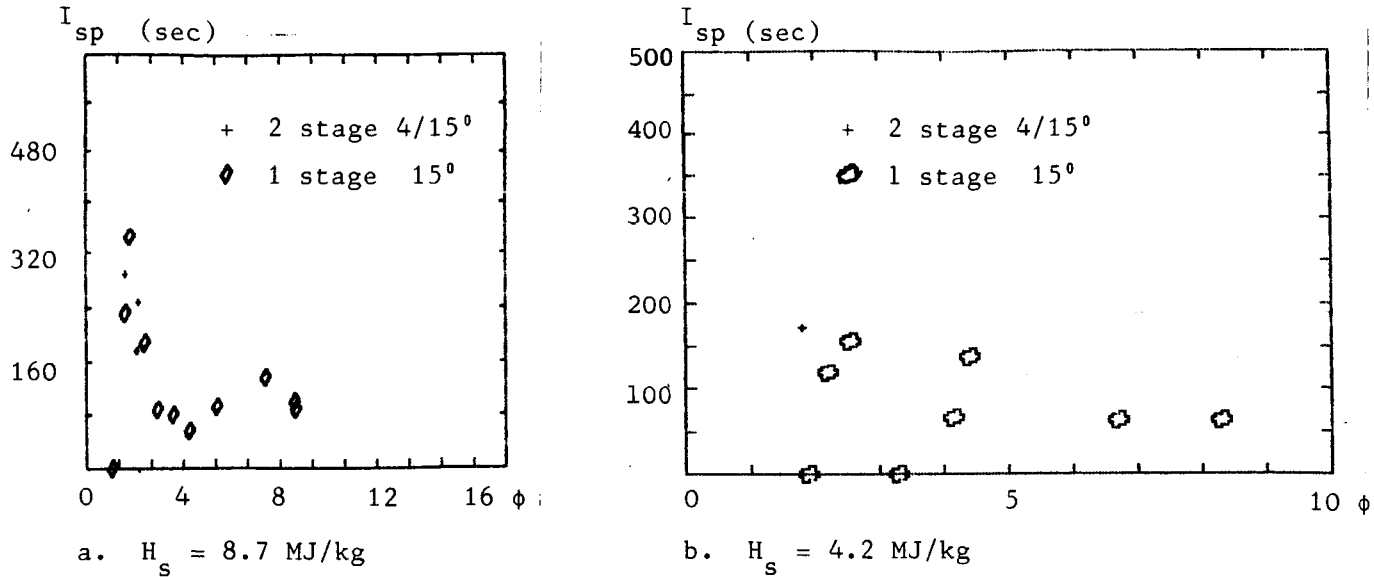

a. H_s = 8.7 MJ/kg

b. H_s = 4.2 MJ/kg

Fig. 49. I_{sp}/ϕ Comparison of dual and single stage expansions. Parallel wall injection, short combustion chamber, M_I = 3.5

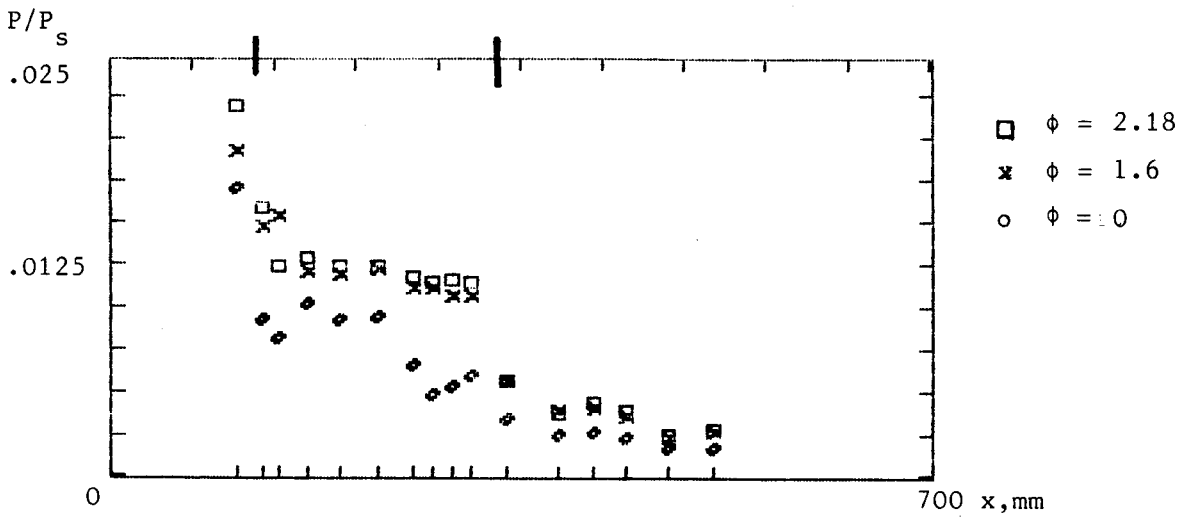

A. H_s = 8.7 MJ/kg

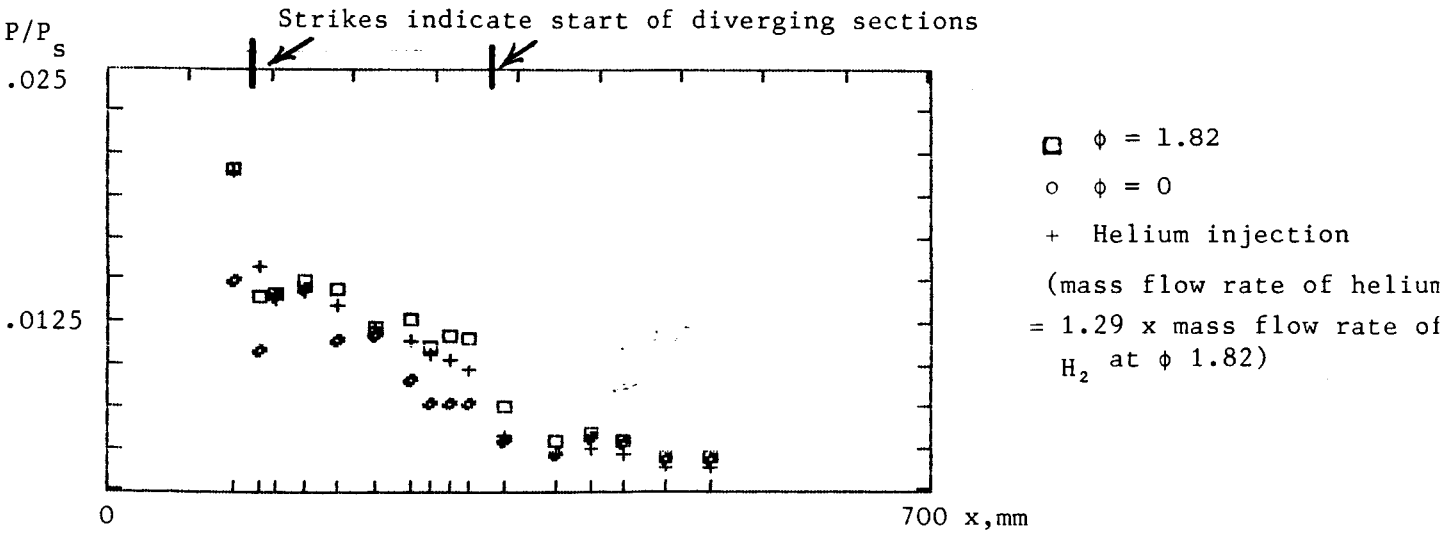

B. H_s = 4.2 MJ/kg

Fig. 50. P/X. Dual stage expansion, short combustion chamber. Parallel wall injection. M_I = 3.5

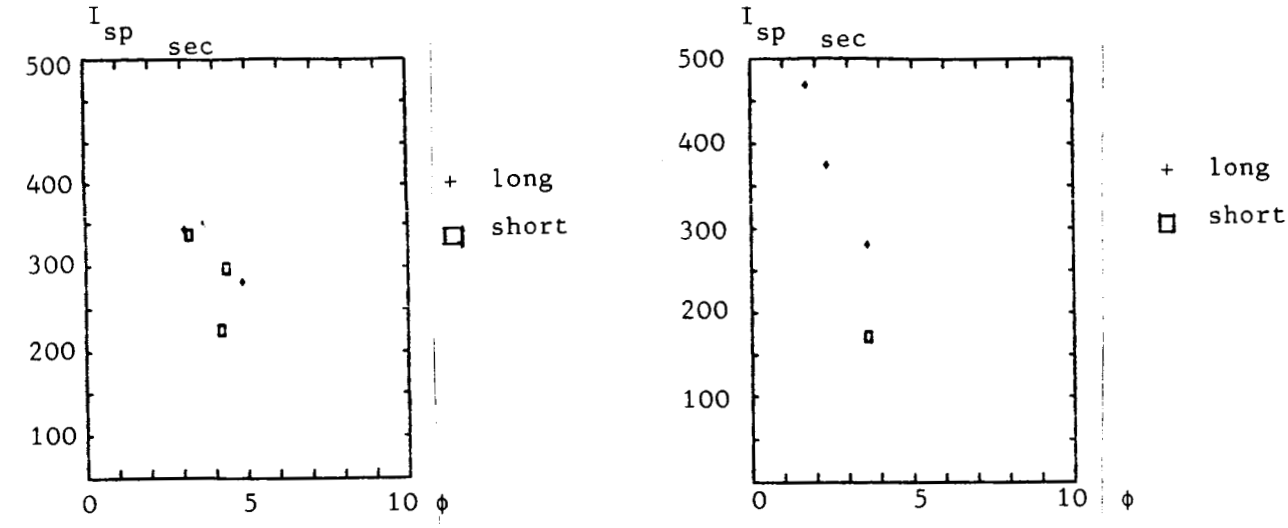

A. H_s = 8.7 MJ/kg

B. H_s = 4.2 MJ/kg

Fig. 51. I_{sp}/ϕ. Dual stage expansion. Long and short combustion chambers. Parallel wall injection. M_I = 3.5.

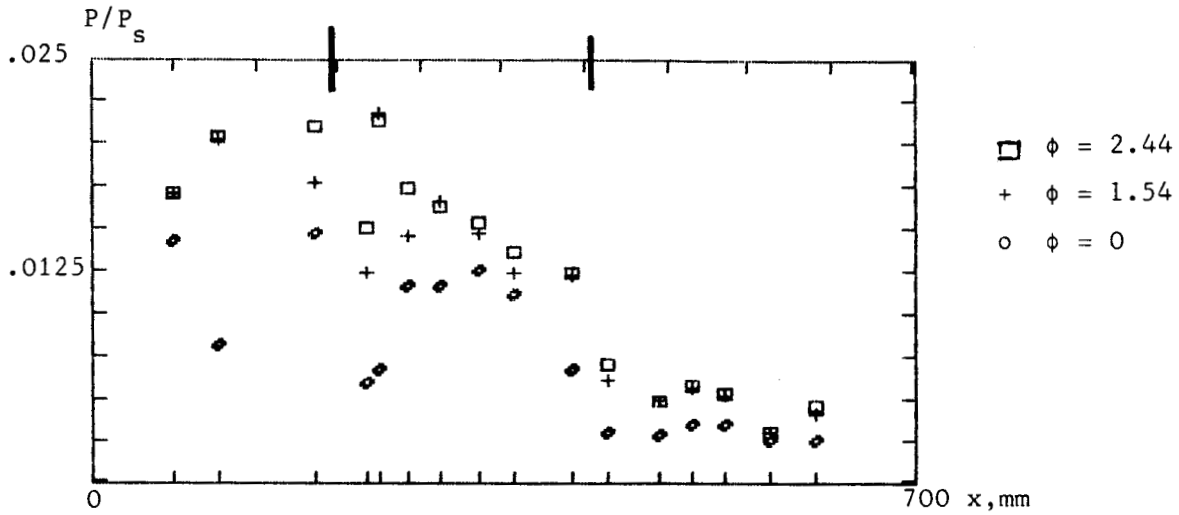

A. H_s = 8.7 MJ/kg

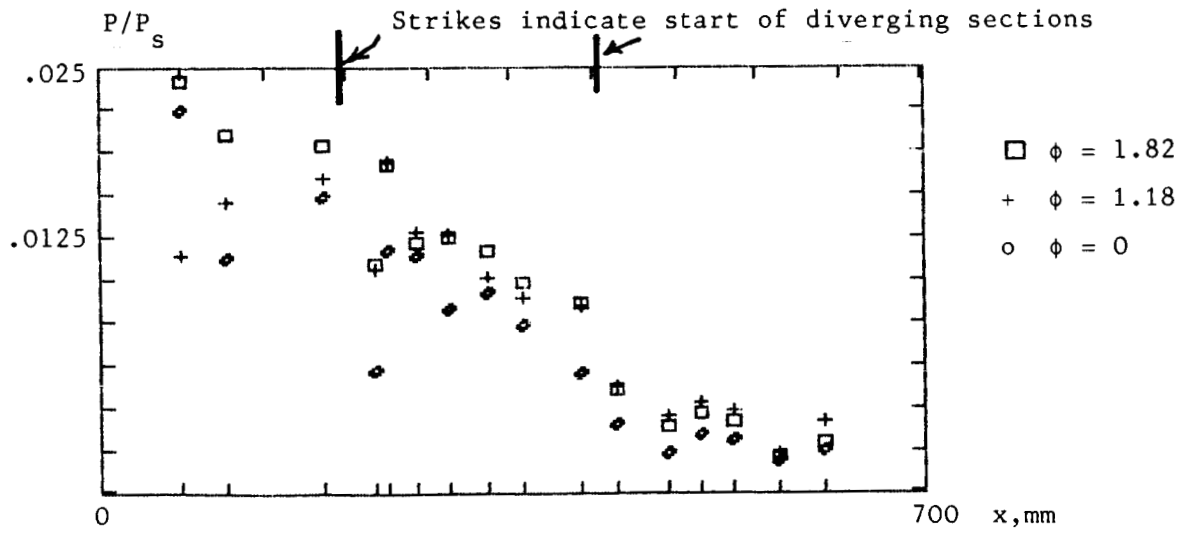

B. H_s = 4.2 MJ/kg

Fig. 52. P/X. Dual stage expansion with long combustion chamber. Parallel wall injection. M_I = 3.5.

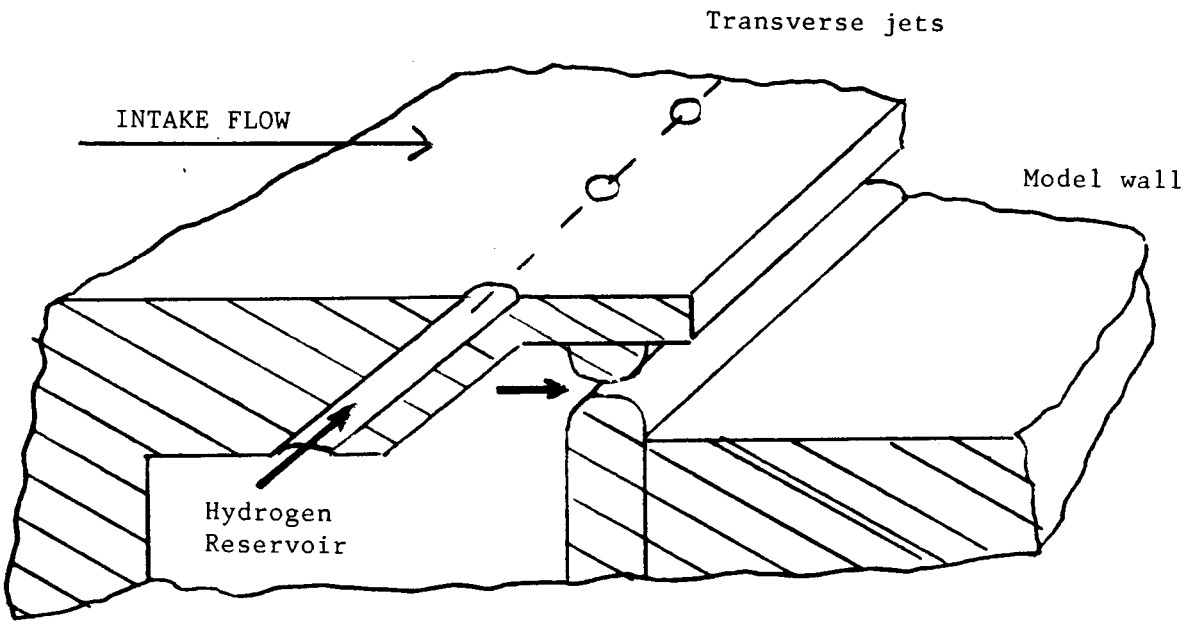

Fig. 53. Arrangement for mixed parallel and transverse wall injection

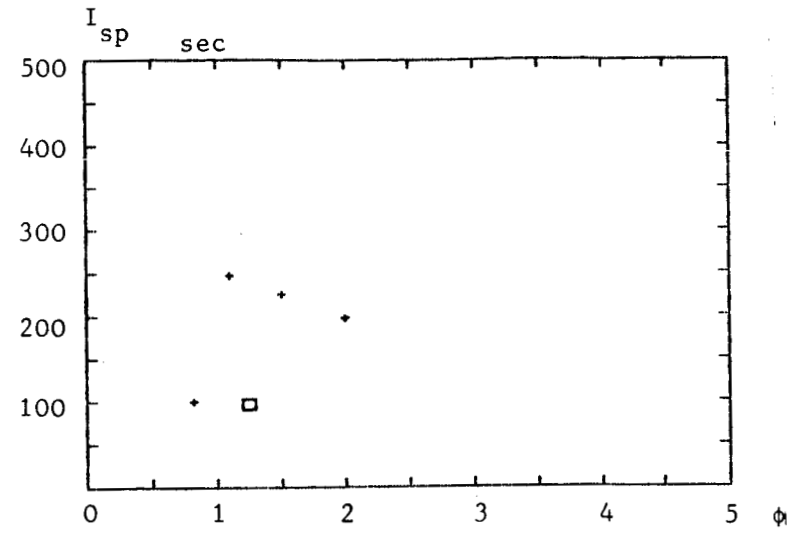

A. 8.7 MJ/kg 27% transverse

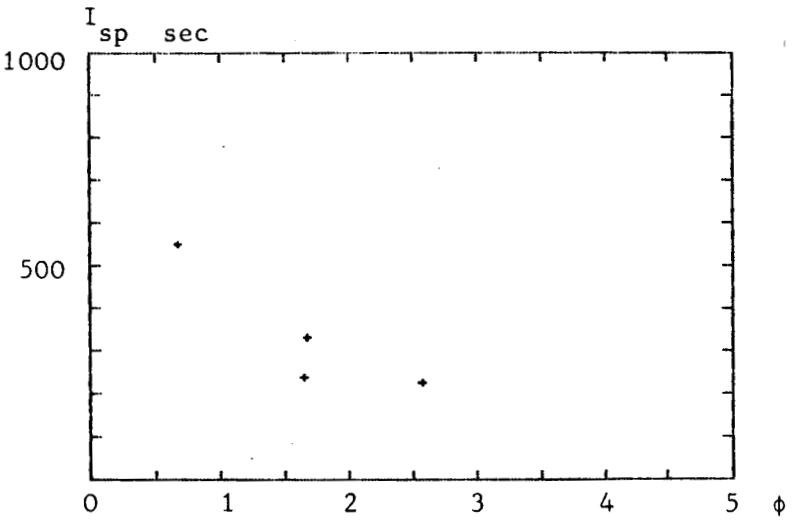

B. 6.1 MJ/kg 27% transverse

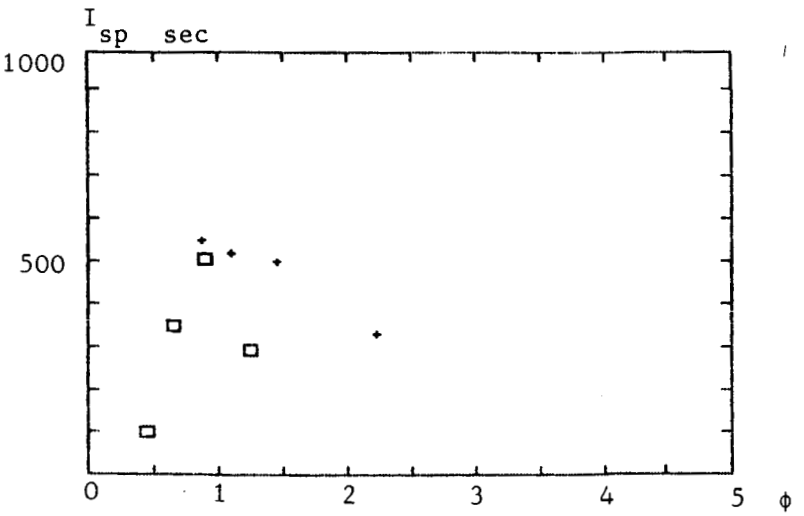

C. 4.2 MJ/kg

Fig. 54. I_{sp}/ϕ. Transverse wall injection dual stage expansion. Long duct. M_I = 3.5

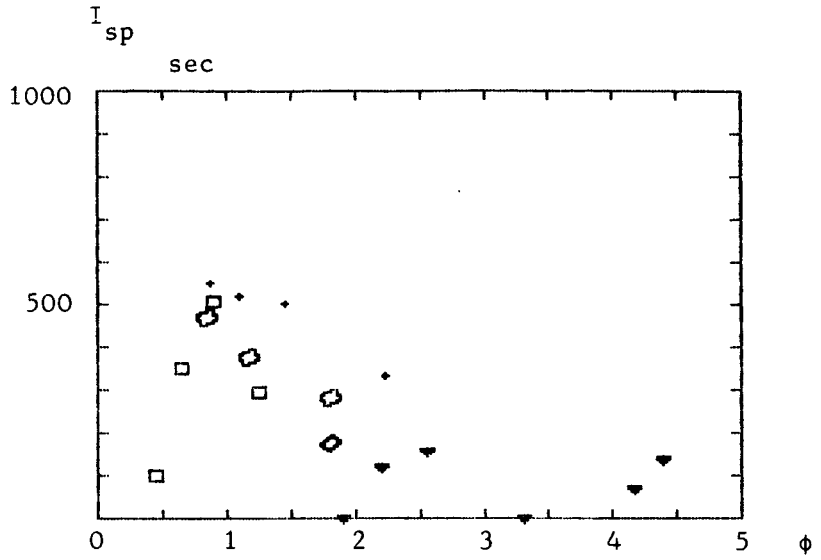

B 4.2 MJ/kg

□ 2 stage expansion, long duct, 79% tranverse

\+ 2 stage expansion, short duct, 27% transverse

◇ 2 stage expansion, long duct, parallel

◇ 2 stage expansion, short duct, pararrel

▼ 1 stage expansion, short duct, parallel

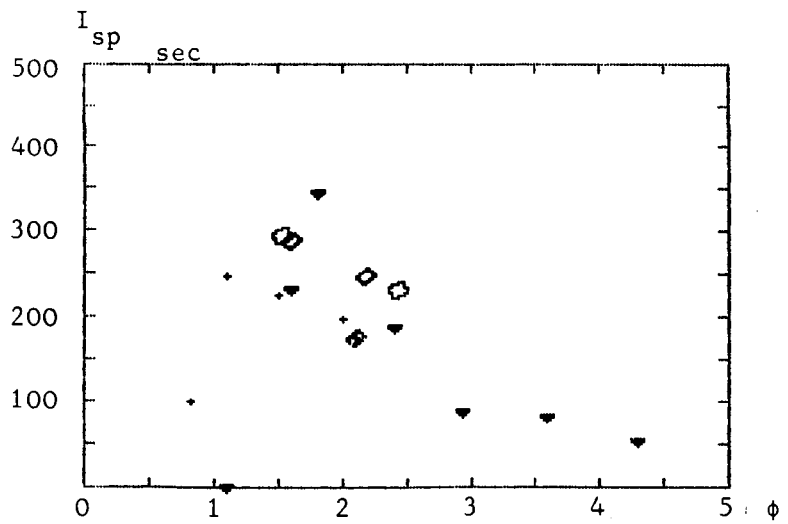

A 8.7 MJ/kg

Fig. 55. I_{sp}/ϕ. Various configurations of wall injection M_I = 3.5

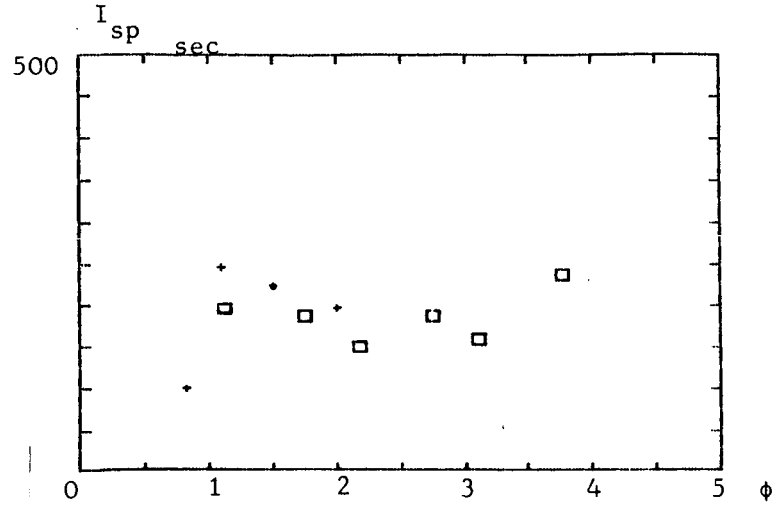

A 8.7 MJ/kg

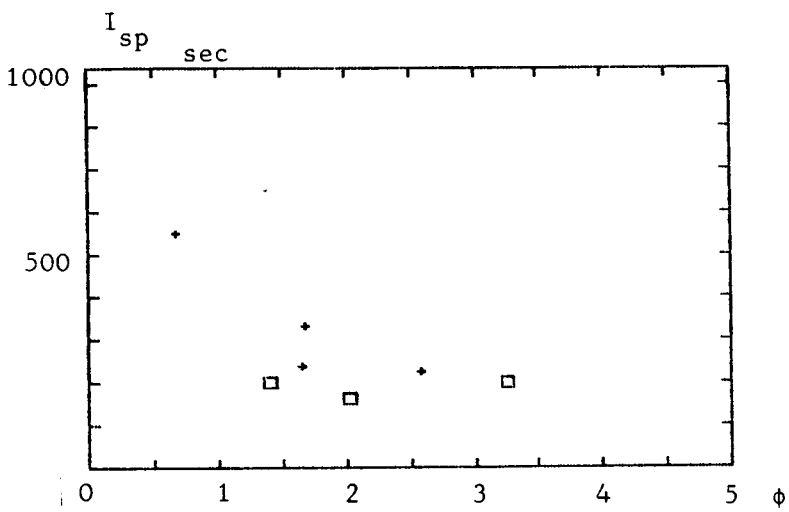

B. 6.1 MJ/kg

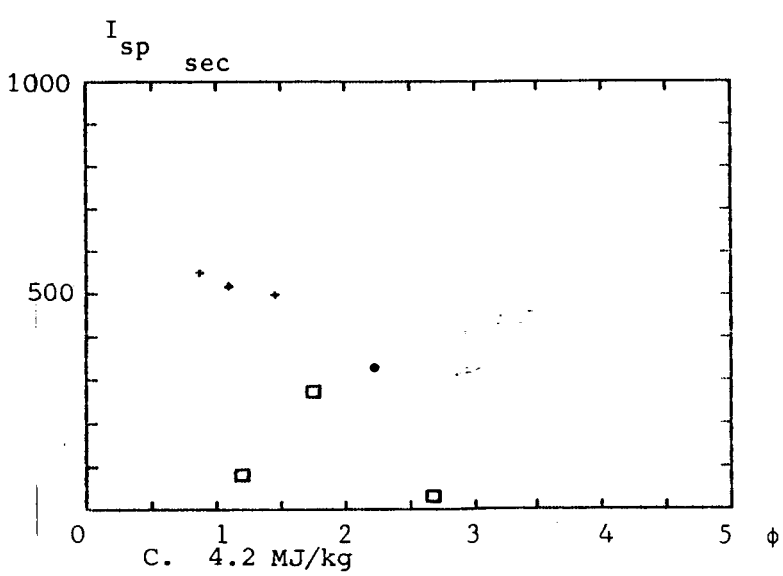

C. 4.2 MJ/kg

Fig. 56. I_{sp}/ϕ. Long duct 2 + 1 stage expansions 27% transverse $M_I = 3.5$

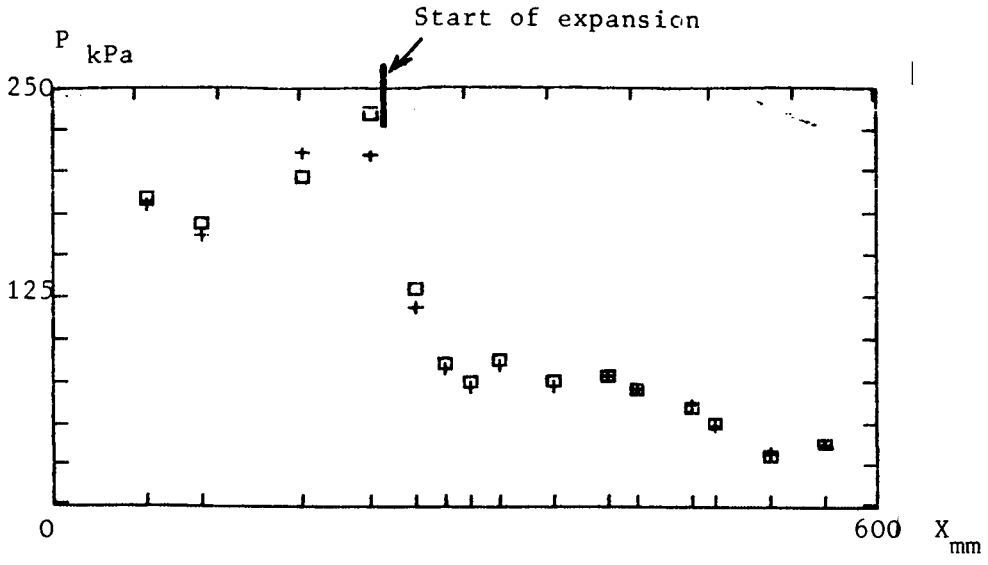

A. P/X

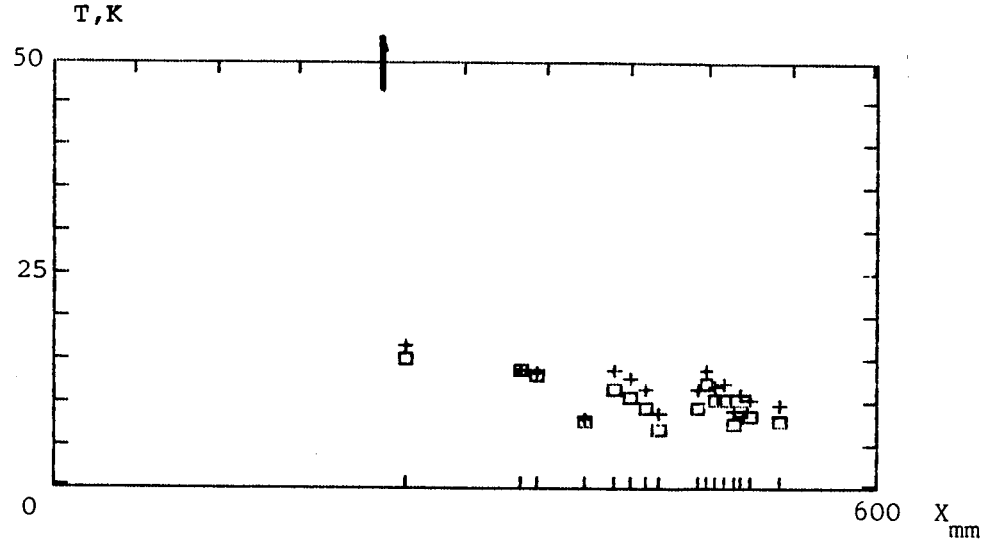

B. T/X

□ ϕ = 2.06 27% transverse injection

\+ ϕ = 2.04 parallel injection

Fig. 57. Comparison of parallel and transverse wall injection. Long duct, single 15° expansion. Hs = 6.1 Mj/kg , M_I = 3.5

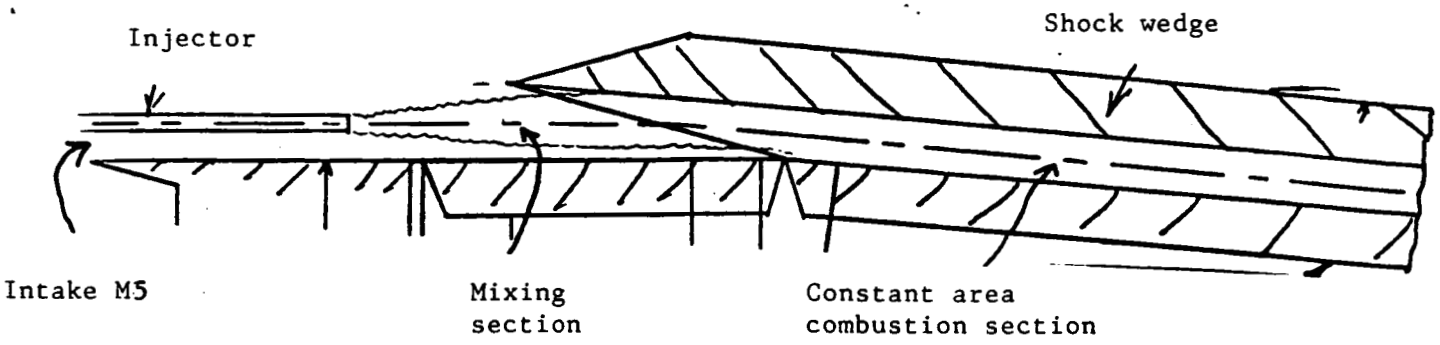

Fig. 58. Experimental shock induced ignition rig for central injection

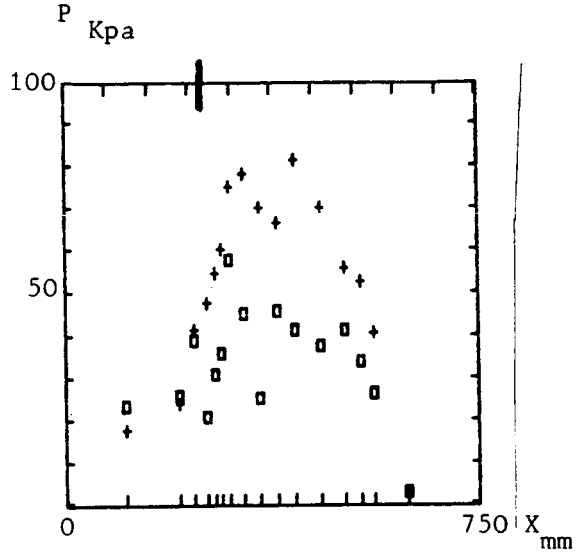

■ ϕ = 0

\+ ϕ = 6.1

A. H_s = 8.7 MJ/kg

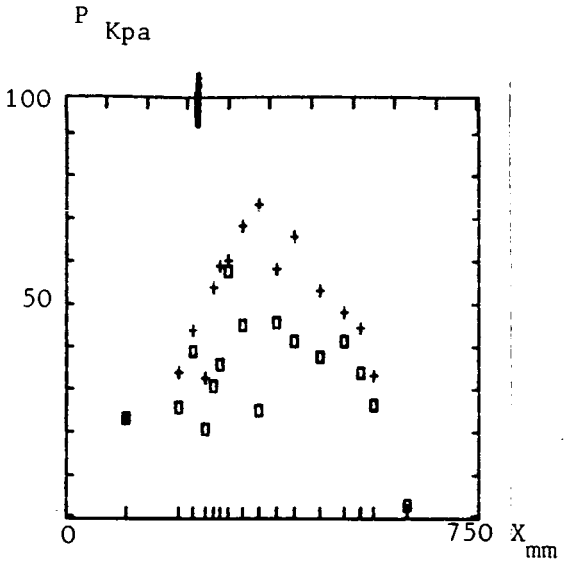

■ ϕ = 0 (H_s = 8.7 MJ/kg)

\+ ϕ = 4.8

B. H_s 6.1 MJ/kg , fuel on

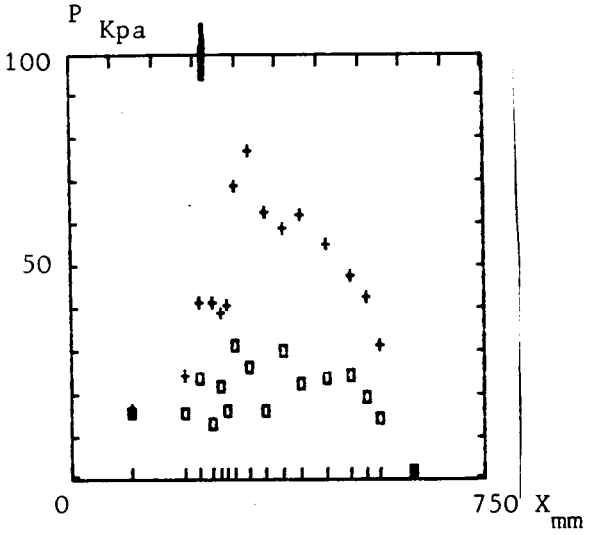

■ ϕ = 0

\+ ϕ = 3.9

C. H_s = 3.43 MJ/kg

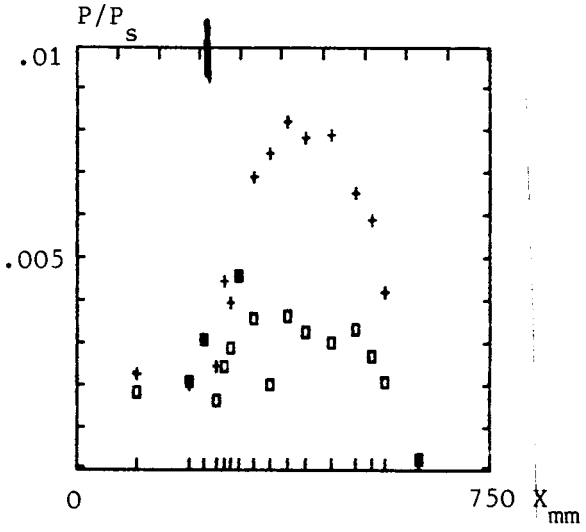

■ ϕ = 0 (8.7 MJ/kg)

\+ ϕ = 4

D. H_s = 2.65 MJ/kg , fuel on

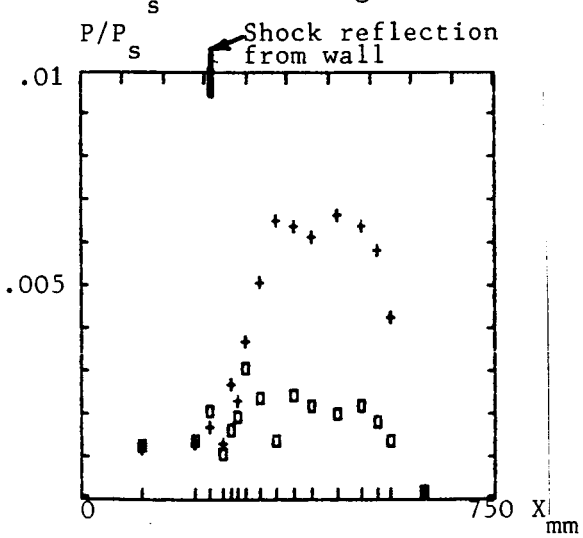

■ ϕ = 0

\+ ϕ = 3.8

E. H_s = 2.3 MJ/kg, fuel on

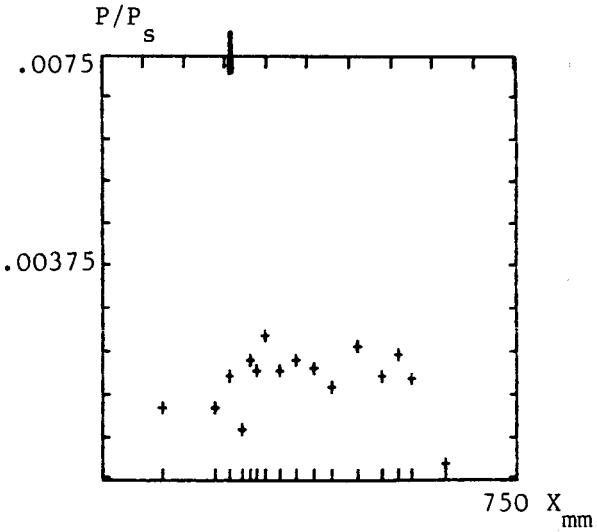

\+ ϕ = 3.7

F. H_s = 1.9 MJ/kg

Fig. 59. P/X. Shock stabalised combustion, central injection M_T = 5, 5° turning angle shock.

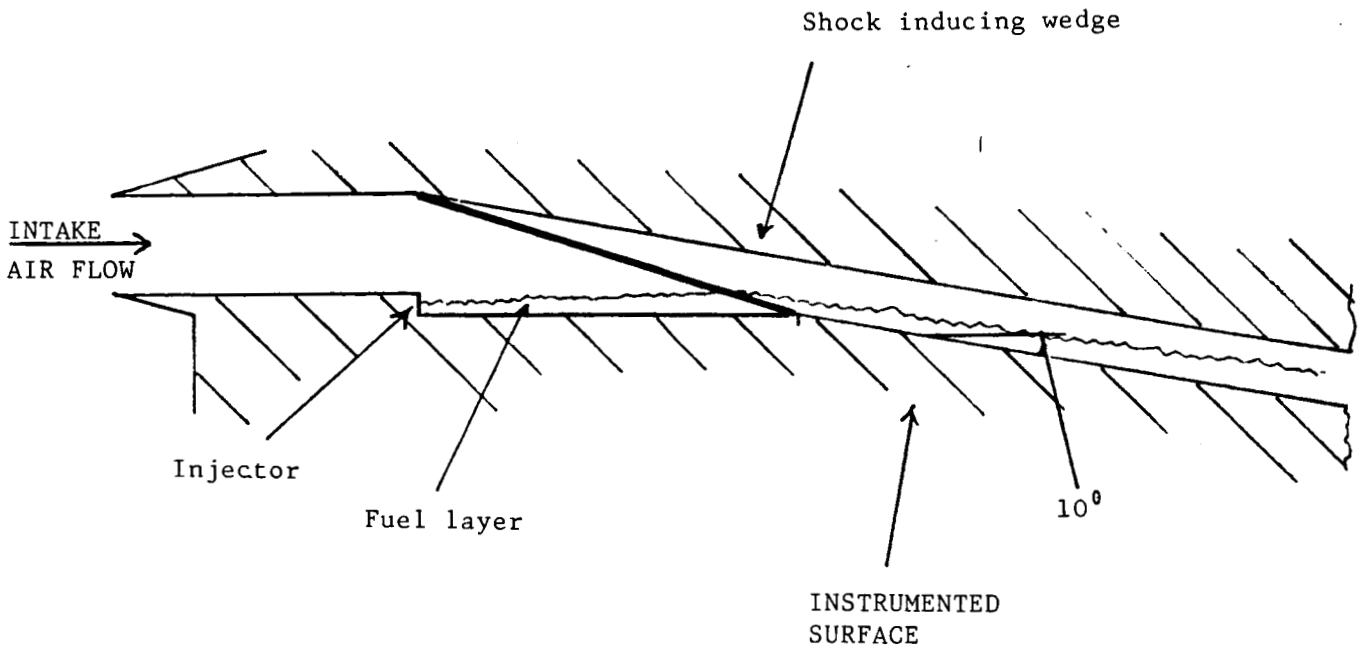

Fig. 60. Wall injection shock induced ignition rig. 10^0 turning angle

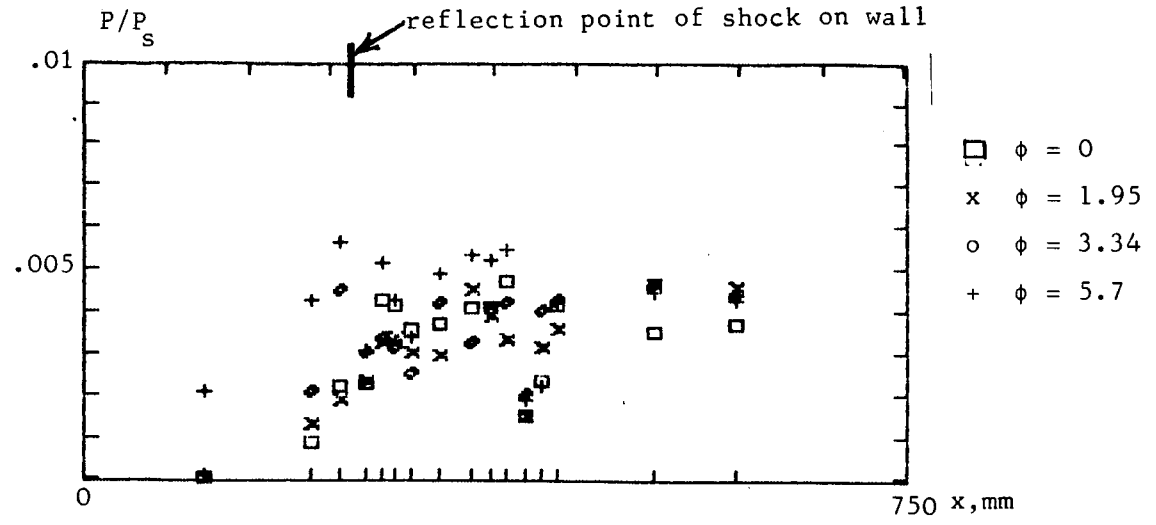

Fig. 61 P/X shock stabilised wall injection. 10° shock. H_s = 8.7 MJ/kg, M_I = 5

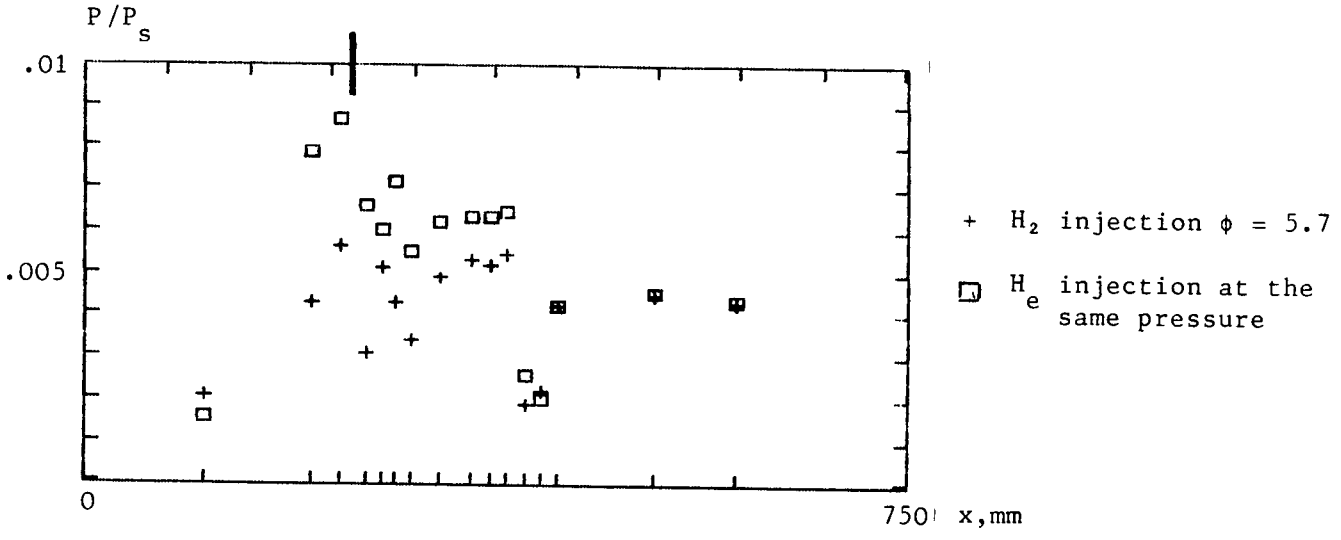

Fig. 62. P/X shock stabilised wall injection. 10° shock. M_I = 5, H_s = 8.7 MJ/kg. Comparison at H_e and H_2 injection.

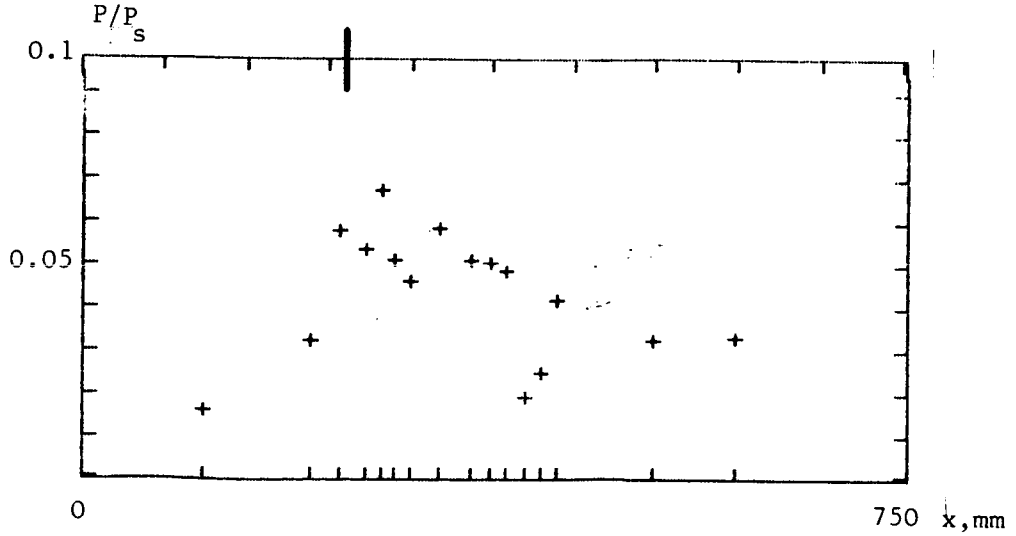

Fig. 63. P/X. Shock stabilised wall injection. 10° shock. M_I = 3.5. H_s = 8.7 MJ/kg. ϕ = 0.91.

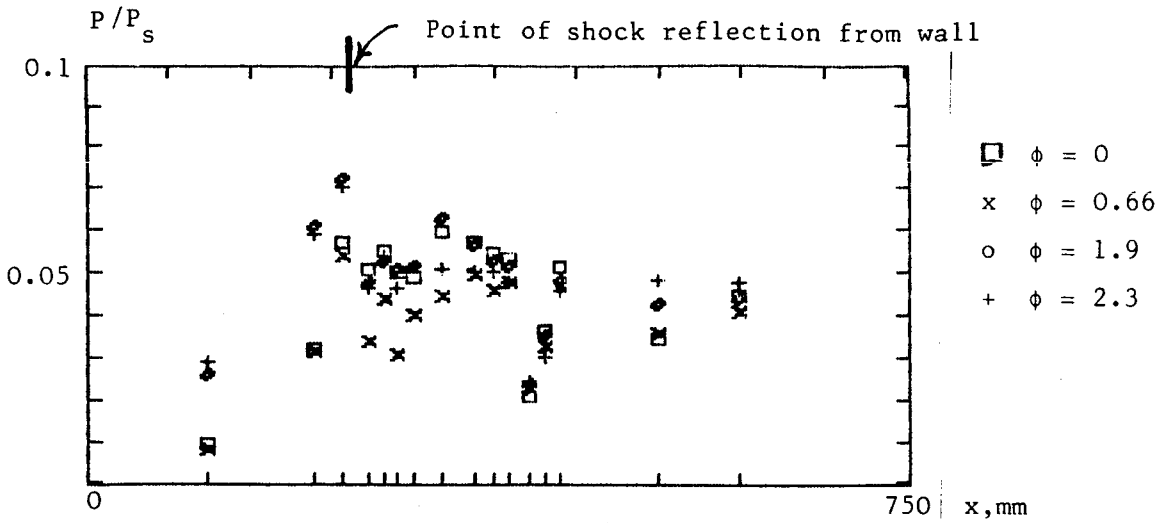

Fig. 64. P/X. Shock stabilised wall injection. 10° shock. M_I = 3.5. H_s = 6.1 MJ/kg.

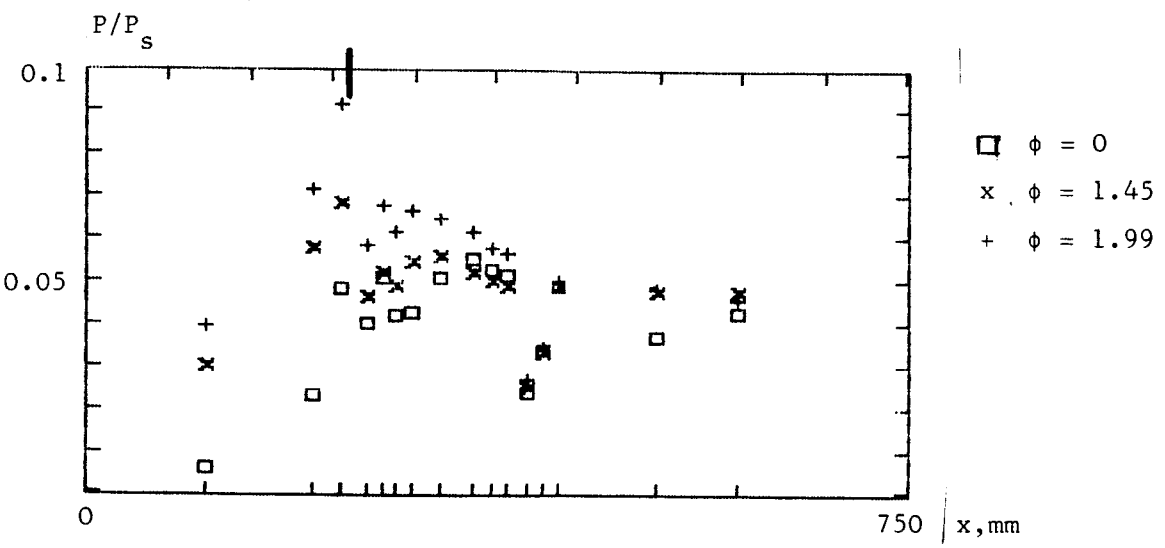

Fig. 65. P/X. Shock stabilised wall injection. 10° shock. H_s = 4.2 MJ/kg , M_I = 3.5

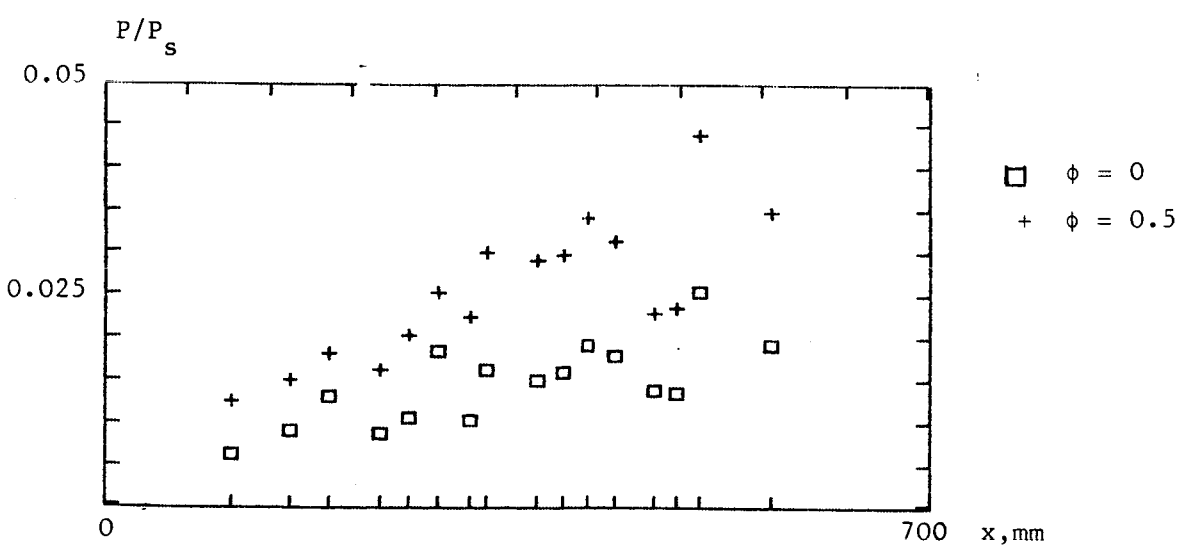

Fig. 66. P/X. Silane injection from wall. M_I = 3.5. H_s = 4.2 MJ/kg

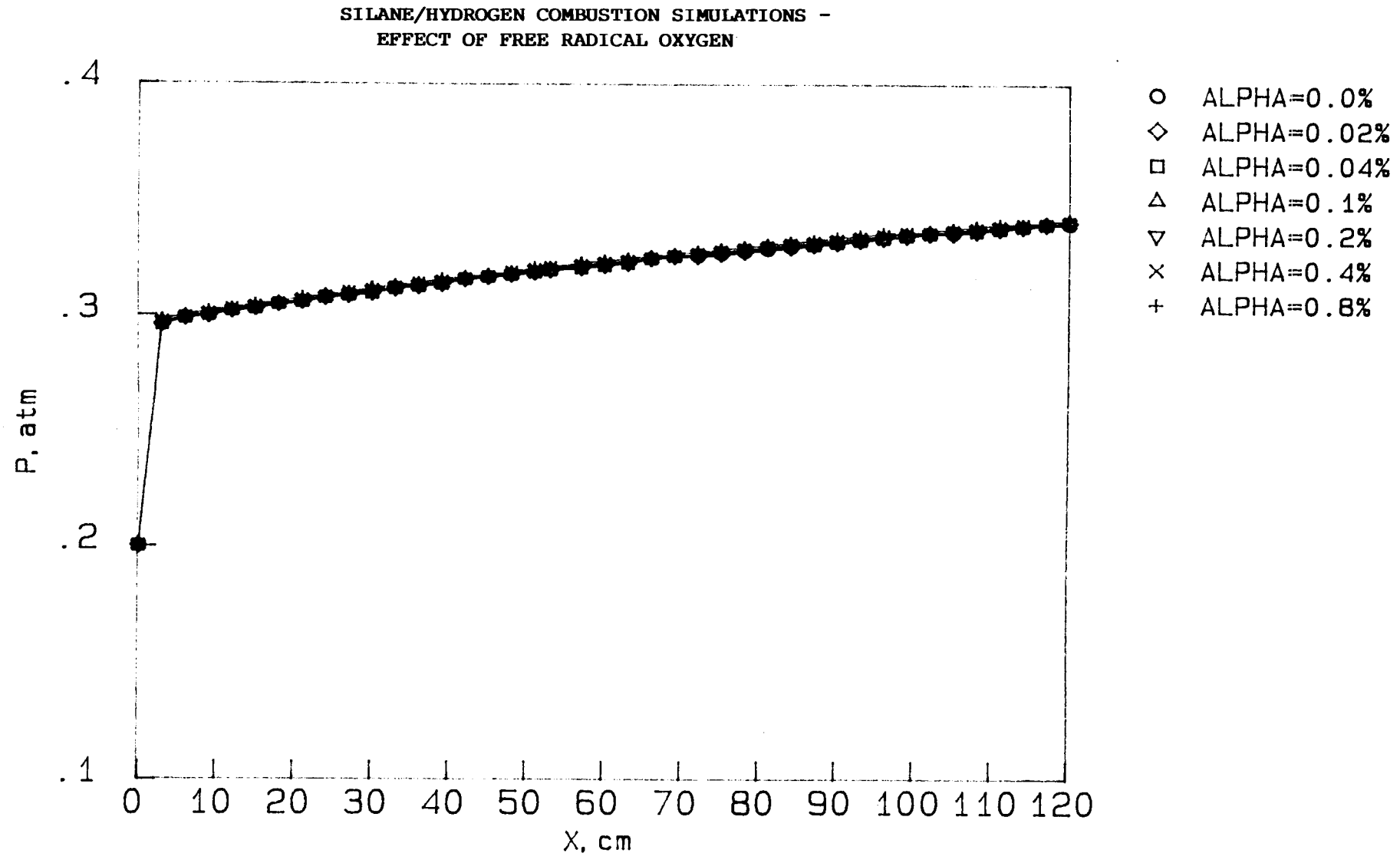

FIG. 67a 20% SiH4/H2, 1500K, 20KPA, MACH 5, PHI=1.0

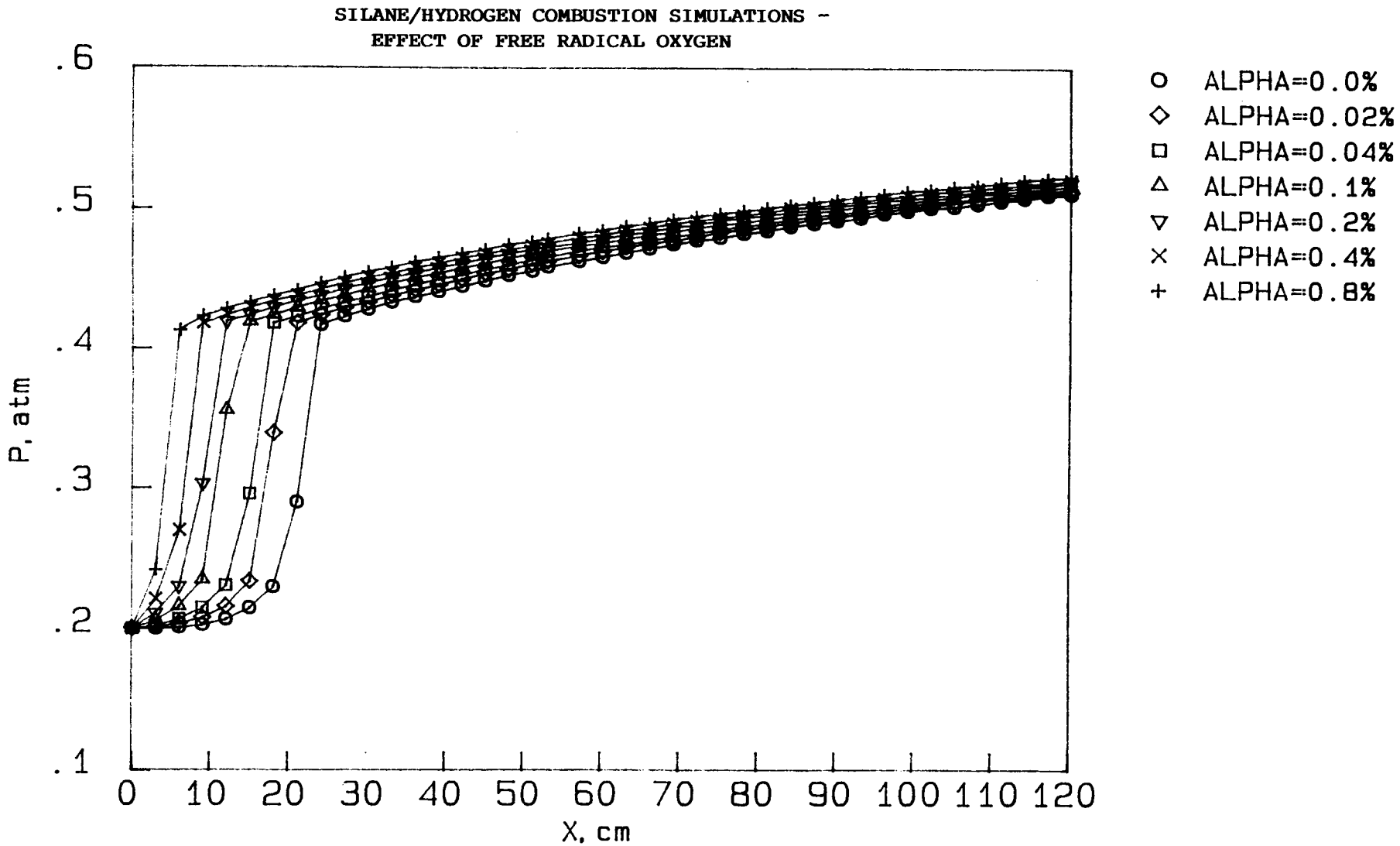

FIG. 67b 20% SIH4/H2, 1000K, 20KPA, MACH 5, PHI=1.0

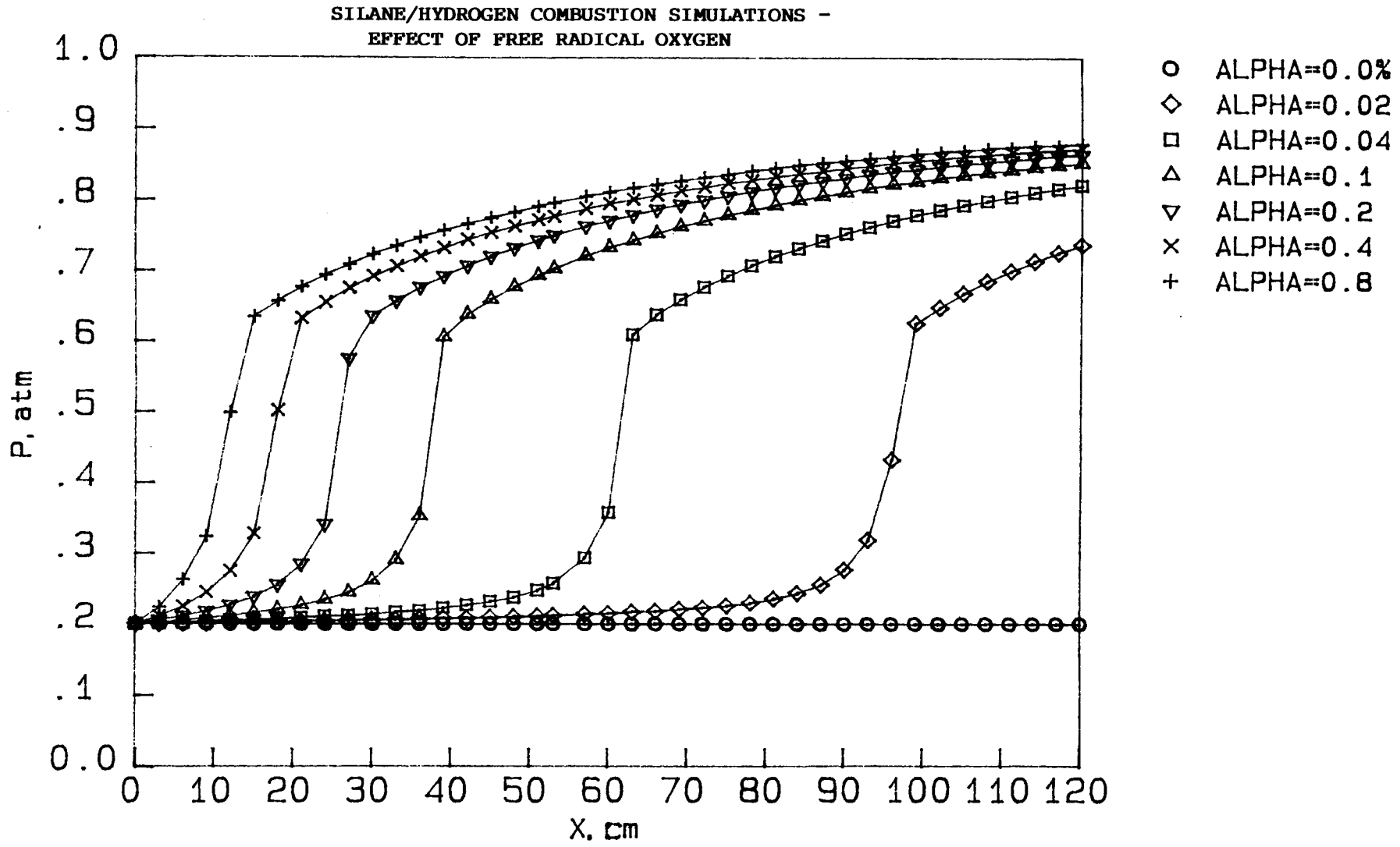

FIG.67c 20% SIH4/H2, 650K, 20KPA, MACH 5, PHI=1.0

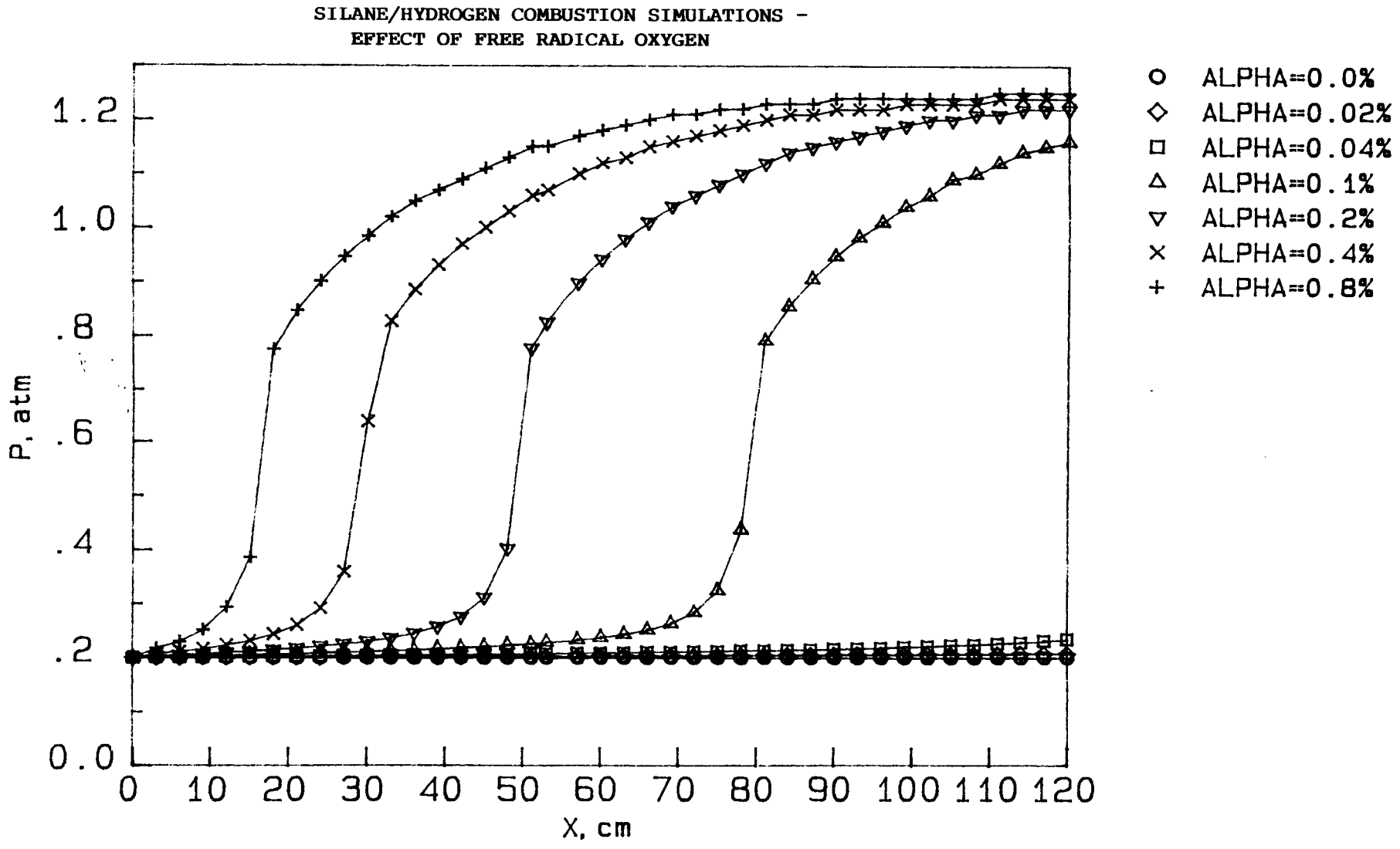

FIG.67d 20% SIH4/H2, 540K, 20KPA, MACH 5, PHI=1.0